Norwegian University of Life Sciences
Faculty of Science and Technology

Philosophiae Doctor (PhD)
Thesis 2021:20

Methods for estimation of major forest attributes based on remotely sensed data for the support of REDD+ measurement, reporting and verification (MRV)

Metoder for estimering av sentrale skoglige egenskaper basert på fjernmålte data til støtte for REDD+ måling, rapportering og verifisering (MRV)

Habitamu Taddese Berie

Methods for estimation of major forest attributes based on remotely sensed data for the support of REDD+ measurement, reporting and verification (MRV)

Metoder for estimering av sentrale skoglige egenskaper basert på fjernmålte data til støtte for REDD+ måling, rapportering og verifisering (MRV)

Philosophiae Doctor (PhD) Thesis

Habitamu Taddese Berie

Norwegian University of Life Sciences
Faculty of Natural Science and Technology

Ås (2021)

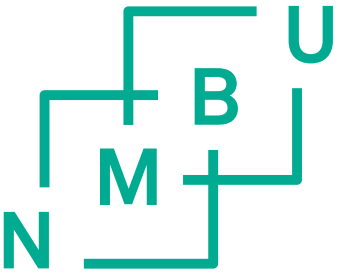

Thesis number 2021:20
ISSN 1894-6402
ISBN 978-82-575-1792-2

Methods for estimation of major forest attributes based on remotely sensed data for the support of REDD+ measurement, reporting and verification (MRV)

Supervisors and Evaluation Committee

PhD supervisors

Prof. Ingunn Burud
Faculty of Natural Science and Technology
Norwegian University of Life Sciences
Postbox 5003, 1432 Ås
Norway

Prof. Terje Gobakken
Faculty of Environmental Science and Natural Resources Management
Norwegian University of Life Sciences
Postbox 5003, 1432 Ås
Norway

Dr Daniel Ayalew Mengistu
Geospatial Data & Technology Center, Department of Geography and Environmental Studies
Bahir Dar University
P. O. Box 1398, Bahir Dar
Ethiopia

Prof. Øystein B. Dick
Faculty of Natural Science and Technology
Norwegian University of Life Sciences
Postbox 5003, 1432 Ås
Norway

Dr Hans Ole Ørka
Faculty of Environmental Science and Natural Resources Management
Norwegian University of Life Sciences
Postbox 5003, 1432 Ås
Norway

Evaluation Committee Members

Dr Lauri Korhonen
University of Eastern Finland, School of Forest Sciences
PO Box 111, FI-80101 Joensuu
Finland

Dr Peter Surovy
Czech University of Life Sciences Prague, Dept. of Forest Management
Suchdolske Namesti 1211/5, 16500 Prague 6
Czech Republic

Associate Professor Oliver Tomic
Faculty of Natural Science and Technology
Norwegian University of Life Sciences
Postbox 5003, 1432 Ås
Norway

Acknowledgements

I feel honoured to thank the individuals and institutions that offered me support throughout this academic endeavour. I would like to thank God for all the wisdom and support I received in my life. My academic journey, in general, has become a reality due to the unwavering support and encouragement of my late mother whom I have a profound gratitude and wish that her soul rests in eternal peace. I dedicate this thesis to her for the bravery she made in investing in the academics beyond her capacity.

I would also like to acknowledge my supervisor prof. Ingunn Burud for the support, guidance, freedom, and encouragement she gave me during the study period. She has offered me an amicable research setting to think and act as an independent researcher. I am thankful to my co-supervisors prof. Terje Gobakken, Dr Daniel Ayalew, prof. Øystein B. Dick and Dr Hans Ole Ørka for all the support I received and the discussions we made. I am indebted to thank prof. Erik Næsset for the significant contributions he made to two of the papers that he co-authored.

Special thanks to the PhD and research colleagues at REALTEK and the officemates for the time we had together and the encouragements. Melesse, Aurora, Amelia, and other officemates and roommates at SiÅs have been nice friends and will be missed. It was a source of encouragement to be accompanied by Dr Zerihun Asrat as a roommate and workmate during the study period.

This PhD work was financed by the "National MRV Capacity Building towards Climate Resilient Development in Ethiopia" project (grant number ETH 14/0002), for which I have ample gratitude. I am very grateful for the logistics support from Hawassa University – Wondo Genet College of Forestry and Natural Resources and Norwegian University of Life Sciences.

I would also like to express my sincere appreciation to my wife Amsal and our beloved children Eldana, Nathan, and Mariamawit for their encouragement, understanding, and affection. They have sacrificed the time and love that I had to offer them. The motivation I received from Daniel T., Belay, Mitiku & the whole family has also been tremendous. My gratitude goes to my brother Walelign for he has been shouldering my responsibilities in the family during my absence. Seble's presence in the family has been a source of stability since she took care of the children during those days.

Habitamu Taddese Berie
Ås, 17 February 2021

Table of Contents

Abbreviations and definitions

AGB	aboveground biomass
AIC	Akaike information criterion
ARVI	atmospherically resistant vegetation index
ASM	angular second moment
B	blue
CC	canopy cover
CO_2	carbon dioxide
CRGE	climate-resilient green economy
CV	coefficient of variation
DBH	diameter at breast height
ESA	European space agency
E-W	east-west (orientation)
ExGI	excessive green index
FBSS	field-based sample survey
FRL	forest reference level
G	green
GLCM	grey level co-occurrence matrix
GLI	green leaf index
GNSS	global navigation satellite system
GPS	global positioning system
IPCC	intergovernmental panel on climate change
L8	Landsat-8
LiDAR	light detection and ranging
LULC	land use/land cover
MD%	relative mean difference
MEA	grey-level co-occurrence matrix mean
Mg ha^{-1}	megagram per hectare
MRV	measurement, reporting and verification
MSI	multispectral instrument
NDGI	normalized difference green index
NDMI	normalized difference moisture index

NDVI	normalized difference vegetation index
NFI	national forest inventory
NIR	near-infrared
N-S	north-south (orientation)
OLI	operational land imager
PS	PlanetScope
QGIS	quantum geographic information system
r	correlation coefficient
R	red
R^2	coefficient of determination
RE	Red-edge
REDD+	reducing emission from deforestation and forest degradation, fostering forest conservation, sustainable forest management, and enhancement of forest carbon stocks
REf	Relative efficiency
REy	RapidEye
RGB	red-green-blue
RMSD%	relative root mean square difference
RMSE%	relative root mean square error
RS	remotely sensed
S2	Sentinel-2
SB	spectral band
SD	standard deviation
SE	standard error
SI	spectral index
SP	sample plot
SR	simple ratio
SWIR	shortwave infrared
UAS	unmanned aerial system
UAV	unmanned aerial vehicle
UNFCCC	the United Nations' framework convention on climate change
US	the United States
USGS	United States geological survey
VAR	grey-level co-occurrence matrix variance
VI	vegetation index (i.e., a type of spectral index)
VTOL	vertical take-off and landing

List of papers

The four research papers, which comprise this work, are listed below. They are labelled with Roman numerals throughout the thesis.

Paper-I: Taddese, H. and Burud, I. 2018. Application of unmanned aerial vehicles in earth resources monitoring: focus on evaluating potentials for forest monitoring in Ethiopia. *European journal of remote sensing*, *51*(1), pp.326-335.

Paper-II: Asrat, Z., Taddese, H., Ørka, H.O., Gobakken, T., Burud, I. and Næsset, E. 2018. Estimation of forest area and canopy cover based on visual interpretation of satellite images in Ethiopia. *Land*, *7*(3), p.92.

Paper-III: Taddese, H., Asrat, Z., Burud, I., Gobakken, T., Ørka, H.O., Dick, Ø.B., Næsset, E. 2020. Use of Remotely Sensed Data to Enhance Estimation of Aboveground Biomass for the Dry Afromontane Forest in South-Central Ethiopia. *Remote sensing,* 12(20): 3335.

Paper-IV: Taddese, H., Gobakken, T., Ayalew, D.M., Ørka, H.O. and Burud, I. (manuscript under review in *Forestry*). Digital Photography for Estimating Canopy Cover in an Afromontane Forest.

Abstract

There is limited information about the status of forest resources in Ethiopia. The available reports based on field sampling are inconsistent and lack precision due to limited sample sizes. Remotely sensed data, which cover a larger area, could be used to supplement the field sampling to improve precision. Therefore, this thesis tried to assess the improvement in estimation efficiency by using different data and methods for assessing forest area, canopy cover and aboveground biomass variables. In paper-I, suitability of unmanned aerial systems for forest monitoring in the Ethiopian context was explored using literature review on existing experiences in different fields across different geographic regions. The review results indicated that unmanned aerial systems have huge potential to contribute to forest assessment in Ethiopia due to the growing technological availability, which offers choices based on the intended purpose and costs. Global experiences indicated the need for preparing operational guidelines and the legal framework within which the system works. In paper-II, manual interpretation of satellite images was used to evaluate the suitability of PlanetScope, RapidEye and Sentinel-2 images for forest area and canopy cover assessment. The results indicated that RapidEye and PlanetScope images, which have relatively high resolution, had similar patterns of estimates for both variables while estimates using the Sentinel-2 images with coarser resolution were dependent on the forest density. Evaluation of sensitivity to sample size showed that the high-resolution images were less sensitive to change in sample size and therefore best suited for studying forest area and CC using manual image interpretation. In paper-III, model-assisted estimation technique was applied to compare the contribution of Landsat-8, Sentinel-2 and PlanetScope image-derived variables for aboveground biomass estimation in a dry Afromontane forest in Ethiopia. Simple models were developed for the variables from each image type and their estimation efficiencies compared. The results indicated that the model-assisted estimates were more precise than that of the field survey. Lastly, in paper-IV, a photo processing method was developed to estimate forest canopy cover from digital photos. The use of Otsu thresholding for photo segmentation offered objective assessment of canopy fractions. The results revealed that the canopy fraction of the central distortion-free 1-3% of the full photo size with thresholds of 10 and 20% estimated canopy cover more precisely than the point-based method. Therefore, the use of a narrow-angle camera for canopy photography is recommended.

Norsk sammendrag

Informasjon om status for skogressurser i Etiopia er begrenset. De tilgjengelige rapportene basert på feltprøver er inkonsekvente og mangler presisjon på grunn av begrensede prøvestørrelser. Fjernmålingsdata som dekker et større område kan brukes til å supplere feltprøvetakingen for å forbedre presisjonen. Jeg har derfor prøvd i dette arbeidet å vurdere forbedringen i estimeringseffektivitet ved å bruke ulike data og metoder for å vurdere skogareal, trekronedekke og biomasse over jord.
I artikkel-I ble egnetheten til ubemannede luftfartøy (droner) for skogovervåking i etiopisk sammenheng undersøkt ved hjelp av litteraturgjennomgang om eksisterende erfaringer innen forskjellige felt på tvers av forskjellige geografiske regioner. Gjennomgangsresultatene indikerte at ubemannede luftfartøy har et enormt potensiale til å bidra til skogvurdering i Etiopia på grunn av den økende teknologiske tilgjengeligheten, som tilbyr valg basert på det tiltenkte formålet og kostnadene. Globale erfaringer indikerte behovet for å utarbeide operasjonelle retningslinjer og det juridiske rammeverket systemet fungerer innenfor.
I artikkel II ble manuell tolkning av satellittbilder brukt for å evaluere egnetheten til PlanetScope, RapidEye og Sentinel-2 bilder for skogareal og trekronedekke. Resultatene indikerte at RapidEye- og PlanetScope-bilder, som har relativt høy oppløsning, ga lignende estimat for begge variable mens estimatene basert på Sentinel-2-bildene med grovere oppløsning var avhengige av skogtettheten. Evaluering av følsomhet for utvalgsstørrelse viste at bilder med høy oppløsning var mindre følsomme for endring i utvalgsstørrelse og derfor best egnet for å studere skogsområde og trekronedekke ut ifra manuell bildetolkning.
I artikkel-III ble modellassistert estimeringsteknikk anvendt for å sammenligne bidraget fra Landsat-8, Sentinel-2 og PlanetScope bildeavledede variabler for estimering av biomasse over bakkenivå i en tørr Afromontane-skog i Etiopia. Enkle modeller ble utviklet for variablene fra hver bildetype og deres estimerte effektivitet sammenlignet. Resultatene indikerte at de modellassisterte estimatene var mer presise enn feltundersøkelsen.
Til slutt ble det i artikkel-IV utviklet en bildebehandlingsmetode for å estimere trekronedekke fra digitale bilder og sammenlignet med punktbaserte data. Bruk av Otsu-terskelverdi for fotosegmentering ga objektiv vurdering av trekroneandel. Resultatene avslørte at bestemmelsen av kronedekke fra den sentrale 1-3% av full fotostørrelse, med terskler på 10% og 20% estimert trekroneandel, var mer presis

enn den punktbaserte metoden. Derfor anbefales bruk av et smalvinkelkamera til fotografering av trekronedekke.

Synopsis

1 Introduction

1.1 General background

Forests, which cover a significant portion of the earth's surface, provide multiple goods and services (Millennium Ecosystem Assessment, 2005; FAO and UNEP, 2020). They have economic and ecological significance at local and global levels. They harbor most of the terrestrial biodiversity on earth and play a major role in the global carbon cycle and hence contribute to climate change mitigation (Pan et al., 2011). Forest is identified as a major carbon sink since it is efficient in absorbing carbon dioxide from the atmosphere and storing it in large biomass per unit area of land (Gibbs et al., 2007; Bonan 2008). Tropical forests were the primary sequesters of atmospheric carbon (i.e. 55% of the total forest carbon stock) in the period from 1990 to 2007 (Pan et al., 2011). However, a recent study shows that tropical forests are the second-largest contributors of terrestrial carbon sequestration next to the boreal forests (Tagesson et al., 2020). This shift in the role of tropical forests as carbon sequester is attributed to the intensified tropical deforestation. The annual gross carbon dioxide emissions from tropical deforestation was estimated at 4.8 gigatons between 2015 and 2017 (Gibbs et al., 2018). Tropical deforestation and forest degradation caused biodiversity losses and carbon emissions (FAO and UNEP, 2020).

A similar trend of deforestation and forest degradation occurred in the remnant forests of Ethiopia. According to the estimates by the World Bank Group, the forest cover of Ethiopia has dwindled through time from about 15% in 1993 to about 12.5% in 2016 while the lowest estimate during this period was 12.3% in 2010. Deforestation and land-use change in Ethiopia emitted an average of 32.4 tCO_2e per year from 1990 to 2016. This represents 23% of Ethiopia's total greenhouse gas emissions over the same period (Global Forest Watch). However, the estimates from different sources were not consistent (MEFCC, 2018). For example, the United Nations' food and agriculture organization (FAO, 2010) estimated the forest cover of Ethiopia as 11.2% of the land area in 2010, which is different from the estimates for the same period by the World Bank Group. Thus, a lack of consistency tells that the

forest monitoring initiatives need to be supported with appropriate data and analysis methods to establish a consistent estimate of forest attributes. In Ethiopia, most of the forest monitoring efforts in the recent past were piecemeal assessments for specific sites and suffered from large uncertainties and low efficiencies (Watson et al., 2013; Duncanson et al., 2015; Kebede and Soromessa, 2018).

In the existing system in Ethiopia, forest inventory data is limited to some attributes only. For example, CC data has not been part of the national forest inventory of many tropical countries including Ethiopia (FDRE, 2017). This could mainly be due to practical difficulties related to the existing measurement techniques for attaining a balance between the financial cost and time for fieldwork on one hand, and accuracy issues on the other hand. However, variables like biomass, forest area and CC have enormous significances for evaluating the economic and environmental benefits of trees and forests. Living biomass of forests is an important indicator of the productivity of forest ecosystems. Biomass data is used to compute carbon stock, which represents the quantity of carbon removed from the atmospheric carbon pool. Thus, biomass assessment provides information about the contribution of forests for combating the impacts of climate change. The forest area variable is useful for monitoring the quantity of area in a landscape occupied by forest and the changes over time. Forest CC is also an important ecological variable, which has a direct relationship with spectral reflectance in optical remotely sensed (RS) data since canopy represents the interface between satellite sensors and forests.

1.2 REDD+ MRV system

The increase in greenhouse gas concentration in the atmosphere due to an increase in anthropogenic activities like excessive use of fossil fuels, land-use change and deforestation causes global warming, which leads to climate change. The UNFCCC has been implemented since 1994 as an international legal framework to combat climate change (Anderson, 1998). One of the recent instruments of the UNFCCC used for mitigating the effects of climate change is through the REDD+ mechanism (i.e., reducing emission from deforestation and forest degradation, fostering forest conservation, sustainable forest management, and enhancement of forest carbon stocks in developing countries), which was endorsed in the 2015 Paris agreement

(UNFCCC, 2015). The idea of the REDD+ mechanism is that developed countries compensate for the forest-based emission reduction by developing countries that have a substantial forest cover. The role of forests in storing carbon was the reason for including forest development and management in the emission reduction strategy. In this process, developed countries enjoy a cost-effective mitigation opportunity for the emissions released from their industries. The Warsaw Framework for REDD+ demands developing countries to formulate a national REDD+ strategy and establish a measurement, reporting and verification (MRV) system among other things (Recio, 2013) to get result-based payments.

Ethiopia ratified the UNFCCC in 1994 and the Kyoto protocol in 2005 as a non-annex-I party and joined the combat against the global climate change (FDRE, 2015). It has initialized a national REDD+ strategy for the period between 2018 and 2030 (FDRE, 2018). The REDD+ program in Ethiopia is embedded within the climate-resilient green economy (CRGE) strategy of the country, which targets at achieving a low carbon sustainable economic development (CRGE, 2011). The national REDD+ strategy of Ethiopia indicated that measurements in the MRV systems rely on field inventory and RS data. However, only Landsat images were used for land use/cover change detection between 2000 and 2013 and will continue to be used as the basis for land use/cover mapping because of their cost-effectiveness.

1.3 Field methods for data collection

Field-based sample survey (FBSS) provides accurate reference data for model calibration and verification (Kleinn, 2003). However, the precision of FBSS estimates is affected by small sample sizes, particularly in developing countries due to cost and accessibility constraints. This is because these countries do not have well-developed transport infrastructure while the majority of the forests exist in difficult terrains (Sandel and Svenning, 2013). FBSS with big plots, large sample sizes and frequent inventory is difficult in such settings. As a result, FBSSs can be cost-prohibitive or infeasible due to poorly developed transport infrastructure (Wondrade et al., 2015).

FBSS provides a basis for determining the relationship between image-derived variables and a dependent variable of interest. The target variable of interest in this

research, particularly aboveground biomass (AGB), is estimated using indirect methods. Site-specific allometric models are used for estimating plot-level AGB in sample plots (SPs). The allometric models of biomass, volume, wood density and other related attributes require field data for calibration and validation (Henry et al., 2010; Chen et al., 2015; Lu et al., 2016; Næsset et al., 2016).

1.4 Remote sensing

The focus of this thesis was exploring the possibilities for enhancing forest information using remote sensing, which is a method for assessing physical objects like forests using sensors on space-borne, air-borne or ground-based platforms without being in physical contact with the object under study. Satellite images, unmanned aerial systems (UASs) and digital photographs used in this study, which represent the three groups of remote sensing platforms, were evaluated for improving forest monitoring in one of the data-scarce tropical areas. All of these data sources have passive sensors and measure reflected energy in the optical region. Experiences show that optical remote sensing has been used for complementing field survey data in many forest types (Koch, 2015).

Although FBSS is often a primary source of data for many of the forest variables, integrating RS data plays an important role in improving estimation efficiency and offering the possibility of wall-to-wall prediction (Næsset et al., 2016). Forestry was the second sector following the military to use remote sensing for supporting field inventory and its relevance grows with the increasing developments in remote sensing technologies (Koch, 2015). RS data have large area coverage and are useful for change monitoring due to the short revisit frequencies. Large area coverage enables assessment of spatial relations among objects and processes. Some of the other reasons for integrating RS data for forest monitoring include low cost due to reduced sampling intensity (some satellite data are freely available), ability to access inaccessible areas (i.e., restricted, remote or difficult to access areas), ability to offer harmonized information (the same sensor used to acquire data of a specific area again and again) and retrospective assessment of changes. On the other hand, the use of RS data has limitations related to long-term availability of data (lifespan of the sensor), weather conditions, lack of technical capacity, object size that can be identified on the

images (versus pixel resolution) and flight permission for airborne data capture (e.g., UASs). These concerns should be considered when dealing with remote sensing methods. Generally, revisit frequency and pixel resolution of satellite images and cloud cover are useful criteria for selecting RS data for forest monitoring.

RS data are used for forest assessment with both design-based and model-assisted estimation techniques (McRoberts, 2010; Næsset et al., 2016). Thus, quantifying the contribution of different types of RS data to reduce uncertainties of estimates is a critical issue for choosing satellite images that offer reasonable estimation (Kleinn, 2003). Freely available medium resolution (i.e. L8 and S2) and low-cost high-resolution (i.e. REy and PS) optical satellite images were used in this study to evaluate their contribution to improving AGB, forest area and CC estimation. This study explored the type of RS data and methods available for use in forest monitoring at different spatial scales.

1.5 Research objectives

The general objective of the research in this thesis was to examine the role of remote sensing data and methods for forest monitoring. Most of the research work evaluated the efficiency of using RS images solely or in combination with FBSS data for estimating forest area, CC and AGB. Optical satellite images and terrestrial photographs offered data for AGB, forest area and CC estimation while feasibility of UASs for forest monitoring was explored through literature review.

Specifically, the objectives of this thesis, which comprises of four papers, were to:

- ✓ Assess the importance of UASs for forest resources monitoring (paper-I);
- ✓ Estimate forest area and CC based on manual interpretation of satellite images of different pixel resolutions (paper-II);
- ✓ Enhance AGB estimation by integrating optical RS data with that of field survey (paper-III); and
- ✓ Develop a method for digital photo processing to estimate forest CC (paper-IV).

1.6 Motivation

The motivation behind this study was improving the consistency and precision of forest information. This was further driven by the availability of inexpensive RS data (some of them freely available) for improving estimation of forest parameters. A recent study by Nguyen et al. (2020) indicated that freely available satellite image products like that of Landsat could be used for AGB estimation in tropical areas where inventory data are not available or outdated. Some low-cost RS data like UASs could also be cost-efficient and more reliable for some forest parameters. UASs are particularly useful for small-scale forest monitoring at district or compartment levels. Manual image interpretation methods could be more applicable for large-scale forest assessment at national or regional scales.

Advances in computing capabilities have also fostered the potentials of integrating different data sources for modelling difficult-to-measure variables like biomass and CC. The lack of information about what feasible methods are available for integrating RS images with FBSS data for biomass estimation in the study area inspired us for testing different methods. The use of RS data for assessing forest variables is important for providing spatially explicit information over temporal regimes and reducing uncertainties, which are required in the REDD+ MRV (Kleinn, C. 2003; Sheng, 2017). The IPCC guidelines encourage countries to establish transparent, consistent and accurate MRV systems.

Therefore, with these background justifications in mind, the four papers in this thesis were framed in the following structure. Paper-I explored the suitability of UASs for natural resources monitoring in Ethiopia based on a systematic review of the literature. Paper-II evaluated image types for estimating forest area and CC using manual interpretation in different forest densities in Ethiopia. Paper-III evaluated the performance of different optical satellite image types for enhancing AGB estimation in the dry Afromontane forest of the south-central Ethiopia. The use of digital photography in paper-IV was also motivated by the need for fast, easy to use and efficient methods for reliable CC assessment.

2 Materials and methods

2.1 Study area description

Ethiopia, located in eastern Africa, geographically extends approximately from 33° to 48° E longitude and from 3° to 15° N latitude (Figure 1-I). It has huge topographic diversity, stretching from the lowest Danakil depression (which is about 125 m below sea level) to the peak of the Simien Mountains, which is over 4500 m above sea level. The great East African rift valley that runs from northeast to southwest divides the country into north, northwest, and southwest highlands and the western lowlands on one side, and the eastern and southeastern highlands and the associated lowlands on the other side (Friis et al., 2010). Such topographic diversity created a wide range of climate and a diverse flora and fauna, with a considerable amount of it being endemic (Tewoldeberhan, 1991). As a result, the country has diverse biomes of which the Afromontane forest type is one of them.

Seven sites (sites A-G in Figure 1-II) were selected for the study of manual interpretation of satellite images for forest area and CC estimation. These sites represent the major biomes in the country that were used for sampling design in the recent national forest inventory (FDRE, 2017). The vegetation types in Ethiopia are classified into four major biomes (Friis et al, 2010). The first category is the dry Afromontane biome, which consists of the undifferentiated Afromontane forest; dry single dominant Afromontane forest of the Ethiopian highlands; Afromontane woodland, wooded grassland, and grassland. Besides, the transition between Afromontane vegetation and *Acacia-Commiphora* bushland, as well as Ericaceous and Afroalpine belts, are included in this category. The dry Afromontane forests cover the north, central, and eastern highlands of the country. The second category is the moist Afromontane biome that comprises mainly primary or mature secondary moist evergreen Afromontane forest. It also contains edges of moist evergreen Afromontane forest, bushland, woodland, and wooded grassland, as well as transitional rainforest. The moist Afromontane forests dominate the southwest and south-central areas of Ethiopia. The third category of biomes is the *Combretum-*

Terminalia biome, which includes the *Combretum-Terminalia* woodland and wooded grassland as major components. The *Combretum-Terminalia* biome covers the northwest, west and southwest lowlands, including the wooded grassland of the western Gambela region. The fourth category is the *Acacia-Commiphora* biome, which includes *Acacia-Commiphora* woodland and bushland, acacia wooded grassland of the rift valley as well as desert and semi-desert vegetation. The *Acacia-Commiphora* biome dominates the northeast, east, and south lowlands of the country.

Site A, which is the dry Afromontane forest biome, was selected for field data collection for papers III and IV since a priori knowledge of the site helped image interpretation and that the site is the most accessible of all the other sites to conduct achievable fieldwork. This site, known as Degaga-Gambo forest, contains both natural and plantation forests. The Degaga-Gambo forest is a state-owned enterprise. It is located on the eastern escarpment of the central rift valley of Ethiopia (Figure 1). It extends geographically from 38˚45' to 38˚56' E longitude and from 7˚13' to 7˚33' N latitude. The study forest has an area of 14,176 ha with an altitudinal range from 2100 to 2730 m above sea level. The area has a bimodal rainfall distribution with the main rainy season being from July to September while the short rainy season is from March to May (Duriaux and Baudron, 2016). The mean annual precipitation and temperature in the area are 1245 mm and 14.9 ˚C, respectively.

Studies (e.g., by Brown, 1969; Evangelista et al., 2007) indicated that the natural forest is a habitat for wild animals including endemic mammals like the mountain nyala (*Tragelaphus buxtoni*). The natural forest management by the forest enterprise and its proximity to Lake Langano, which is a major tourist destination in Ethiopia, make it one of the mountain nyala hunting sites (Evangelista et al., 2007). These forests have been severely encroached and degraded because of their accessibility for settlement and agriculture (Lemenih and Bongers, 2011). The main economy of the local people relies on crop production, animal husbandry and ecotourism activities. Rural villages and small townships are surrounding the forest. The main source of household energy for these settlements is illegal wood collection from these forests.

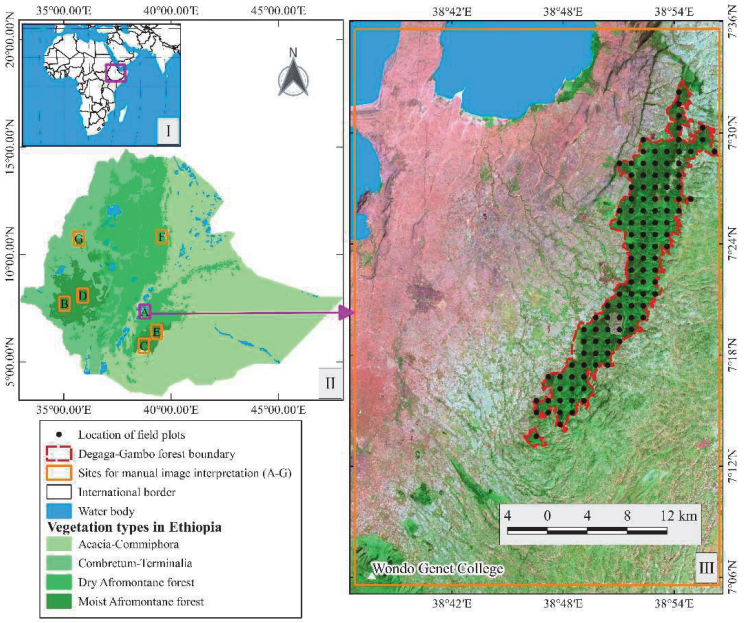

Figure 1: Location of research sites for manual image interpretation (A-G) in Ethiopia (II) and the field plot distribution in site A (III). The base map of the plot distribution map on the right panel (III) is SWIR-NIR-R band rendering of the Landsat-8 image acquired on 16 January 2019. Note that SWIR, NIR and R represent the shortwave infrared, near-infrared and red SBs, respectively.

2.2 Data Sources

Details of the overall process of data acquisition and analysis is shown in Figure 2 and further elaborated in the sections below. The data used in this thesis came from various sources. Field measurement was conducted in Degaga-Gambo forest (Figure 1-III: site A) for acquiring data for the target variables (i.e. biomass and CC). Digital photographs were captured from defined grid locations in the field plots (see Figure 3 for details). Besides, RS data were obtained from different sources. Satellite images of L8, S2, REy and PS were downloaded from respective websites. L8 image was downloaded from the United States geological survey earth explorer website (USGS). S2 images were downloaded from the European Space Agency - Copernicus Open Access Hub (ESA) while the PS and REy images were obtained from the Planet explorer website (Planet Explorer) upon the permission we got from the company. An extensive literature review was conducted for all the research papers and the thesis write-up.

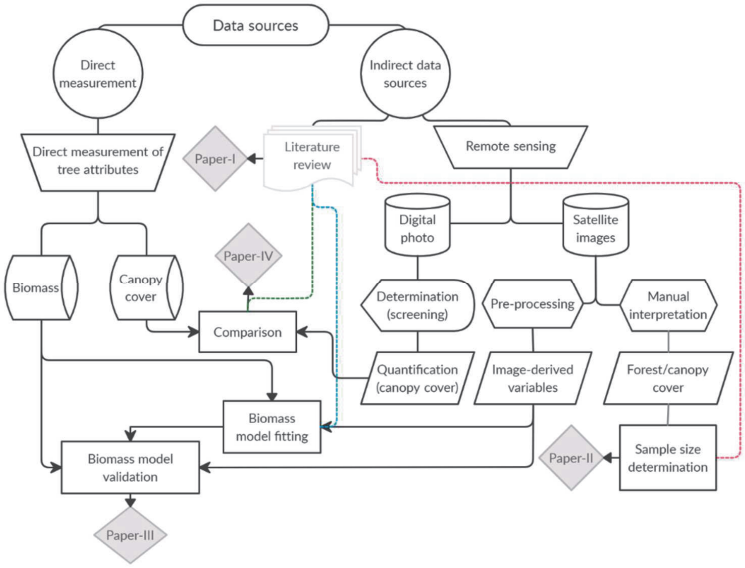

Figure 2. Overview of the research methodology. The rectangular boxes represent the outputs of the process while the diamond symbols refer to the decision outcomes (papers). The circular

shapes represent the broader class of data sources while the cylinders refer to the raw data. Other symbols refer to intermediate grouping of data or processes.

2.2.1 Literature review

The first paper in this thesis was developed based on a systematic review of existing literature (Ćosović et al., 2020). Literature review was also an important part of the other papers and the whole thesis work. A specific combination of search terms were used to get relevant information about a subject of interest. Literature search was conducted in the Web of Sciences, Scopus and Google Scholar databases.

For example, the specific combination of the search terms used in paper-I were alternative names of UAS, fields of application and 'Ethiopia'. The alternative names of UAS used in the scientific literature are 'unmanned aerial system', 'unmanned aircraft system', 'unmanned aerial vehicle' and 'drone'. The main application areas related to the interest of this evaluation are agriculture, flood control, wildlife monitoring, wildland forest fire management, forestry, hazard management, remote sensing, coastal wetland mapping, mapping of invasive species and environmental management. The assessment included the current experiences in Ethiopia on the use of UASs. Furthermore, opportunities and potential concerns in the use of UASs were explored. The paper was structured in accordance with these core issues.

2.2.2 Field survey

Papers III and IV relied on data from a field survey. For this purpose, forest inventory was carried out in 111 circular plots (paper-III), of which 76 selected plots were used for paper-IV. The reason for the variability in the number of samples was that paper-III relied on the probability distribution of the sample data at each of the systematically distributed locations to apply model-assisted estimation. For paper-IV, CC data was not collected for plots that fell in non-forest classes and some plots with data that had defects were removed during data pre-processing. The field data were collected in the dry seasons of 2018 and 2019. Systematic sampling design was employed to locate the SP centers. This sampling design was chosen due to its simplicity, the possibility of eliminating the phenomenon of clustered selection of samples and hence resulting in more precise estimates as compared to other

sampling techniques. This was so since the resource distribution does not follow a defined pattern in which systematic sampling could be biased. The Degaga-Gambo forest boundary (Figure 1-III) was used as the sampling frame within which SP locations were distributed at 1.18 km spacing in both the N-S and E-W directions. A handheld Garmin 78 GPS (global positioning system) unit was used to navigate to the location of the SPs. Precise positions of the plot centers were measured using differential GNSS with rover and base units of Topcon legacy-E + 40 channels dual-frequency receivers (Topcon Positioning Systems Inc.). These receivers record pseudo-range and carrier phase of GPS and GLONASS. The base station was set up at Wondo Genet College of Forestry and Natural Resources campus. The Euclidean distance between the base station and the plot centers ranged between 21.70 and 57.20 km with an average distance of 41.80 km. To determine the position of the base station using precise point positioning, the GPS and GLONASS data were recorded continuously for 24 hours (Kouba, 2009). The rover was mounted on a 2.98 m carbon rod at the plot center to record for 41.50 minutes on average using a one-second logging rate. The recordings were post-processed using the Magnet tools software (Magnet Tools). The standard error (SE) of the post-processed planimetric plot coordinates ranged from 0.02 to 1.11 m with a mean of 0.23 m.

The point locations were used to create circular SPs of 1000 m^2. All trees within the SP with DBH (i.e., diameter of trees at 1.30 m above the ground) ≥ 5 cm were identified by species and measured for DBH. Total tree height, bark thickness and diameter at stump height (i.e., diameter at 0.30 m above the ground) were measured for 10 systematically selected sample trees in each plot (Sullivan et al., 2018). For SPs with 10 trees or less, all of the trees were measured for these variables. Tree height was measured using the Haglöf VL5 hypsometer (Haglöf Company Group) while diameter was measured using a caliper or measuring tape based on tree size. A maximum DBH of 270 cm was measured.

For CC assessment in paper-IV, a network of N-S and E-W lines were created at 3 m interval in both directions starting from the plot center (Figure 3). A total of 109 points were created at the nodes of these line networks within a 1000 m^2 circular plot. Two measurements of CC were taken at the nodes. One set of measurements was

visual observation of CC vertically above the point while the other was photo capture. The visual observation was a count of obstruction by the forest canopy, which was recorded as "hit" or "miss" of canopy above the point in the zenith direction. The counts were converted into CC and used for evaluating the photo-based methods.

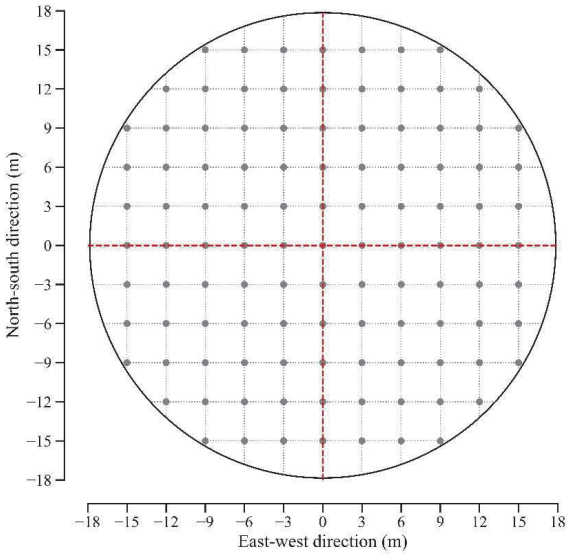

Figure 3. Design of the nodes (dots) within a circular SP of 17.85 m radius for CC measurement. The CC data were collected at the intersections of the broken lines within the circular plot at an interval of 3 m in both N-S (N is upwards) and E-W (E is rightwards) directions from the center of the SP, which is represented by the intersection of the broken red lines.

2.2.3 Remotely sensed data

For paper-II, RS data of the seven study sites distributed across the country were manually interpreted for estimating forest area and CC (Figure 1-II). Selection of the seven sites was subjective to accommodate sample sites representing a wide range of vegetation types in the country. The seven sites represented the four major biomes of the country, mainly the dense remnant forests in the southwest and south-central Ethiopia. The recent trends of forest loss/gain were also considered for site selection (Global Forest Watch). Some of the sites were selected since recent forest cover

changes are taking place in them. Site A is very accessible to the home institution of the interpreters such that prior knowledge of the area helps image interpretation. In each of the seven sites, plots of size 2052 km^2 (36 km × 57 km) were created for image interpretation. There were 228 square SPs of 70 m × 70 m (with an area of the sampling unit of 0.5 hectare) in each site. Two forest professionals performed the manual interpretation on S2, REy and PS images. They discussed the basics of image interpretation and shared experiences prior to the task. Both interpreters had similar exposure to the study sites. It was not possible to check the differences between interpreters and thus the average data of the two interpreters were used for analysis. Land use types were determined for each plot based on the IPCC definitions of land use/land cover (LULC) categories (Penman et al., 2003) i.e., forest land, cropland, grassland, wetland, settlements, and other lands. This data was used to estimate forest area proportion in each site. Within these sampling units, 49 square subplots of 2 m × 2 m were used as observation windows to identify whether they covered tree canopies or not. CC was estimated as the proportion of tree-covered subplots in the 0.5-hectare plot.

A detailed description of the characteristics of S2, REy, PS and L8 images are given in papers II and III. Predictor variables, which were used for AGB modelling in Paper-III, were derived from L8, S2 and PS satellite images. These images were acquired in January 2019, which is the dry season when it is easier to distinguish trees from other background objects. The image acquisition time was also needed to coincide with the field inventory period. The selected images had could cover < 5%. Image variables of the spectral band (SB) reflectance and spectral indices (SIs) were derived from the three satellite image types. Besides, image texture variables of PS were tested if they could portray spatial patterns of vegetation (and hence biomass) due to their high spatial resolution (Sousa et al., 2017). The SBs used in this study (i.e., blue, green, red, near-infrared, shortwave infrared-1 (for both L8 and S2), red-edge (only for S2)) have spatial resolutions of 30 m for L8 and 10 or 20 m for S2 (see Table 1 for details of the resolutions of individual bands).

Six scenes of orthorectified scaled products of PS (Level-3B) were downloaded from the Planet Explorer website (Planet Explorer). These images contain information about top of atmosphere radiance for the blue, green, red and near-infrared SBs.

Table 1. Major characteristics of the satellite systems and image properties used in this study.

Satellite	Sensor [a]	Spectral Bands [b]	Spatial Resolution
Landsat-8 (L8)	OLI	B, G, R, NIR, SWIR1	30 m: all SB
Sentinel-2 (S2)	MSI	B, G, R, RE, NIR, SWIR1	10 m: visible, NIR; 20 m: RE, SWIR1
PlanetScope (PS)	4-band frame imager; NIR filter	B, G, R, NIR	3 m: all SB
RapidEye (REy)	MSI	R, G, B, RE, NIR	5m

Source: USGS Earth Explorer for L8 and S2; Planet Explorer for PS and REy images.

[a] *OLI and MSI stand for operational land imager and multispectral instrument sensors.*

[b] *B, G, R, NIR, SWIR1 and RE represent the blue, green, red, near-infrared, shortwave infrared-1 and red-edge spectral bands (SBs), respectively.*

2.3 Data analyses

The first paper in this thesis is a review exploring the potentials, existing experiences, opportunities and concerns related to the use of UASs for forest monitoring in Ethiopia. A systematic review of the literature was conducted to study the basic characteristics of UASs, their application areas and operational guidelines. Such data were organized according to pre-defined thematic outlines. Existing global experiences on the major application areas, current practices, technological advances and operational regulations were reviewed to identify the opportunities and concerns about the proper use of the technology supported with contextualized operational guidelines and legal frameworks for limiting any potential misuse.

In paper-II, forest area and CC were computed for the three image types across the seven sites. Land use types at each SP of 0.5 ha were coded as 1 if forest and 0 otherwise, and mean forest area was computed. CC was computed for the three image types in the seven respective sites and each land use type. Unbiased estimators of the mean and variance of forest area and CC were computed. SE of the mean was computed as the square root of its variance. See the material and methods section of paper-II for details of the equations for calculating the estimators.

To assess the effects of the number of observations on the precision of both forest area and CC, four different resample sizes (m = 50, 100, 150, and 200) were used for bootstrap sampling with replacement, and the SE of the boot statistics were computed and compared with the SE of the original sample size (i.e. 228). The results of this study were compared by site (forest density) and image type (spatial resolution).

Both FBSS and satellite data were used for developing AGB estimation models in paper-III. Field-measured variables of individual trees were converted to tree-level AGB using allometric models developed for the study forest by Asrat et al. (2020). The biomass of individual trees were aggregated to plot-level and scaled to Mg ha^{-1} to compare them with the plot-level independent variables. The plot-level independent variables were computed as the mean and standard deviation of SB reflectance, SI and texture variables within the boundary of the SPs. The images were atmospherically corrected band reflectance values and SIs (from all the three image types) and texture variables from the high-resolution PS images. Due to the absence of previous studies of similar nature in this forest type, selection of suitable image-derived predictor variables was a challenge (Adame-Campos et al., 2019). Therefore, predictor variables were selected based on correlation analysis with the observed AGB. Correlation analysis was also used to discard multicollinearity among the independent variables. Consequently, the variables that had a stronger relationship with AGB and less intercorrelated were selected. Indicators like the Pearson's correlation coefficient and variable inflation factor were used to evaluate the strength of linear relationships and the multicollinearity effect among the variables. Those variables with the largest correlation coefficient and the least variable inflation factor were selected. To control overfitting problem, the number of predictor variables in each image type was limited to a maximum of two. Generalised linear models for the individual image types were created by regressing the observed AGB with the selected image-derived variables. Model performance was evaluated by leave-one-out cross-validation technique. The relative root mean square error (RMSE%), relative mean difference (MD%), coefficient of determination (R^2) and the Akaike information criterion (AIC) were used to evaluate the predictive power of the models.

Image-derived population data were obtained by tessellating the study site into square grid cells of 1000 m^2 and applying area-weighted mean and standard deviation of the pixel values. Predictions using the selected models were used to estimate the mean and variance estimators of AGB. The gain in precision of the estimates when using model-assisted technique was evaluated by comparing the model-assisted estimation uncertainties for each image type with that of the FBSS. This gain in precision was evaluated using an index called relative efficiency. A relative efficiency is greater than one implies the amount of additional precision gained due to the use of the RS data for estimating AGB compared to the pure FBSS.

For paper-IV, the binary count data of the ocular observations at the nodes of square grids in each of the sampling plots were converted to plot-level estimates of CC. Similarly, the digital photographs taken at the same locations were processed to photo-based CC estimates. The photos were cut into eight concentric squares of different sizes (100, 44.4, 11.1, 2.8, 1.8, 1.0, 0.4, and 0.1% of the original 3000 × 3000 pixels photo size) towards the photo center to study the influence of view angle on CC estimates. Otsu thresholding was used to binarize the digital photos into canopy and non-canopy segments to compute canopy fraction (in %). The canopy fraction obtained from each photo was classified into canopy and sky using seven threshold values (i.e., 10%, 20%, 30%, 40%, 50%, 60% and 70%). The canopy fractions greater than the thresholds were classified as canopy; or sky, otherwise. The resulting canopy and sky values were used to compute plot-level CC. Finally, the photo-based estimates of CC using different photo sizes and classification thresholds were compared against the point-based estimates. A two-sample t-test was used to assess the significance of variation between the photo-based and point-based estimates of CC. Coefficient of variation (CV) was used to evaluate the extent of variation of the plot-level data from the mean CC. The efficiency of photographic methods for CC estimation was evaluated using R^2, relative root mean square difference (RMSD%), relative mean difference (MD%) and CV(%). See paper-IV for the equations.

3 Results and discussion

3.1 Feasibility of using UASs for forest monitoring in Ethiopia

Paper-I assessed the feasibility of UASs for forestry applications in Ethiopia. It identified different types of unmanned aerial vehicles (UAVs), which are the platforms of the UASs, suitable for various applications. Among the different types of UAVs, the fixed-wing and rotary-wing types were identified as suitable for forest inventory due to affordability. The rotary-wing UAVs have the advantage that they need small space for landing as compared to the fixed-wing types. This makes the rotary-wing UAVs preferable in intact forests where sufficient landing spaces are rarely available. Whereas the fixed-wing UAVs are more suited to applications that demand longer flight endurance. The fixed-wing UAVs have a simple structure, which makes them easy for maintenance (Klimkowska, et al., 2016).

Most of the civilian use UASs have inbuilt sensors that record the red, green and blue (RGB) light. In recent years, the possibility of integrating additional sensors of the red-edge, near-infrared and thermal infrared SBs and laser scanning systems has enhanced the efficiency of capturing additional data for multiple applications (Colomina and Molina, 2014; Zahawi et al., 2015). The red edge and near-infrared are better suited for assessing the spatial distribution of vegetation while the laser scanning systems help to study the vertical structure of forests.

The original purpose of UAS technologies was for military, patrolling international borders and governance (Budiyono, 2008; Callam, 2010; Muchiri and Kimathi, 2016). Through time, UASs have gained acceptance in other civilian fields like agriculture, forestry, disaster management, environmental monitoring and wildlife management among others (UNOCHA, 2014; Feng et al, 2015; Jeanneret and Rambaldi, 2016; Popescu et al., 2017). In forestry, they are used to assess forest dynamics, stand species composition, stand structure and disturbances. They have been used to study attributes of forests such as tree height, crown width, basal area, stem number, gross stock volume and AGB (Puliti et al., 2015; Zahawi et al., 2015; Banu et al., 2016; Goodbody et al., 2017; Hird et al., 2017; Torresan et al., 2017).

Advances in UAV platform design and sensor development offered many opportunities for a wider application of UASs. There is a growing interest in UASs due to the reduced size of the vehicles, affordability, low energy consumption, flexibility, options for a variety of sensors and the high spatial resolution data (Colomina and Molina, 2014; Christensen, 2015; Puliti et al., 2015; Banu et al., 2016; Gaitani, et al, 2017; Hird et al., 2017). UASs provide high spatial resolution images based on demand-based temporal patterns of data acquisition, which makes the technology very efficient. Data from UAS can also be used to calibrate coarse resolution data like satellite images. Thus, the UAS technology has a potential for supporting forestry and environmental monitoring.

Although to a limited extent, there have been experiences of using UASs in Ethiopia, particularly by development projects and aid agencies. Delivery of medical supplies in remote areas, security, railway construction projects, animal disease control and the film industry have been the major application areas of UASs in the country. Experiences across different countries revealed that the use of UASs has associated concerns, which need to be addressed through strict regulations to avoid misuse of the technology for risky missions like terror attacks and to protect any risk to the traditional aviation. Obviously, the concern with potential threats cannot be resolved by sidestepping the use of the technology. Instead, it is highly recommended that full-fledged regulations are formulated and enforced for successful use of the technology. Recently, the Ethiopian civil aviation authority enacted a regulation to import, assemble and operate UASs in Ethiopia (CAA, 2020). The enactment of the UAS regulation will foster the possibility of using UASs in diverse fields including forestry and environmental monitoring.

3.2 Manual image interpretation for forest area and CC estimation

The results in paper-II indicated that manual image interpretation is a useful technique for estimating forest area and CC at large scale level like at national or regional scale. This technique was efficient in terms of financial and time costs as compared to the FBSS techniques. In the current study, it was possible to record data for an area of 390 km^2 per hour on average. This amount of time is not sufficient even

to travel to the SP locations for an FBSS. Estimates of forest area and CC using the PS and REy images showed similarities consistently over the study sites, although there were marginal differences, in which case the estimates using REy images were smaller in most cases. The estimates using S2 images differed from the other two image types in most of the study sites, and the differences in mean forest area or CC estimates were much larger and statistically significant ($p < 0.01$) for sites with dense vegetation (i.e. sites B, D, E and G in Figure 1-II). There were insignificant differences among the image types in sites with low vegetation densities (i.e. sites A, C and F). In such situations, the S2 images that have relatively coarser spatial resolution than the PS and REy images would produce a reasonably comparable estimate of forest area or CC.

Comparison of CC by LULC classes for the three image types revealed that the estimates for forestland were significantly larger than that for the other LULC types with a magnitude of 0.57 from PS, 0.59 from REy, and 0.58 from the S2 images. The CC estimates were similar across the image types for homogenous surfaces like forest, cropland and grassland LULC types. Whereas, in heterogeneous LULC types like in settlements and other LULC classes in which different objects exist, coarser-resolution images tended to either overestimate or underestimate CC as compared with estimates from finer resolution images.

These variations in the results among the image types might not be related to the true value due to the absence of ground-truthing data. The estimates using PS and REy images were robust and capable of producing comparable results in biomes with different vegetation densities. This could be due to a relatively higher spatial resolution of the PS and REy images compared with the S2 ones. This is in agreement with the findings of previous studies that indicated an increase in overall accuracy with improvement in image resolution (Churches et al., 2014; Draksler, 2017). Another factor contributing to the differences could be the presence of more missing data in S2 that could reduce the number of observations and hence affect the quality of the estimates (Lohr, 2009). The revisit frequency also influences the data availability at cloudy locations. The more frequent revisit time of PS is highly favourable for REDD+ MRV, since 85% of the images used for interpretation were

acquired within one month (May 2017) while for REy and S2, only a maximum of 34% and 40% of the images were acquired within a single month, respectively. Generally, among the image types, the high-resolution PS images resulted in better precision. The results suggest that careful selection of satellite images is needed for estimating forest area and CC using visual interpretation. For low-density forest sites, the freely available S2 images may be safely used, whereas, for dense forest sites, higher resolution images such as PS and REy should be considered for a reliable estimation. Obviously, the choice may also depend on the purpose of the study and the availability of resources.

This study also evaluated how sample size affected the uncertainty of estimates from different image types. The results from bootstrap sampling showed an increase in SE with a decrease in sample size for both variables, regardless of site and image type. On average, the increase in SE when resampling with a sample size of 200 (instead of 228 sample observations) was less than 9% for both variables (i.e. forest area and CC) regardless of image type. Sample size of 150 generated average estimates with a SE inflation of less than 24% for all of the image types. Similarly, when the sample size was reduced to 100, the SE increased by almost 50%. The use of only 50 samples increased the SEs by more than 100% in all of the cases. In general, overall estimates using PS and REy images were less sensitive to the reduction of sample size for both forest area and CC.

When resources allocated for data collection are limited, it is important to apply appropriate sampling designs and use adequate sampling intensities (Jayaraman, 2000; Lenth, 2001; Böttcher et al., 2009; Falkowski et al., 2009). Such methods provide alternatives to obtain reliable estimates of forest area and CC at a lower cost of image procurement, especially for dense forests where low-resolution images have deficiencies, and the quality of information pays off. The findings of bootstrap sampling revealed that the precision of the estimates is sensitive to changes in the number of observations. Therefore, the decision to reduce sample size should strike a balance between cost and anticipated accuracy.

3.3 Enhancing AGB estimation using optical RS data

3.3.1 Relationship of image-derived variables with AGB

Statistical test for significance of correlation coefficients of the relationship of image-derived variables with AGB revealed moderate correlation (Schober et al., 2018). AGB had a moderate negative correlation with SB reflectance variables. Whereas it had moderate positive relationships with most SIs. It was revealed from the exploratory analysis that standard deviation of SIs (of S2 and PS) and texture variables (of PS) were also moderately correlated with AGB.

For the L8 and S2 data, SIs were less correlated with AGB as compared to the SB reflectance variables. Table 2 shows that from the SIs, NDMI had considerable relationship with AGB while ARVI, NDVI and SR have weaker correlations. The SBs were moderately related to AGB with correlation coefficients ranging from -0.38 (NIR of L8) to -0.49 (SWIR1 of S2). From the S2 variables, the standard deviation of the SIs (namely GLI, NDGI and VI) had relatively stronger positive associations with AGB. Similarly, for the PS variables, the mean of SBs of G, R and B showed the strongest relationship with AGB followed by that of VI and NDGI SIs. Image texture data of PS had also moderate relationships with AGB (Table 2).

Table 2. Correlation of image-derived variables from L8, S2 and PS images with aboveground biomass (AGB). See Table 1 for description of the SBs. NDMI, ARVI, NDVI, SR, GLI, NDGI, VI and ExGI are the normalized difference moisture index, atmospherically resistant vegetation index, normalized difference vegetation index, simple ratio, green leaf index, normalized difference green index, vegetation index and excessive green index, respectively. ASM, VAR and MEA are the angular second moment, grey-level co-occurrence matrix variance and mean texture variables, respectively. The notations for SBs and spectral indices (SIs) of all the image types are MMM_mean or MMM_std representing the mean and standard deviation of the variable MMM. For texture variables of PS, BnXXX_mean is the mean of XXX texture variable of band Bn where n =1, 2, 3, 4 for B, G, R, NIR, respectively. Similarly, BnXXX_std is the standard deviation of the texture variable as described above for the BnXXX_mean, except replacing 'mean' by 'std'.

L8		S2		PS	
Variable	**correlation**	**Variable**	**correlation**	**Variable**	**Correlation**
NDMI_mean	0.39***	GLI_std	0.44***	VI_mean	0.44***
ARVI_mean	0.27**	NDGI_std	0.43***	NDGI_mean	0.44***
NDVI_mean	0.23*	VI_std	0.43***	B4ASM_std	0.37***
SR_mean	0.19*	NDMI_mean	0.31***	B4ENE_std	0.35***
NIR_mean	-0.38***	NIR_mean	-0.42***	NIR_mean	-0.38***
B_mean	-0.41***	R_mean	-0.43***	B3VAR_mean	-0.39***
R_mean	-0.42***	B_mean	-0.46***	B2VAR_mean	-0.39***
G_mean	-0.45***	RE_mean	-0.48***	B1VAR_mean	-0.39***
SWIR1_mean	-0.48***	G_mean	-0.49***	B3MEA_mean	-0.40***
		SWIR1_mean	-0.49***	B2MEA_mean	-0.40***
		ExGI_mean	-0.51***	B1MEA_mean	-0.40***
				B_mean	-0.46***
				R_mean	-0.46***
				G_mean	-0.48***

* p-value < 0.05; ** p-value < 0.01; *** p-value < 0.001.

The observed moderate relationship of image-derived variables with AGB demonstrated the potential of optical RS data for AGB modelling. The negative correlation coefficients between SB reflectance and AGB are in line with the results of similar studies conducted in various forest types (Lorenzen and Jensen, 1988; Gizachew et al., 2016; Bao et al., 2019). This negative relationship could be explained by a shadow effect and large moisture contents within the complex forest stands where AGB is large (Lu et al., 2005; Prasad et al., 2009; Wang et al., 2016). The presence of scattered big trees in SPs with large AGB results in larger shadows than

the SPs with medium and small-sized trees that had lower moisture content and smaller AGB. The high moisture content and large shadows in SPs with big scattered trees had smaller reflectance values in the images. The biomass in these plots is very large. On the other hand, SPs with medium tree sizes had relatively larger spectral reflectance values while they had relatively smaller biomasses. This resulted in an inverse relationship between biomass and SB reflectance.

The positive relationship of most of the SIs with AGB found in this study is also following the patterns of previous research findings (Lorenzen and Jensen, 1988; Gizachew et al., 2016; Macedo et al., 2018). The standard deviation of some SIs had demonstrated remarkable potential to relate with AGB, which is in agreement with the results by Næsset et al. (2016) in Tanzania. The GLI, ExGI and NDGI SIs, which had limited usage for biomass studies, showed great potential for predicting AGB in this forest. Thus, an in-depth study is required to understand the potential of these SIs for AGB estimation in other forest types too.

Furthermore, inter-resolution comparison of SBs showed that the limited spectral properties of PS images might have restricted their potential to characterize AGB. We observed that the S2 data contain a range of SBs that were more sensitive to AGB than the PS data, which have a higher spatial resolution.

3.3.2 Variable selection for the AGB prediction models

Most of the image-derived variables have problem of intercorrelation (Wang et al., 2016; Lu et al., 2019), suggesting the importance of a careful screening of these variables for AGB modelling. Accordingly, variables with minimal intercorrelation were selected for the AGB prediction models for each image type. Therefore, for L8 data, the SWIR1 band reflectance had a stronger correlation with AGB than the other variables. The suitability of the SWIR1 SB for AGB estimation was in line with the results of other studies (Horler and Ahern, 1986; Roy and Ravan, 1996; Risdiyanto and Fakhrul, 2017). For green vegetation, the SWIR1 reflectance is controlled by the amount of water in the leaf biomass of the canopy. This could also be due to the low diffuse reflection of light at the SWIR1, and hence shadows are better contrasted. Low diffuse reflection is associated with distinct luminance of the leaf, background

objects and shadow, thereby enhancing the contrast among them. The presence of thick layers of fragmented tree canopy and shadows in SPs with large AGB yielded low reflectance in the SBs, including the SWIR1 band as portrayed with the negative coefficient in the selected models.

The S2 model had two independent variables (SWIR1 and standard deviation of GLI). Inclusion of the standard deviation of GLI in this model indicates the importance of this variable to capture spatial variation in the forest canopy structure since GLI can identify green leaves and stems from the background soil surface (Louhaichi et al., 2001). This variable could reflect the level of disturbance, terrain variation or presence of very big scattered trees in the natural forest.

For the PS data, all the SB reflectance variables demonstrated considerable potentials for AGB modelling. All the four SBs has a moderate correlation with AGB. However, their performances were not different from that of the corresponding SBs of the lower resolution S2 images despite their superior spatial resolution. The G SB had a stronger correlation than the other variables.

3.3.3 Selected AGB models by image type

Given the complex forest structure and topography in the study area, the L8 and PS models had equivalent performance and explained a considerable amount of variation in the FBSS AGB with R^2 of 29% and 27%, respectively. The calibration RMSEs of the L8 and PS models were 71.06% and 71.79%, respectively. This was comparable with the results of other studies conducted even in intermediate vegetation cover conditions where it is easier to get a stronger relationship between image data and AGB (Magnussen et al, 2019).

The S2 model had predictor variables of the SWIR1 band reflectance and standard deviation of GLI. It had the least AIC among the models (1385.06) and minimal overfitting problem with relative RMSEs of the model fit and validation of 64.87% and 67.12%, respectively (Table 3). Unlike the selected L8 and PS models, the S2 model explained a larger amount (about 41%) of the variability in AGB. Generally, the predictive power of the S2 model prevailed over that of the other models.

Table 3. Selected models and performance indicators for AGB estimation in the Degaga-Gambo forest using independent variables from L8, S2 and PS images.

Image	Model [c]	AIC	Calibration	Validation	Prediction
			RMSE (%)	RMSE (%)	Correlation [d]
L8	$\widehat{AGB} = \exp(6.9967 - 16.1492 \times SWIR1)$	1403.31	71.06	73.23	0.54
S2	$\widehat{AGB} = \exp(6.1310 - 11.4874 \times SWIR1 + 12.7865 \times GLI\_std)$	1385.06	64.87	67.12	0.64
PS	$\widehat{AGB} = \exp(11.7696 - 75.2766 \times G)$	1406.00	71.79	75.17	0.52

[c] *std refer to the area-weighted standard deviation of the image-derived variables within the grid cells.*

[d] *Pearson's correlation coefficient between ground reference and model-predicted values of AGB for the models in each image type. Square of the coefficients is the same as the model R^2.*

3.3.4 Model-assisted estimation and mapping of AGB

Table 4 shows the estimated mean AGB, estimates of mean deviation, SE of the mean AGB estimates and relative efficiency (REf) for the selected models. The model-assisted estimates of mean AGB were 179.67, 177.79 and 184.27 Mg ha^{-1} using the L8, S2 and PS models, respectively. These estimates were within 95% confidence interval of the pure FBSS AGB estimate (i.e. 155.15 - 213.76 Mg ha^{-1}). The estimated mean AGB using the PS model was closer to the field-estimated mean AGB (i.e. 184.35 Mg ha^{-1}) than the estimates using the other models were. The estimated mean AGB using the L8 and PS models had the largest and smallest MDs, respectively. The PS model-assisted estimate was relatively less precise followed by the L8 model. The estimates revealed that the L8 and PS models resulted in equivalent estimation efficiencies (i.e., 1.40 and 1.37, respectively). Among the three models, the S2 model-assisted estimation was the most precise with a SE of 11.40 Mg ha^{-1}. As a result, REf of the S2 model-assisted estimation (i.e. 1.68) was greater than what was obtained using the other models.

Table 4. Estimated mean AGB (Mg ha^{-1}), mean deviation (MD) in Mg ha^{-1}, standard error (SE) of the mean (Mg ha^{-1}) and relative efficiency (REf) of the model-assisted estimation.

Estimator data source	Estimated mean AGB	Estimated MD	SE	REf
Model-assisted; L8-model	179.67	1.71	12.49	1.40
Model-assisted; S2-model	177.79	0.62	11.40	1.68
Model-assisted; PS-model	184.27	-0.13	12.62	1.37
Field-based	184.35	---	14.79	---

The spatial patterns of AGB prediction maps, which are shown as Figure 4 in Paper-III, indicated the spatial consistency of predictions across all the models (Kleinn, 2003).

The REf when using the L8 model in this study was slightly larger than the findings by Næsset et al. (2016) for the Miombo woodlands in Tanzania using the global Landsat products. The selected S2 model contributed more strongly to improving estimation precision than the L8 and PS models did. This improvement in estimation efficiency is equivalent to reducing the number of field SPs required to attain the same precision to approximately 59% of the sample size required for a pure FBSS. The REf when using the S2 model was smaller than that of the REy images used for AGB estimation in the Miombo woodlands in Tanzania (Næsset et al., 2016). This might be attributed to the heterogeneity of the forest in the current study or the interaction effect of forest types and spatial resolution of the images. Besides, Næsset et al. (2016) commented that the small study area covered in their study might have resulted in overly optimistic results. However, the results in the current study were similar to the findings by Navarro et al. (2019) who studied AGB of mangrove plantations using S2 images in Senegal. Therefore, the results of the current study are reasonable given the heterogeneity of the terrain and forest conditions, which influence the relationship of image data and AGB (Roy and Ravan, 1996).

Although there might be some variations between the models in this regard, they were able to predict only to a limited range of the ground reference AGB. This shows a saturation problem for which canopy shadow is mainly responsible in the SPs with large AGB (Lu et al., 2005). Therefore, future efforts should focus on synchronizing

other auxiliary variables like canopy density and canopy height from airborne laser scanning data with the identified variables to improve model performance.

The understory vegetation biomass, which was not accounted for in the FBSS AGB, could have had a major influence on the image-derived variables. This might partly explain the moderate improvement in the precision of the model-assisted estimates compared to the pure FBSS estimate. The effect of understory vegetation on the relationship between image-derived variables and AGB was more obvious in the high-resolution PS images. A greater compliance of the RS data with AGB would happen for homogeneous forests in which the understory vegetation cover is minimal and the forest CC is uniform. Therefore, further studies are needed in pure plantation forests to attain an optimum efficiency of RS data for AGB estimation beyond the ones we got in this study.

Generally, the selected models of each satellite data source based on the identified variables improved AGB estimations, which were reinforced by other research findings. The freely available S2 data were particularly useful indicating that they possess sensible spectral and spatial properties for AGB estimation.

3.4 Digital photography for forest CC estimation

3.4.1 Photo-based methods for CC estimation

The photo-based estimates of CC rely on correct segmentation of the photo pixel values into canopy and sky segments. For this purpose, the determination of an appropriate threshold for segmentation is vital. Otsu thresholding offered objective thresholds for segmenting the pixel values of the digital photographs.

This study was conducted in a dense CC condition where the minimum and mean CC estimates using the point-based method were 33.9% and 80.6%, respectively (Table 5). The canopy fraction estimates using the photo-based method were compared with the point-based data to identify the appropriate photo processing techniques for estimating CC. The results indicated that the mean canopy fraction estimates using digital photos increased with photo size, ranging from 64.3 to 77.9% (Table 5). This pattern is in line with previous studies that used digital photos to estimate CC

(Korhonen et al., 2006; Bianchi et al., 2017). Despite the increase in the mean canopy fraction with an increase in photo size, all of the photo-based estimates were smaller than the point-based estimates of CC. Besides, the variance of the estimates increased with photo size from 269.9 for the smallest photo to 721.5 for the biggest photo. The canopy fraction estimates for all the photo sizes were both biased and less precise. Therefore, the canopy fractions were thresholded to get logical estimates of CC. Introduction of the threshold variable in the photo processing methods enabled estimation of CC with a minimum deviation from the point-based data. The CC estimates based on the threshold classes (regardless of the photo sizes) indicated that the estimates decreased by more than 50% (from 85.32 to 41.62%) with the increase in thresholds (from 10 to 70%) while their variance increased (from 182.5 to 272.6). When photo size is not taken into consideration, the CC estimates at 10 and 20% thresholds were slightly greater than the point-based CC. This could be because the photos that had a significant amount of canopy gaps were classified as canopy due to the use of smaller thresholds.

Table 5. The plot-level minimum, maximum, mean, and standard deviation (SD) of the canopy cover (CC, in %) estimates of the photo-based methods using different photo sizes and thresholds and that of the point-based method. Analysis of variance of the effects of the photo size, classification threshold, and their interactions is also shown for the photo-based method.

Variable	Factor	Minimum CC	Maximum CC	Mean CC	SD	F-score [f]	p-value
Photo size [e] (pixels)	100	13.8	99.1	64.3	16.4	56.2	<0.001
	200	8.3	99.1	65.4	17.4		
	300	6.4	100.0	66.2	18.2		
	400	2.8	100.0	66.8	18.8		
	500	2.8	100.0	67.2	19.4		
	1000	0.9	100.0	69.3	22.0		
	2000	0.0	100.0	74.0	25.6		
	3000	0.0	100.0	77.9	26.9		
Threshold of classification (%)	10	36.7	100.0	85.3	13.5	721.8	<0.001
	20	35.8	100.0	82.2	14.2		
	30	34.9	100.0	78.3	14.9		
	40	33.0	100.0	73.4	15.7		
	50	24.8	100.0	66.0	16.5		
	60	1.8	100.0	55.4	17.4		
	70	0.0	86.2	41.6	16.5		
Interactions [g]	---			---	---	8.0	< 0.001
Point-based estimation	---	33.9	100.0	80.6	13.4	---	---

[e] *photo size refers to the length of one side of the square-shaped photos (in number of pixels).*

[f] *significant at 95% confidence level.*

[g] *details of estimated CC for the interaction of photo size and threshold variables are presented in Table 6.*

The effect of overestimation increased with an increase in the size of the photos (Table 6). Results of the CC estimates from the full-size photos analysed with different thresholds had extreme values, indicating the huge uncertainty associated with the use of the entire photo for CC estimation. This could be attributed to the distortions

of tree canopy positions and gaps and their geometries towards the edge of the photos. The results revealed that the CC estimates using the central slices of the photos were more precise indicating the higher certainty associated with the use of these portions of the photos for estimating CC. Only a small central part of the vertical photo (less than 3% of the size of the original photo) was useful for CC estimation comparable to the point-based data. At this central portion of the photos, the photo elements are relatively free from distortion and had a strong coherence with the point-based data. The geometry of canopy openings were relatively preserved and resulted in a minimal bias in the CC estimates. This result was supported by other research findings that recommended a narrow-angle of view to obtain a reliable CC data using photographic techniques (Korhonen et al., 2006; Chianucci, 2016). The photo-based CC estimates that strongly correlated with the point-based estimates came from only a few combinations of the photo sizes and thresholds. Photos with sizes of 300 × 300 pixels, 400 × 400 pixels and 500 × 500 pixels (which represented 1, 1.8 and 2.8% of the original photo size) offered better estimates of CC at 10% and 20% thresholds. The suitability of the 10% and 20% thresholds could be attributed to the fact that all the SPs had large CC. Photo sizes smaller than 300 × 300 pixels underestimated CC for all the thresholds. Hence, very small photo sizes (<1% of the full photo size) could not provide reliable estimates of CC. This may be attributed to the effect of solar illumination that exaggerated canopy gap fraction estimates, which is a common problem mentioned in previous studies (Rich, 1990).

Table 6. Effect of photo sizes and thresholds on CC estimates from digital photos.

Photo size (number of pixels)	Threshold (%)						
	10	**20**	**30**	**40**	**50**	**60**	**70**
100 × 100	76.86	73.97	70.43	66.50	61.20	54.50	46.55
200 × 200	78.93	76.01	72.61	68.11	62.14	54.76	45.48
300 × 300	80.43*	77.27*	73.77	69.30	63.04	54.75	44.48
400 × 400	81.49*	78.57*	74.83	70.44	63.84	54.75	43.57
500 × 500	82.48*	79.56*	75.72	71.04	64.12	54.57	42.87
1000 × 1000	87.99	83.65	79.56**	73.82	65.99	54.29	39.80
2000 × 2000	95.91	92.04	87.14	80.70**	70.96	55.87	35.41
3000 × 3000	98.47	96.16	92.67	86.89	76.63	59.41	34.78

* *These estimates are very close to the point-based mean CC (i.e., 80.55%) at the thresholds of CC for forest definition by the FAO and Ethiopia (FAO, 2000; FDRE, 2016). Their MD% were not significant. As a result, the combinations of photo sizes and thresholds that gave these estimates were more reliable than the other options.*

** *These estimates are also close to the point-based estimates but the thresholds used for these estimations are beyond the accepted thresholds in the forest definitions mentioned above. Although the estimates are close to the point-based data, they had larger variances compared with the other (i.e., the above) group. Therefore, these were not the focus of discussion.*

3.4.2 Evaluation of the photo-based estimates of CC

Figure 4 shows the patterns of RMSD% and MD% of the photo-based estimates of CC from the point-based estimate for all the possible combinations of the photo sizes and thresholds. These patterns dictated the selection of the useful parameters of photo processing for deriving CC estimates. The results indicated that combinations of the three photo sizes (i.e., 300 × 300 pixels, 400 × 400 pixels and 500 × 500 pixels) with 10% and 20% thresholds yielded the smallest deviation in terms of both RMSD% and MD% criteria.

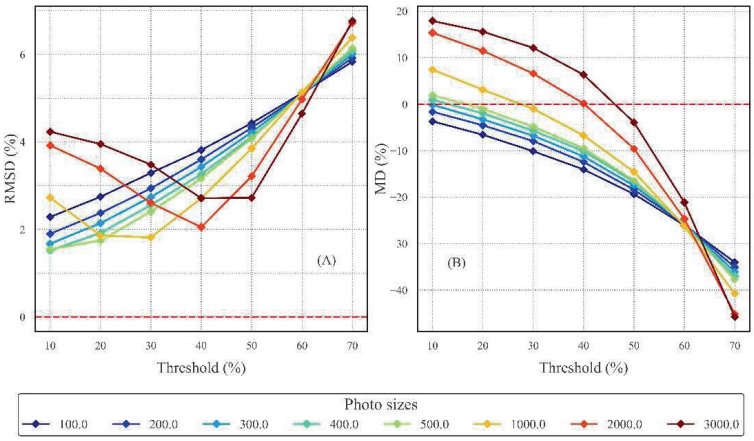

Figure 4. Deviation of the photo-based estimates from the point-based data (A) RMSD% (relative root mean square difference) and (B) MD% (relative mean difference) of the photo-based CC data using the different photo sizes (different colours; see legend) and thresholds.

Results of correlation analysis (Pearson's correlation test; p-value < 0.05 for all) indicated that the photo-based estimates at 10% threshold had stronger correlations with the point-based data (i.e., 0.95 - 0.96 for the photo sizes of 300 × 300 pixels, and 400 × 400 pixels and 500 × 500 pixels). The estimates using the same respective photo sizes at 20% threshold had correlation coefficients of 0.92, 0.94 and 0.95 with the point-based data. The observed strong linear relationship between photo-based and point-based estimates of CC indicates the huge potential that digital photography can offer as a quick and accurate method for estimating CC. Due to the flexibility in the methods, estimation precision was improved by selecting distortion-free parts of the photos and appropriate thresholds. None of the MD% for the optimum photo processing variables was statistically different from zero at a 5% significance level.

The CV for the 500 × 500 pixels photo size with a 10% threshold was the smallest of all the possible combinations. For the identified optimum photo sizes, the estimates of CC with a 10% threshold had a relatively smaller CV than the 20% threshold equivalents and even that of the point-based data (CVs less than 16.15% for all the three photo sizes). This might be due to the objective sampling and data processing

in the photo-based methods. The results of MD% estimates followed a similar pattern (Table 7). The MD% of the CC estimates of all the identified optimum combinations of the photo size and threshold were not significantly different from zero at 95% confidence level. The CC estimates for the photo size of 300 × 300 pixels at the 10% threshold resulted in the least MD% (-0.13).

Table 7. The estimates of mean, SD, and coefficient of variation (CV) of the photo-based CC using the selected photo sizes and thresholds and their relative mean differences (MD%) from the point-based data. The unit of all the estimators is percentage.

Combinations of thresholds and photo size	Mean CC	SD	CV	MD% [h]
10% threshold and 300 × 300 pixels	80.4	13.0	16.1	-0.1
10% threshold and 400 × 400 pixels	81.5	12.7	15.6	0.9
10% threshold and 500 × 500 pixels	82.5	12.6	15.3	1.9
20% threshold and 300 × 300 pixels	77.3	13.1	17.0	-3.3
20% threshold and 400 × 400 pixels	78.6	13.0	16.6	-2.0
20% threshold and 500 × 500 pixels	79.6	13.1	16.5	-1.0
Point-based data	80.6	13.5	16.8	---

[h] *the MD% were insignificant at 95% level of confidence.*

4 Discussion

The research work of the four papers in this thesis has shown that remote sensing played a vital role in supporting the provision of information in the dry Afromontane forest, which is one of the tropical forest types. This forest is among the major forest types that have a huge potential for REDD+ programs. However, the forest is also among the least-studied and data-scarce forest types. Therefore, integration of RS data with FBSS is needed for enhancing resource assessment and monitoring in this site. Forest area, CC and biomass are few of the major forest variables worth accurate estimation, particularly, for REDD+ MRV. An accurate estimation of forest area is a basic information in land resources assessment that helps quantify the resource stock. Understanding the location and size of the resource is important for planning FBSS and for analysing the total resource stock in that population. An accurate estimation of forest CC plays multiple roles since CC is an important attribute of forests. Similarly, there is a growing need for accurate AGB estimation due to its significance as a source of renewable energy, pulp and paper, construction materials, and for computing the carbon stock sequestered in the living biomass of trees, to mention some.

The research results in this thesis tried to illustrate the importance of remote sensing methods and RS data for supporting forest assessment and monitoring in a tropical forest type. Remote sensing offers opportunities for forest monitoring through provision of auxiliary data. Besides acting as complements for ground sampling methods, sampling strategies based on RS data are used in computing some useful forest variables for which wall-to-wall assessment is a challenging task. Sampling is particularly useful for very high-resolution RS data obtained from commercial sources. Whereas freely available medium resolution images are used as complements to FBSS data for a wall-to-wall prediction.

The gain in estimation efficiency and feasibility of the methods are the main attributes for evaluating the use of RS data in forest monitoring. RS data of different spatial resolutions were effectively used in this work to estimate major forest variables at

different spatial scales. The growing availability of high-resolution data from PS and REy satellites offered opportunities for improving forest information through large-scale forest surveys. This was in agreement with the study results by Puliti et al. (2018), which utilized data from UASs and S2 for forest growing stock volume estimation through hierarchical model-based inference. Both the PS and REy images used in the current study provided a more precise estimation of forest area and canopy cover using manual image interpretation. The PS data had also significant contribution for AGB estimation, which has a direct association with the REDD+ MRV initiatives being implemented to combat the changing climate. Improvements in AGB estimation have significant influence on quantifying the amount of greenhouse gas emission reduction, which increases the confidence that the REDD+ projects can have for tackling the global climate change challenge. The enhanced estimation efficiencies can help the parties involved in the REDD+ projects to get a fair share of benefits. Therefore, REDD+ projects can make use of the data and methods used in this thesis for forest monitoring in resourceful territories, which could otherwise be hampered by cost limitations when mapping extensive forest areas with limited resource stocks. The results also indicated that data from satellites providing low and medium-resolution images (e.g. L8 and S2), which are freely available, could be used for wall-to-wall prediction and mapping of forest resources. These data improved estimation performance, in terms of precision, particularly of AGB estimation in the Degaga-Gambo forest. Therefore, integration of these freely available data, particularly the S2 data, in the national forest inventories is highly recommended since the estimates using only the FBSS had limited precision (Watson et al., 2013). This study did not entail additional technical justification for the use of the commercial PS data over the freely available S2 data for AGB estimation. However, the use of the PS and the REy images for forest area and CC was considerably advantageous in dense forest conditions were the precision of estimates could justify the additional costs.

Although AGB models using the L8, S2 and PS data contributed to improving AGB estimation in the study forest, the performance of the S2-model was better than the other two types. The selected AGB models from the high-resolution (PS) and low-resolution (L8) data had similar performances in terms of the gain in estimation precision. The S2 images have additional spectral bands that helped AGB estimation

more than the contribution of the high spatial resolution of the PS images. Although the comparison was not exhaustive since the systems have differences in spectral properties, the study results suggest that AGB is more influenced by spectral resolution than spatial resolution. An in-depth investigation is thus required to examine the effect of spatial and spectral resolution of image data on the efficiency of AGB estimation.

The study has also indicated that the use of digital photography played a vital role in forest CC estimation. It provided more precise CC information than the point-based method did. The possibility of retaining archival data for change detection and the flexibility of the analysis methods are some of the advantages of the photo-based approach for CC estimation. The study suggested that further research related to the efficient use of digital photography for CC estimation is needed. The multiple benefits of CC information in the field of ecological monitoring, agroforestry management, silviculture, erosion control, and others inspire in-depth research to advance the methods of digital photography for efficient estimation of forest CC. Studies geared towards site and species specificity may provide more dependable information. The number of photos required for optimising different aspects of efficiency needs to be investigated. The results of other techniques of photo processing need to be compared with the current results. Such studies will enhance the importance of digital photography for producing reliable CC information.

Generally, the study results will benefit environmental management, ecological protection, natural resources management and initiatives on combating the global climate change. These findings can be used to support the REDD+ MRV programs in Ethiopia and other countries of a similar situation. Furthermore, the study results and the methods used in this thesis can be used as points of reference for further research in the field.

5 Identified gaps for future study

This thesis explored the various data types and methods for forest area, biomass and CC assessment. In paper-I, it was indicated that the suitability of UASs for forest resources monitoring requires conducting case studies. There is a need for future efforts to study the importance of UAS data for specific forest attributes including crown cover, biomass, forest density and tree height.

In paper-II, the use of manual image interpretation for large-scale forest area and CC assessment did not have ground-truth data to make inference on the accuracies. Future research is needed to verify the results with ground truth data. Moreover, two persons did the image interpretation; hence, the comparison between interpreters was not possible. Therefore, future research initiatives should be designed to include the error assessment due to subjectivity. The effect of season on image selection for manual interpretation should also be explicitly evaluated.

In paper-III, AGB assessment relied on optical RS data. Due to the rugged topographic setting and complex forest structure, a synergy of other RS data like LiDAR data could enhance the model performance beyond what has been achieved. Furthermore, the current methods could also reveal better performance for plantation forests where the forest structure is not as such heterogeneous.

In paper-IV, which dealt with the use of photographic methods for CC estimation, a more accurate reference data could be used to make a profound conclusion about the reliability of the estimates. Further research is also needed to determine the optimum sample size (number of photos) required per plot.

6 Conclusion

The first paper explored existing literature about the potential uses of UASs in the forestry sector in Ethiopia. There is ample evidence on the possible uses of UASs in forestry. Those lessons can be adopted and customized to the Ethiopian conditions and used to supplement the existing FBSS methods. However, due care should be taken into account when using UASs in rough topographic settings as the identified feasible systems have very limited range of flight altitude. Besides, experiences indicated that UAS operation guidelines and regulations should be set explicitly so that security is not threatened.

In paper-II, visual image interpretation was applied to evaluate the use of PS, REy, and S2 satellite images for forest area and CC estimation. The study results showed that PS and REy images produced similar estimates of both variables for all of the study sites and LULC classes. The S2 image estimates varied significantly from the two other types of images in study sites with relatively denser forest cover but resulted in similar estimates in sites with less dense forests. In visual image interpretation, very high-resolution images should be given priority. In case of using expensive and very high-resolution images, a sampling approach could reduce the overall costs compared with the wall-to-wall acquisitions. Sample size determination depends on the balance between inventory costs and the required level of precision.

In paper-III, the variable exploratory assessment identified important image-derived variables for AGB estimation in the dry Afromontane forest, including GLI, ExGI and NDGI that were seldom used for AGB modelling. A detailed examination of the importance of these variables for AGB assessment in various forest conditions is recommended. The simple models selected in this study for each image type enhanced AGB estimation. Of the variables used in the models, the SWIR1 band reflectance, which lacks in the PS data, was a useful variable of the L8 and S2 models in this forest type. The study suggested that the additional spectral information of L8 and S2 images was more determinant of AGB estimation than the higher spatial resolution of the PS images. The remote sensing-assisted estimation techniques used

in this study complemented the FBSS estimates of AGB by improving precision. The method can be used to improve the quality of estimates obtained from limited sample sizes used in forest inventories in many developing countries.

In paper-IV, the study results indicated that the use of the central less distorted sections of digital photos for CC estimation demands setting a reasonable threshold for classifying the canopy fractions into canopy and sky. For dense forests like the ones in this study area, 1 – 3% of the central part of the photo and 10% or 20% thresholds resulted in a strong relationship with the point-based data. The photo-based method with these photo sizes and thresholds provided a more precise CC than the point-based method. For the photo-based method to be effective, narrow-angle camera lenses are recommended for capturing relevant canopy photos. Further research is needed to identify suitable focal length ranges for a more efficient assessment of CC in different forest density conditions. The methods of CC estimation used in this study could be relevant for supporting silvicultural management in tropical species-rich forests where light competition is severe. It can also provide useful information like availability of adequate shade trees for agro-forestry systems like the traditional forest-coffee production practices. This method can contribute to advancing the methods of CC estimation in different forest types.

By and large, the selection of methods for estimation of forest attributes should depend on the purpose, cost, anticipated accuracy and workload. Furthermore, technical training and experience sharing are needed for using most of these methods. Therefore, the higher education institutions should incorporate such technical contents into their academic curricula. They should also design short-term refresher courses on these topics for supporting the capacity of experts such that national inventories will be more efficient.

References

Adame-Campos, R.L.; Ghilardi, A.; Gao, Y.; Paneque-Gálvez, J. and Mas, J.F. 2019. Variables selection for aboveground biomass estimations using satellite data: a comparison between relative importance approach and stepwise Akaike's information criterion. *ISPRS Int. J. Geoinf., 8*(6), p.245, https://doi.org/10.3390/ijgi8060245.

Anderson, J.W. 1998. *The Kyoto Protocol on Climate Change*; Resources for the Future: Washington DC, USA; pp. 1–21. Available online: https://media.rff.org/documents/RFF-RPT-kyotoprot.pdf (accessed on 17 September 2019).

Asrat, Z.; Eid, T.; Gobakken, T. and Negash, M. 2020. Aboveground tree biomass prediction options for the Dry Afromontane forests in south-central Ethiopia. *For. Ecol. Manag., 473*, pp.1-14, https://doi.org/10.1016/j.foreco.2020.118335.

Banu, T.P.; Borlea, G.F. and Banu, C. 2016. The use of drones in forestry. *J. Environ. Sci. Eng. B*, *5*(11), pp.557-562, https://doi.org/10.17265/2162-5263/2016.11.007.

Bao, N.; Li, W.; Gu, X. and Liu, Y. 2019. Biomass Estimation for Semiarid Vegetation and Mine Rehabilitation Using Worldview-3 and Sentinel-1 SAR Imagery. *Remote Sens., 11*, pp.1-20, https://doi.org/10.3390/rs11232855.

Bianchi, S.; Cahalan, C.; Hale, S. and Gibbons, J.M. 2017. Rapid assessment of forest canopy and light regime using smartphone hemispherical photography. *Ecol. Evol., 7*(24), pp.10556-10566, https://doi.org/10.1002/ece3.3567.

Bonan, G.B. 2008. Forests and climate change: Forcings, feedbacks, and the climate benefits of forests. *Science*, *320*, pp.1444–1449, http://dx.doi.org/10.1126/science.1155121.

Böttcher, H.; Eisbrenner, K.; Fritz, S.; Kindermann, G.; Kraxner, F.; McCallum, I. and Obersteiner, M. 2009. An assessment of monitoring requirements and costs of 'reduced emissions from deforestation and degradation'. *Carbon Balanc. Manag., 4(1)*, pp.1-14, https://doi.org/10.1186/1750-0680-4-7.

Brown, L.H. 1969. Observations on the status, habitat and behaviour of the mountain nyala (*Tragelaphus buxtoni*) in Ethiopia. *Mammalia, 33*(4), pp.545-597, http://dx.doi.org/10.1515/mamm.1969.33.4.545.

Budiyono, A. 2008. Advances in unmanned aerial vehicles technologies. In *International symposium on intelligent unmanned system* (pp.1-13).

CAA (Civil Aviation Authority): starts issuing drone import license (2020, August 29). The Reporter Ethiopia. Retrieved from: https://www.thereporterethiopia.com/article/civil-aviation-authority-starts-issuing-drone-import-license (accessed on 03 Sept. 2020).

Callam, A. 2010. Drone wars: Armed unmanned aerial vehicles. *Int. Affairs Review, 18* (3)**.**

Chen, Q.; Laurin, G.V. and Valentini, R. 2015. Uncertainty of remotely sensed aboveground biomass over an African tropical forest: Propagating errors from trees to plots to pixels. *Remote Sens. Environ., 160*, pp.134-143, https://doi.org/10.1016/j.rse.2015.01.009.

Chianucci, F. 2016. A note on estimating canopy cover from digital cover and hemispherical photography. *Silva Fenn., 50*(1), pp.1-10, https://doi.org/10.14214/sf.1518.

Christensen, B.R., 2015. Use of UAV or remotely piloted aircraft and forward-looking infrared in forest, rural and wildland fire management: evaluation using simple economic analysis. *N. Z. J. For. Sci., 45*(1), pp.1-9, https://doi.org/10.1186/s40490-015-0044-9.

Churches, C.E.; Wampler, P.J.; Sun, W. and Smith, A.J. 2014. Evaluation of forest cover estimates for Haiti using supervised classification of Landsat data. *Int. J. Appl. Earth Obs. Geoinf., 30*, pp.203–216, https://doi.org/10.1016/j.jag.2014.01.020.

Colomina, I. and Molina, P. 2014. Unmanned aerial systems for photogrammetry and remote sensing: A review. *ISPRS J. Photogramm. Remote Sens., 92,* pp.79-97, https://doi.org/10.1016/j.isprsjprs.2014.02.013.

Ćosović, M.; Bugalho, M.N.; Thom, D. and Borges, J.G. 2020. Stand structural characteristics are the most practical biodiversity indicators for forest management planning in Europe. *Forests*, *11*(3), p.343, https://doi.org/10.3390/f11030343.

CRGE (Climate-Resilient Green Economy). 2011. *Ethiopia's Climate-Resilient Green Economy: Green Economy Strategy*. Federal Democratic Republic of Ethiopia. Available online: https://www.oneplanetnetwork.org/resource/ethiopias-climate-resilient-green-economy-strategy (accessed on 8 November 2020).

Draksler, A. 2017. The effect of satellite image resolution and minimum mapping unit on the accuracy of forest cover maps; Technische Universit¨at M¨unchen: Munich, Germany.

Duncanson, L.; Rourke, O. and Dubayah, R. 2015. Small sample sizes yield biased allometric equations in temperate forests. *Sci. Rep., 5*, pp.1-13, https://doi.org/10.1038/srep17153.

Duriaux, J.Y. and Baudron, F. 2016. Understanding people and forest interrelations along an intensification gradient in Arsi-Negele, Ethiopia. In *Agrarian Change in Tropical Landscapes*; Deakin, L.; Kshatriya, M. and Sunderland, T. (Eds); Center for International Forestry Research (CIFOR): Bogor, Indonesia, pp.14–53.

ESA (European Space Agency) - Copernicus Open Access Hub. Available online: https://scihub.copernicus.eu/dhus/#/home (accessed on 23 August 2019).

Evangelista, P.; Swartzinski, P. and Waltermire, R. 2007. A profile of the mountain nyala (*Tragelaphus buxtoni*). *African Indaba, 5*(2), pp.1-47; special report.

Falkowski, M.J.; Wulder, M.A.; White, J.C. and Gillis, M.D. 2009. Supporting large-area, sample-based forest inventories with very high spatial resolution satellite imagery. *Prog. Phys. Geogr., 33*(3), pp.403-423, https://doi.org/10.1177/0309133309342643.

FAO (Food and Agricultural Organization of the United Nations). 2010. Global Forest Resources Assessment. FAO forestry paper No. 163, Rome, Italy. Available online: http://www.fao.org/3/i1757e/i1757e.pdf (accessed on 06 September 2020).

FAO and UNEP. 2020. The State of the World's Forests 2020. Forests, biodiversity and people. Rome, Italy. Available online: https://doi.org/10.4060/ca8642en (accessed on 21 July 2020).

FDRE (Federal Democratic Republic of Ethiopia). 2015. Ethiopia's Second National Communication to the United Nations Framework Convention on Climate Change. Addis Ababa, Ethiopia. Available online: https://unfccc.int/resource/docs/natc/ethnc2.pdf (accessed on 08 November 2020).

FDRE (Federal Democratic Republic of Ethiopia). 2017. Ethiopia's Forest Reference Level Submission to the UNFCCC. Available online: https://redd.unfccc.int/files/ethiopia_frel_3.2_final_modified_submission.pdf (accessed on 03 August 2020).

FDRE (Federal Democratic Republic of Ethiopia). 2018. National REDD+ Strategy (2018-2030). Ministry of Environment, Forest and Climate Change, National REDD+ Secretariat. Available online: https://www.forestcarbonpartnership.org/system/files/documents/Ethiopia%20REDD%20Strategy_June%2025%20%202018.pdf (accessed on 07 November 2020).

Feng, Q.; Liu, J. and Gong, J. 2015. Urban flood mapping based on unmanned aerial vehicle remote sensing and random forest classifier - a case of Yuyao, China. *Water, 7*(4), pp.1437-1455, https://doi.org/10.3390/w7041437.

Friis, I.; Demissew, S. and Van Breugel, P. 2010. *Atlas of the potential vegetation of Ethiopia*. The Royal Danish Academy of Science and Letters, Volume 58: Copenhagen, Denmark.

Gaitani, N.; Burud, I.; Thiis, T. and Santamouris, M. 2017. High-resolution spectral mapping of urban thermal properties with Unmanned Aerial Vehicles. *Build. Environ., 121*, pp.215-224, https://doi.org/10.1016/j.buildenv.2017.05.027.

Gibbs, H.K.; Brown, S.; Niles, J.O. and Foley, J.A. 2007. Monitoring and estimating tropical forest carbon stocks: making REDD a reality. *Environ. Res. Lett., 2*(4), pp.1-13, http://dx.doi.org/10.1088/1748-9326/2/4/045023.

Gibbs, D.; Harris, N. and Seymour, F. (2018, October 04). By the Numbers: The Value of Tropical Forests in the Climate Change Equation. World Resources Institute. https://www.wri.org/blog/2018/10/numbers-value-tropical-forests-climate-change-equation (accessed on 24 September 2020).

Gizachew, B.; Solberg, S.; Naesset, E.; Gobakken, T.; Bollandsas, O.M.; Breidenbach, J.; Zahabu, E. and Mauya, E.W. 2016. Mapping and estimating the total living biomass and carbon in low-biomass woodlands using Landsat 8 CDR data. *Carbon Balance Manag*., *11*, pp.1–14, https://doi.org/10.1186/s13021-016-0055-8.

Global Forest Watch. Available online: https://www.globalforestwatch.org/dashboards/country/ETH/ (accessed on 06 September 2020).

Goodbody, T.R.; Coops, N.C.; Marshall, P.L.; Tompalski, P. and Crawford, P. 2017. Unmanned aerial systems for precision forest inventory purposes: A review and case study. *For. Chron., 93*(1), pp.71-81, https://doi.org/10.5558/tfc2017-012.

Haglöf Company Group. Available online: http://www.haglofsweden.com/index.php/en/products/instruments/height/541-the-vertex-laser-geo-all-you-need-in-a-rangefinder-hypsometer (accessed on 12 November 2019).

Henry, M.; Besnard, A.; Asante, W.A.; Eshun, J.; Adu-Bredu, S.; Valentini, R.; Bernoux, M. and Saint-André, L. 2010. Wood density, phytomass variations within and among trees, and allometric equations in a tropical rainforest of Africa. *For. Ecol. Manag., 260*, pp.1375–1388, https://doi.org/10.1016/j.foreco.2010.07.040.

Hird, J.N.; Montaghi, A.; McDermid, G.J.; Kariyeva, J.; Moorman, B.J.; Nielsen S.E. and McIntosh, A.C.S. 2017. Use of unmanned aerial vehicles for monitoring recovery of forest vegetation on petroleum well sites. *Remote Sens., 9*(5), pp.1-20, https://doi.org/10.3390/rs9050413.

Horler, D.N.H. and Ahern, F.J. 1986. Forestry information content of Thematic Mapper data. *Int. J. Remote Sens., 7*, pp. 405–428, https://doi.org/10.1080/01431168608954695.

Jayaraman, K. 2000. *A Statistical Manual for Forestry Research*, FORSPA. Available online: http://www.fao.org/3/a-x6831e.pdf (accessed on 10 November 2017).

Jeanneret, C. and Rambaldi, G. 2016. Drone governance: *a scan of policies, laws and regulations governing the use of unmanned aerial vehicles (UAV) in 79 countries*. CTA Working Paper.

Kebede, B. and Soromessa, T. 2018. Allometric equations for aboveground biomass estimation of *Olea europaea* L. subsp. cuspidatain Mana Angetu Forest. *Ecosyst. Health Sustain., 4*, pp. 1-12, https://doi.org/10.1080/20964129.2018.1433951.

Kleinn, C. 2003. New technologies and methodologies for national forest inventories. *UNASYLVA-FAO,* pp.10-15. Available online: http://www.fao.org/tempref/docrep/fao/005/y4001e/y4001e01.pdf (accessed on 20 November 2020).

Klimkowska, A.; Lee, I. and Choi, K. 2016. Possibilities of UAS for maritime monitoring. *Int. Arch. Photogramm. Remote Sens. Spat. Inf. Sci., 41*, pp.885-891, https://doi.org/10.5194/isprs-archives-XLI-B1-885-2016.

Koch, B. 2015. Remote Sensing supporting national forest inventories NFA. In *FAO Knowledge Reference for National Forest Assessments*; FAO: Rome, Italy; pp.77–92. Available online: http://www.fao.org/3/a-i4822e.pdf (accessed 16 December 2019).

Korhonen, L.; Korhonen, K.T.; Rautiainen, M. and Stenberg, P. 2006. Estimation of forest canopy cover: a comparison of field measurement techniques, *Silva Fenn., 40*(4), pp.577-588, https://www.doi.org/10.14214/sf.315.

Kouba, J. 2009. A Guide to Using International GNSS Service (IGS) Products. Available online: https://www.researchgate.net/profile/Jan_Kouba/publication/228663800_A_guide_to_using_International_GNSS_Service_IGS_products/links/54fcc30c0cf270426d102cd3.pdf (accessed on 18 May 2020).

Lemenih, M. and Bongers, F. 2011. Dry forests of Ethiopia and their silviculture. In: Günter S., Weber M., Stimm B., Mosandl R. (eds) *Silviculture in the Tropics. Tropical Forestry*, vol. 8. Springer, Berlin, Heidelberg. https://doi.org/10.1007/978-3-642-19986-8_17.

Lenth, R.V. 2001. Some practical guidelines for effective sample size determination. *Am. Stat., 55(3)*, pp.187–193, https://doi.org/10.1198/000313001317098149.

Lohr, S. 2009. *Sampling: Design and Analysis*, second edition; Nelson Education: Scarborough, ON, Canada.

Lorenzen, B. and Jensen, A. 1988. Reflectance of blue, green, red and near-infrared radiation from wetland vegetation used in a model discriminating live and dead aboveground biomass. *New Phytol., 108*, pp.345–355, https://doi.org/10.1111/j.1469-8137.1988.tb04173.x.

Louhaichi, M.; Borman, M.M. and Johnson, D.E. 2001. Spatially located platform and aerial photography for documentation of grazing impacts on wheat. *Geocarto Int., 16*, pp. 65–70, https://doi.org/10.1080/10106040108542184.

Lu, D.; Batistella, M. and Moran, E. 2005. Satellite estimation of aboveground biomass and impacts of forest stand structure. *Photogramm. Eng. Remote Sens., 71*, pp.967–974, https://doi.org/10.14358/PERS.71.8.967.

Lu, D.; Chen, Q.; Wang, G.; Liu, L.; Li, G. and Moran, E. 2016. A survey of remote sensing-based aboveground biomass estimation methods in forest ecosystems. *Int. J. Digit. Earth, 9*(1), pp.63-105, https://doi.org/10.1080/17538947.2014.990526.

Lu, N.; Zhou, J.; Han, Z.; Li, D.; Cao, Q.; Yao, X.; Tian, Y.; Zhu, Y.; Cao, W. and Cheng, T. 2019. Improved estimation of aboveground biomass in wheat from RGB imagery and point

cloud data acquired with a low-cost unmanned aerial vehicle system. *Plant Methods, 15*, pp.1–16, https://doi.org/10.1186/s13007-019-0402-3.

Macedo, F.L.; Sousa, A.M.O.; Gonçalves, A.C.; Marques da Silva, J.R.; Mesquita, P.A. and Rodrigues, R.A.F. 2018. Aboveground biomass estimation for *Quercus rotundifolia* using vegetation indices derived from high spatial resolution satellite images. *Eur. J. Remote Sens., 51*, pp. 932–944, https://doi.org/10.1080/22797254.2018.1521250.

Magnet Tools (version 1.0). 2012. Topcon Positioning Systems Inc.: Livermore, CA, USA. Available online: https://www.tigersupplies.com/files/bcf31975-d2e6-44c2-ba66-7bad3a95cdb3HLP_MAGNET_Office_Tools_v1_0_EN.pdf (accessed on 21 September 2019).

Magnussen, S.; Næsset, E. and Gobakken, T. 2019. An application niche for finite mixture models in forest resource surveys. *Can. J. For. Res., 49*, pp.1453–1462, https://doi.org/10.1139/cjfr-2019-0170.

McRoberts, R.E. 2010. Probability-and model-based approaches to inference for proportion forest using satellite imagery as ancillary data. *Remote Sens. Environ., 114*(5), pp.1017-1025, https://doi.org/10.1016/j.rse.2009.12.013.

MEFCC (ministry of environment, forestry and climate change). 2018. National Forest Sector Development Program, Ethiopia. Volume I, Situation Analysis. Available online: https://www.undp.org/content/dam/ethiopia/docs/2018/National%20Forest%20sector%20Development%20Programme%20Volume%201%20Situation%20Analysis.pdf (accessed on 08 September 2020).

Millennium Ecosystem Assessment. 2005. *Ecosystems and human well-being* (Vol. 5, p. 563). United States of America: Island press. Available online: http://www.bioquest.org/wp-content/blogs.dir/files/2009/06/ecosystems-and-health.pdf (accessed on 08 November 2020).

Muchiri, N. and Kimathi, S. 2016. A Review of Applications and Potential Applications of UAV. In *Proceedings of Sustainable Research and Innovation Conference* (pp. 280-283).

Næsset, E.; Ørka, H.O.; Solberg, S.; Bollandsås, O.M.; Hansen, E.H.; Mauya, E.; Zahabu, E.; Malimbwi, R.; Chamuya, N.; Olsson, H. and Gobakken, T. 2016. Mapping and estimating forest area and aboveground biomass in miombo woodlands in Tanzania using data from airborne laser scanning, TanDEM-X, RapidEye, and global forest maps: A comparison of estimated precision. *Remote Sens. Environ., 175*, pp.282–300, https://doi.org/10.1016/j.rse.2016.01.006.

Navarro, J.A.; Algeet, N.; Fernández-Landa, A.; Esteban, J.; Rodríguez-Noriega, P. and Guillén-Climent, M.L. 2019. Integration of UAV, Sentinel-1, and Sentinel-2 data for mangrove plantation aboveground biomass monitoring in Senegal. *Remote Sens., 11*, pp.1–23, https://www.doi.org/10.3390/rs11010077.

Nguyen, T. H.; Jones, S.; Soto-Berelov, M.; Haywood, A. and Hislop, S. 2020. Landsat Time-Series for Estimating Forest Aboveground Biomass and Its Dynamics across Space and Time: A Review. *Remote Sens*., *12*(1), pp.1-25, https://doi.org/10.3390/rs12010098.

Pan, Y.; Birdsey, R.A.; Fang, J.; Houghton, R.; Kauppi, P.E.; Kurz, W.A.; Phillips, O.L.; Shvidenko, A.; Lewis, S.L.; Canadell, J.G. and Ciais, P. 2011. A large and persistent carbon sink in the world's forests. *Science, 333*(6045), pp.988-993, https://www.doi.org/10.1126/science.1201609.

Penman, J.; Gytarsky, M.; Hiraishi, T.; Krug, T.; Kruger, D.; Pipatti, R.; Buendia, L.; Miwa, K.; Ngara, T.; Tanabe, K. and Wagner, F. 2003. *Good practice guidance for land use, land-use change and forestry*; IPCC: Geneva, Switzerland.

Planet Explorer. Available online: https://www.planet.com/explorer/ (accessed on 3 September 2019).

Popescu, D.; Ichim, L. and Stoican, F. 2017. Unmanned aerial vehicle systems for remote estimation of flooded areas based on complex image processing. *Sensors, 17*(3), 446, https://doi.org/10.3390/s17030446.

Prasad, B.; Babar, M.A.; Carver, B.F.; Raun, W.R. and Klatt, A.R. 2009. Association of biomass production and canopy spectral reflectance indices in winter wheat. *Can. J. Plant. Sci., 89*, pp.485–496, https://doi.org/10.4141/CJPS08137.

Puliti, S.; Saarela, S.; Gobakken, T.; Ståhl, G. and Næsset, E. 2018. Combining UAV and Sentinel-2 auxiliary data for forest growing stock volume estimation through hierarchical model-based inference. *Remote Sens. Environ., 204*, pp.485-497, https://doi.org/10.1016/j.rse.2017.10.007.

Puliti, S.; Ørka, H.O.; Gobakken, T. and Næsset, E. 2015. Inventory of small forest areas using an unmanned aerial system. *Remote Sens., 7*(8), pp.9632-9654, https://doi.org/10.3390/rs70809632.

Recio, M.E. 2013. The Warsaw framework and the future of REDD+. *Yearbook of International Environmental Law*, *24*(1), pp.37-69, https://doi.org/10.1093/yiel/yvu060.

Rich, P.M. 1990. Characterizing plant canopies with hemispherical photographs. *Remote sensing reviews, 5*(1), pp.13-29, https://doi.org/10.1080/02757259009532119.

Risdiyanto, I. and Fakhrul, M. 2017. Examination of multi-spectral radiance of the Landsat 8 satellite data for estimating biomass carbon stock at wetland ecosystem. *Preprints, pp.*1–14, https://doi.org/10.20944/preprints201704.0020.v1.

Roy, P.S. and Ravan, S.A. 1996. Biomass estimation using satellite remote sensing data—an investigation on possible approaches for natural forest. *J. Biosci., 21*, pp.535–561, https://doi.org/10.1007/BF02703218.

Sandel, B. and Svenning, J.C. 2013. Human impacts drive a global topographic signature in tree cover. *Nature Communications*, *4*(1), pp.1-7, https://doi.org/10.1038/ncomms3474.

Schober, P.; Boer, C. and Schwarte, L.A. 2018. Correlation coefficients: appropriate use and interpretation. *Anesth. Analg., 126*, pp.1763-1768, https://doi.org/10.1213/ANE.0000000000002864.

Sheng, J. 2017. Effect of uncertainties in estimated carbon reduction from deforestation and forest degradation on required incentive payments in developing countries. *Sustainability, 9*(9), pp.1-14, https://doi.org/10.3390/su9091608.

Sousa, A.M.; Gonçalves, A.C. and Silva, J.R.M. 2017. Aboveground biomass estimation with high spatial resolution satellite images. *Biomass Volume Estimation and Valorization for Energy. Rijeka: InTech*, pp.47-70, https://dx.doi.org/10.5772/65665.

Sullivan, M.J.; Lewis, S.L.; Hubau, W.; Qie, L.; Baker, T.R.; Banin, L.F.; Chave, J.; Cuni-Sanchez, A.; Feldpausch, T.R.; Lopez-Gonzalez, G. and Arets, E. 2018. Field methods for sampling tree height for tropical forest biomass estimation. *Methods Ecol. Evol., 9*(5), pp.1179-1189, https://doi.org/10.1111/2041-210X.12962.

Tagesson, T.; Schurgers, G.; Horion, S.; Ciais, P.; Tian, F.; Brandt, M.; Ahlström, A.; Wigneron, J.P.; Ardö, J.; Olin, S. and Fan, L. 2020. Recent divergence in the contributions of tropical and

boreal forests to the terrestrial carbon sink. *Nat. Ecol. Evol., 4*(2), pp.202-209, https://doi.org/10.1038/s41559-019-1090-0.

Tewoldeberhan, G.E. 1991. Diversity of the Ethiopian flora. In Engels, J.; Hawkes, J. and Worede, M. (Eds.), *Plant Genetic Resources of Ethiopia* (pp. 75-81). Cambridge: Cambridge University Press. https://doi.org/10.1017/CBO9780511551543.005.

Topcon Positioning Systems Inc. Available online: https://www.topconpositioning.com/gb/gnss-network-solutions (accessed on 16 September 2019).

Torresan, C.; Berton, A.; Carotenuto, F.; Gennaro, S.F.D.; Gioli, B.; Matese, A.; Miglietta, F.; Vagnoli, C.; Zaldei A. and Wallace, L. 2017. Forestry applications of UAVs in Europe: a review. *Int. J. Remote Sens., 38*(8-10), pp.2427-2447, https://doi.org/10.1080/01431161.2016.1252477.

UNFCCC. 2015. Adoption of the Paris Agreement Proposal by the President. In *Proceedings of the Paris Climate Change Conference-COP 21*: Paris, France, pp. 1-31. Available online: https://unfccc.int/resource/docs/2015/cop21/eng/l09.pdf (accessed on 16 September 2019).

UNOCHA (United Nations Office for the Coordination of Humanitarian Affairs). 2014. Unmanned aerial vehicles in humanitarian response. Available online: https://docs.unocha.org/sites/dms/Documents/Unmanned%20Aerial%20Vehicles%20in%20Humanitarian%20Response%20OCHA%20July%202014.pdf (accessed on June 02, 2017).

USGS (United States Geological Survey) - Earth Explorer. Available online: https://earthexplorer.usgs.gov/ (accessed on 23 August 2019).

Wang, Q.; Pang, Y.; Li, Z.; Sun, G.; Chen, E. and Ni-Meister, W. 2016. The potential of forest biomass inversion based on vegetation indices using multi-angle CHRIS/PROBA data. *Remote Sens., 8*, pp.1-17, https://www.doi.org/10.3390/rs8110891.

Watson, C.; Mourato, S. and Milner-Gulland, E.J. 2013. Uncertain emission reductions from forest conservation: REDD in the Bale Mountains, Ethiopia. *Ecol. Soc., 18*(3), pp. 1-16, http://dx.doi.org/10.5751/ES-05670-180306.

WBG (World Bank Group). World development indicators database - Forest area (percentage of land area). Available online at https://data.worldbank.org/indicator/AG.LND.FRST.ZS (accessed on 05 September 2020).

Wondrade, N.; Dick, O.B. and Tveite, H. 2015. Estimating aboveground biomass and carbon stock in the lake Hawassa watershed, Ethiopia by integrating remote sensing and allometric equations. *Forest Research: Open Access, 4*, pp.1-11, https://doi.org/10.4172/2168-9776.1000151.

Zahawi, R.A.; Dandois, J.P.; Holl, K.D.; Nadwodny, D.; Reid, J.L. and Ellis, E.C. 2015. Using lightweight unmanned aerial vehicles to monitor tropical forest recovery. *Biol. Conserv., 186*, pp.287-295, https://doi.org/10.1016/j.biocon.2015.03.031.

Individual papers

PAPER-I

EUROPEAN JOURNAL OF REMOTE SENSING, 2018
VOL. 51, NO. 1, 326–335
https://doi.org/10.1080/22797254.2018.1432993

Taylor & Francis
Taylor & Francis Group

REVIEW ARTICLE

OPEN ACCESS Check for updates

Application of unmanned aerial vehicles in earth resources monitoring: focus on evaluating potentials for forest monitoring in Ethiopia

Habitamu Taddese Berie [a,b] and Ingunn Burud[a]

[a]Faculty of Science and Technology, Norwegian University of Life Sciences, Ås, Norway; [b]Wondo Genet College of Forestry and Natural Resources, Hawassa University, Shashemene, Ethiopia

ABSTRACT

Application of unmanned aerial systems was limited to the military until the last decade when we see dramatic growth of interest by civilian users. Among the many fields of application of unmanned aerial vehicles (UAVs), forestry has diverse uses ranging from forest cover assessment to species classification and real-time forest fire monitoring.

Inspired by the potential uses of the technology, this study is a review of literature on the types and uses of UAVs, the challenges and opportunities, current experiences and the future prospects of using UAVs for forest resources monitoring in Ethiopia.

The study has identified potential uses of UAVs for forestry applications. It has also shown that there is perceived need for accurate, demand-based and cost-effective tools for forest resources monitoring in developing countries including Ethiopia. Hence, the use of small UAVs in the forestry sector in Ethiopia is believed to be a supplementary method to the existing methods of spatial data capture for filling the gap of information and improving the quality of forest information that is needed to comply with international standards.

The results of this study indicate that Ethiopia can make use of the technology and improve its forest information system. However, while doing so, rules and regulations must be put in place to avoid the challenges that come along with introducing the technology. If properly used, the technology will enhance the forest management decision-support system of the country.

ARTICLE HISTORY
Received 29 June 2017
Revised 20 January 2018
Accepted 23 January 2018

KEYWORDS
Forestry; unmanned aerial vehicle; high-resolution images; multispectral data; infrared; canopy

Introduction

Drone or unmanned aerial vehicle (UAV) is a lightweight flying device similar to an aircraft; however, different from an aircraft since it is not operated by a pilot on-board. Based on how its movement is controlled, it can be an autonomous or a remotely piloted type. Broadly classified, small unmanned aerial systems (UAS) use a platform less than 10 kg in weight (Watts, Kobziar, & Percival, 2010). There are different models of UAV; however, most of them are hand-launched and operated remotely. A UAV is the aerial platform component of UAS, which also has a ground control station and communication components. Based on the types of wing, UAVs might broadly be classified as fixed-wing or rotary-wing type. The fixed-wing UAS move horizontally and need a larger open space for take-off and landing. On the other hand, the rotary-wing UAS move vertically; thus, requiring a small open space for landing.

Originally, UAS were used for military applications like reconnaissance and surveillance. Furthermore, a significant part of the civil applications of UAS technologies has been aerial photography and remote sensing for many decades (Colomina & Molina, 2014). However, they are becoming widely used in civil applications, especially in recent years. Now, UAS are becoming important in many fields like agriculture, cultural heritage management, search and rescue missions, infrastructure inspection, natural resources management and urban planning. These diverse applications are linked with the recent advances in the platform and sensor technologies (Budiyono, 2008). Image handling and processing systems have also shown improvement and provide opportunity for increasing interest in the use of UAS in many sectors. Therefore, such a huge interest in the use of UAS has grown because of the improvements in the technology and the increasing demand for timely and accurate information to cope up with the changing environment (Puliti, Ørka, Gobakken, & Næsset, 2015).

Because of climate change, sustainable forest management is becoming a global concern. Consequently, countries are encouraged to generate accurate forest information on a continuous basis to ensure that they have reduced net greenhouse gas emissions to the atmosphere. That is the reason for the institutionalization of the Reducing Emissions from Deforestation and forest Degradation plus (REDD+) schemes and other international conventions. Those conventions

CONTACT Habitamu Taddese Berie habtu1976@gmail.com; habitamu.taddese.berie@nmbu.no

require the member countries to quantify and report the reduced greenhouse gas emission because of reducing deforestation and forest degradation as well as ensuring sustainable forest resources management. For many years, this task has been carried out using the complementary methods of ground-based surveys and remote sensing data analysis. However, the use of UAS maybe a much better method since it provides accurate, flexible and cost-effective techniques (Banu, Borlea, & Banu, 2016; Colomina & Molina, 2014; Puliti et al., 2015).

Located in the horn of Africa very close to the Sahara desert, Ethiopia is one of the countries that has suffered from the impacts of climate change. The country is one of the signatories of the REDD+ negotiations and other international environmental conventions. Ethiopia has been striving to combat the impacts of climate change since it is vulnerable to recurrent drought and other environmental crises. As a result, it has designed and implemented a strategy that emphasizes restoring degraded lands and sustainable forest management called the Climate Resilient Green Economy strategy.

In response to the international conventions, Ethiopia needs to generate reliable forest information that conforms in quality to the international standards and can be ready to be reported whenever required. The existing ground-based methods of forest data collection are costly and slow to meet the time limit of reporting. On the other hand, satellite remote sensing methods based on the freely available Landsat images do not meet the quality criteria. This is mainly because Landsat images have too small spatial resolution to correctly identify and interpret trees. As a result, the information generated using these images has low accuracy.

Cognizant of the current trend of development, it seems that Ethiopia can benefit from the emerging UAS technologies to generate reliable forest information at the required time frames. Hence, this study was intended to explore the existing facts about applications of UAS technologies in forestry in various parts of the world to identify the potentials of the technology and initiate case studies to test if they can be adapted to the settings in Ethiopia.

Methods

This study focuses on review of the recent scientific publications in the field of UAS and their applications, particularly in forestry. Then, significance of the technology for forest resource monitoring in Ethiopia was evaluated based on the international experiences and existing realities in the country. A systematic approach was employed to search for all relevant scientific papers that relate to the topics.

A bibliographic survey on the Google Scholar and Scopus databases of scientific publications has been carried out. The keywords used in the search process include various combinations of the alternative nomenclatures of the system, fields of application and the name Ethiopia, which is the focus of this paper. The options of nomenclature that were used as keywords include "unmanned aerial systems", "unmanned aircraft systems", "unmanned aerial vehicles" and "drone" since these are the commonly used terms in scientific papers. The various application areas related to the interest of this study were agriculture, flood control, wildlife monitoring, wildland forest fire management, forestry, hazard management, remote sensing, coastal wetland mapping, mapping of invasive species and environment. Furthermore, the keyword "Ethiopia" was used to specify existing literature related to the uses of UAS in the country.

The review was organized according to the applications. The papers in each category were reviewed in accordance with these sections. A synthesis of the established global knowledge base in the use of UAS for various applications with emphasis on forestry has been made. The current experiences, legal frameworks, possible challenges and opportunities of using UAS in Ethiopia were reviewed. The existing methods of forest inventory in the country, their limitations and the prospects of future inventories were examined. Finally, feasibility of the technology in forest monitoring was evaluated based on international experiences and the local settings.

Types of UAV

UAVs are classified into various types based on different criteria. Most of the criteria for classifying UAVs include size and payload, flight endurance, flight range, altitude and capabilities. These characteristics are interrelated. Most of the time, large UAS carry more payload, fly at a higher altitude, move a longer distance and hence have better flight endurance and capability than small ones.

Based on wing types, UAVs are classified into the following five major types. The first type are the rotary-wing UAVs, which use batteries and have shorter flight times (Paneque-Gálvez, McCall, Napoletano, Wich, & Koh, 2014). This type of UAV includes the helicopter, quadracopter, octocopter and other varieties of multicopters. This type of UAV has the advantage that it needs small space for landing as compared to the fixed-wing UAV.

The second type of UAV are the fixed-wing UAVs, which are more suited to applications that demand longer flight endurance. They require large space for take-off and landing. As a result, they are not suitable for areas crowded with tall objects like buildings,

trees, wind farm vanes and other infrastructures. However, they have simple structure, which is easy for maintenance (Klimkowska, Lee, & Choi, 2016).

The third type of UAV are the groups of light-weight aerial systems called blimps such as balloons and airships, which are lighter than air and have long flight endurance, fly at low speeds and generally are large sized (Gupta, Ghonge, & Jawandhiya, 2013).The fourth group of UAV are the flapping-wing UAVs, which have flexible and morphing small wings, similar to birds and flying insects.

The fifth class of UAV are the Vertical Take-Off & Landing (VTOL) UAVs, which do not require take-off or landing run (Watts, Ambrosia, & Hinkley, 2012). These UAVs are typically used in situations where limitations of terrain require this specialized capability. However, high power requirements for hovering flight limit the flight durations for VTOL UAV, except in the large sizes for which increased lifting capabilities accommodate large fuel capacity. The advantages of VTOL UAV are the portability of the platforms for remote area operations without the necessity for runway complexes. These platforms are useful in rescue operations in a complex urban structure environment (narrow streets, buildings, etc.).

Thus, there is a choice to select the most appropriate technology that conforms to the prevailing environmental settings and purpose.

UAS sensors

Most of the UAS have inbuilt sensors, which record the red, green and blue (RGB) part of the electromagnetic spectrum. However, in recent years, introduction of additional sensors has enhanced the efficiency of capturing additional data. This was achieved by including the red-edge, near infrared and thermal infrared spectral bands and laser scanning systems (Colomina & Molina, 2014; Zahawi et al., 2015).

Innovations in sensor technology have fostered the successful implementation of UAS for forestry applications. For example, infrared sensors, including the thermal imaging systems, were used for forest fire monitoring (Allison et al., 2016; Hoffmann et al., 2016; Martínez-De Dios, Merino, Caballero, & Ollero, 2011; Merino, Caballero, Martínez-de-Dios, Maza, & Ollero, 2012; Scholtz et al., 2011). Predicting canopy cover and studies related to wood volume and biomass estimation became possible using laser scanners (Getzin, Nuske, & Wiegand, 2014; Zahawi et al., 2015).

This development in sensor technology has paved additional opportunity for studying the status of natural resources and the challenges facing them. This will enhance the potential uses of UAS technologies for multiple user groups, including forestry professionals, by providing more spectral data that can be applied to a wide range of uses.

General applications of UAS

The original purpose of UAS technologies was for military, patrolling international borders and governance (Budiyono, 2008; Callam, 2015; Finn & Wright, 2012; Gregory, 2011; Muchiri & Kimathi, 2016; Wall & Monahan, 2011). Through time, UAS technology has become important in many application fields. It is applied in management of crops, fisheries, forests and other natural resources among others (Jeanneret & Rambaldi, 2016).

In the agricultural sector, UAS have gained interest in precision agriculture to increase production (Simelli & Tsagaris, 2015). Scientists used UAS to study nutrient content of crops. For instance, UAS were used to estimate the amount of nitrogen status of turf-grasses in the University of Pisa, Italy (Caturegli et al., 2016). According to Shi et al. (2016), UAS technology was used to measure plant height of crops like maize and sorghum. UAS were also used in different countries to study plant biophysical properties like leaf area index and yield, and the growing environment. The technology has been used to investigate weed, pest and disease infestations. For example, small UAS were used to detect symptoms of disease and pest attacks on oil-bearing trees in Greece (Psirofonia, Samaritakis, Eliopoulos, & Potamitis, 2017). Planting patterns in sugarcane were supervised using UAS imagery in Nicaragua, Central America (Luna & Lobo, 2016). Promising results were obtained indicating huge potential of the technology in precision agriculture in the future (Felderhof, Gillieson, Zadro, & Van Boven, 2008).

The use of UAS is also becoming common in flood control; natural hazard management and infrastructural changes (Galarreta, Kerle, & Gerke, 2015; Giordan, Manconi, Remondino, & Nex, 2017; Perks, Russell, & Large, 2016). Studies show that UAS were used to identify disaster damages and serve humanitarian response services during disaster events in flood-affected Asian countries like Taiwan and China (Feng, Liu, & Gong, 2015; Popescu, Ichim, & Stoican, 2017; UNOCHA, 2014).

Moreover, the emerging technology has been applied for coastal wetland mapping and environmental management (Boon, Greenfield, & Tesfamichael, 2016; Klemas, 2015). Due to the excellent spatial resolution of products from UAS, they are preferred choices for cadastral mapping (Crommelinck et al., 2016).

UAS have also attracted wildlife ecologists in many parts of the world, including those in African countries, for wildlife monitoring and rangeland management (Christie, Gilbert, Brown, Hatfield, & Hanson,

2016; Hodgson, Baylis, Mott, Herrod, & Clarke, 2016; Rango et al., 2009; Wich, 2015; Wolf, 2017). This approach was found to be a cheaper and safer technique of studying a vast area of wildlife and their habitats than ground-based techniques (Gonzalez et al., 2016; Linchant, Lisein, Semeki, Lejeune, & Vermeulen, 2015).

Forestry applications of UAS

This paper emphasizes on assessing the possible areas of application of UAS in the forestry sector. Several studies carried out in various parts of the world indicate that UAS have ample potential in assessing forest resources. This is mainly because UAS provide the possibility of making a non-destructive and accurate measurement of many attributes of trees (forests). The current growth of the UAS technologies has put great hope that the technology can be used to study forest dynamics, stand species composition, disturbances and other attributes of forests (Banu et al., 2016). The following paragraphs explain some of the most common uses of UAS in the forestry sector, which are thought to be good lessons for Ethiopia and other countries of similar desire.

Several research works done by different scholars reveal that UAS were applied in estimation of dendrometric parameters. Studies in Canada and European countries (Goodbody, Coops, Marshall, Tompalski, & Crawford, 2017; Hird et al., 2017; Puliti et al., 2015; Torresan et al., 2017) have shown that UAS were capable of estimating tree height, crown width, basal area, stem number; and modelling gross stock volume and above ground biomass. The research findings of Zahawi et al. (2015) revealed that UAS technologies are viable for monitoring tropical forest restoration in Costa Rica. Findings of this study revealed that UAS are able to predict canopy height and above-ground biomass at the same level of precision as LiDAR systems.

UAS are also used for tree species classification and quantification of spatial gaps in forests. Burchfield (2014) used UAS for mapping of invasive trees and shrubs in Eastern Kansas of the US. Similarly, multi-temporal UAS imagery differentiated tree species in southern Belgium (Michez, Piégay, Lisein, Claessens, & Lejeune, 2016). The possibility to fly at any required time and acquire high spatial resolution imagery provides the opportunity to study plant identification, which has been difficult using ordinary satellite remote sensing systems. Getzin et al. (2014) used UAS images to analyse canopy gap patterns of forests in Germany. Such a study of spatial gap patterns of forest canopy is relevant as a biodiversity indicator. In addition, UAS were used to determine canopy height of a mixture of uneven-aged broadleaved stands with a predominance of oaks and even-aged coniferous stands in Belgium and the US (Dandois & Ellis, 2013; Lisein, Pierrot-Deseilligny, Bonnet, & Lejeune, 2013).

Other studies have indicated that UAS have potential for post-fire recovery monitoring and forest protection. Scientific investigations indicated that UAS have contributed to wildland fire monitoring, especially in difficult topographic settings (Cruz, Eckert, Meneses, & Martínez, 2016; Ollero & Merino, 2006). It is used to generate information about the vegetation condition, water stress and risk indices before a fire happens. During the fire incidence, UAS that have infrared and visible sensors are important for fire detection and monitoring. In recent studies, these sensors were mounted on UAS to study the structure of ongoing forest fires (Casbeer, Beard, McLain, Li, & Mehra, 2005; Martínez-De Dios et al., 2011; Merino et al., 2012). In these studies, UAS were used to detect real-time behaviour of forest fire like the location and shape of the fire front, the rate of spread, and the fire flame height. A recent study indicated that UAS helped to monitor forest health and to map forest diseases. For example, the visible and infrared sensors were used to produce pest infestation maps in Germany (Lehmann, Nieberding, Prinz, & Knoth, 2015).

Furthermore, researchers have found that UAS are vital tools for 3D reconstruction for growth modelling (Gatziolis, Lienard, Vogs, & Strigul, 2015) and studying biodiversity (Sandbrook, 2015). The technology helped to study seasonal patterns of change of wetland vegetation (Marcaccio, Markle, & Chow-Fraser, 2015). Thus, UAS have significance in studying habitat conditions and understanding the status of biodiversity.

UAS can also support participatory forest management efforts, particularly in developing countries. It can serve as a means of evaluating the impacts of intervention and as a planning tool for new actions. These applications of UAS are believed to enhance community-based forest management schemes in the tropics given external assistance and funding is provided to the poor communities living in these parts of the globe (Paneque-Gálvez et al., 2014).

Opportunities for using UAS

In recent years, UAS technologies are evolving rapidly and becoming appropriate for multiple applications. There are various reasons that make the technologies relatively preferred. UAS applications research carried out in many sectors has shown that the emerging interest in these technologies is related to the reduced size of the vehicles, affordability in terms of cost, low energy consumption, flexibility, minimizing of risks and the resulting high spatial

resolution data (Banu et al., 2016; Christensen, 2015; Colomina & Molina, 2014; Gaitani, Burud, Thiis, & Santamouris, 2017; Hird et al., 2017; Puliti et al., 2015). As a result, a diverse range of end users including foresters makes use of these technologies.

Advances in UAV platform design have contributed to innovation of small UAS that fly at low altitudes to provide very fine spatial resolution images (Anderson & Gaston, 2013; Yuan, Zhang, & Liu, 2015). The cost of data collection and processing using UAS is lower than that of equivalent methods that provide the same accuracy as terrestrial LiDAR and airborne laser scanning systems (Lisein et al., 2013; Puliti et al., 2015).

Besides, UAS technologies are important because they are flexible (Yuan et al., 2015). Mission planning and flight altitude are controlled based on real needs of users. The flight paths are designed to meet the objectives of the flight mission (Colomina & Molina, 2014). Hence, this technology is an efficient method of spatial data collection for a multitude of applications in the forestry sector ranging from species classification to forest fire monitoring and volume or biomass modelling. The technique attracts attention of many professionals since it has the ability to generate data to study a wide area of land with lower cost and better efficiency than ground-based systems.

The other advantage of UAS relates to low energy consumption (Banu et al., 2016). Small UAS use either fuel (gas) or battery as a source of energy. Although the batteries or fuel needs to be charged frequently, the energy required for a mission is small. Therefore, its low energy requirement contributes to the wide acceptance of the technology.

However, the main reason for the growing interest in using UAS technologies stems from the fact that they provide high spatial resolution images based on a demand-based temporal pattern. Applications like cadastre, urban planning, species classification and yield estimation that require detailed information benefit from these technologies (Colomina & Molina, 2014; Gaitani et al., 2017).

Moreover, the use of UAS is a safer method. It does not risk causalities since no human life is endangered during the process. This characteristic of UAS is ideal for military applications. The lack of on-board operators allows UAVs to be used in politically sensitive areas in which the deployment of human soldiers would create too much controversy. Hence, UAS are considered as a highly preferred technology for risk management (Banu et al., 2016; Muchiri and Kimathi, 2016). Therefore, UAS are important in monitoring forest fire and disease outbreaks, especially in areas with rough topography where terrestrial movement is restricted (Watts et al., 2010).

The current use of UAS in forestry applications is under experimental phase and its contribution to the sector will be realized in the near future (Banu et al., 2016). Furthermore, most of the experiments were carried out in European countries and the US. Based on these lessons, further studies have to be conducted in the local settings of developing countries as well so that the UAS can provide service to all potential users. This tests the appropriateness of the technology and provides feedback for further modifications in the UAS to meet local conditions.

Challenges associated with using UAS

UAS could play an important role in complex humanitarian emergency services as they can be used for surveillance in difficult or inaccessible areas. However, there are also risks associated with human welfare if they are misused (Boyle, 2015). Legal and ethical restraints have to be maintained to make use of the potentials of UAS. Some of the potential risks of UAS technologies are mentioned later. Furthermore, this section explains the possible means of mitigating the challenges to use the potentials of the technology properly.

Environmental challenges

Topography and winds on the high mountains might disturb the system or create noise in the products. The UAS platforms may collide with tall buildings and trees and cause problems unless governed by specific regulations.

Big data problem

The speed at which we convert data into meaningful information does not balance with the trend of data generation. The available analysis techniques are not efficient in making use of all the contents in the UAS-collected data. The often unstructured, heterogeneous big data require a smart interplay between skilled data scientists and domain experts (Wolfert, Ge, Verdouw, & Bogaardt, 2017). Therefore, skill capacity development to process and extract relevant information is a requirement for organizations to make the best use of the potentials of the technology.

Responsibility

UAS, like any aerial remote sensing system, require detailed flight planning. Although, it is an unmanned system, the crewmembers involved in the flight mission have to be known and responsible for what will happen during the flight.

Legal issues

There should be strict rules and regulations that govern how the UAS should function. A study conducted in Africa, Caribbean and Pacific countries indicates that some countries have well developed regulations that provide a workable environment for UAS operations while other countries do not have rules and regulations designed for UAS that are operational in their territories (Jeanneret & Rambaldi, 2016). Absence of regulations will open up room for misuse of the technology. The study has indicated that other countries have banned the use of UAS, which will influence their benefits from the technologies. This measure might be taken because of observed challenges of misuse of the technology. We suggest that well-established regulations will bring the extreme views of different countries together as long as the technologies provide service and are properly used to benefit the community.

Air safety and security issues

The military uses unmanned aircraft for intelligence, surveillance and reconnaissance, as well as direct attack on targets. When everybody can buy and fly UAS, it will be a convenient situation for misuse like terrorist attacks. The UAS may also collide with other flying objects or among themselves unless properly regulated. Therefore, we anticipate that the government of Ethiopia take the issue seriously and develop regulations that inhibit misuse of the technology. Otherwise, it will be a disaster to allow them to fly everywhere.

Privacy

The use of UAS might be disturbing when they fly over an area where people do not want to recognize their presence. The fact that they fly at low altitude close to the earth's surface enhances the effect. Rules and regulations should address this issue.

UAS regulation of every country should address all these challenges (Anderson, 2012). Each country has to set well-thought-out regulations to avoid human-induced problems and reduce the effect of natural challenges. The UAS regulations should take into account the international laws and be enforced accordingly. This technology will create misery to the global community unless regulated by national and international laws.

Anderson (2012) stated that there will be good uses and bad ones, but the same is true of any tool. The user has to exploit the good things and regulations need to limit the associated challenges. Our experience with regard to the current situation of UAS conforms to the suggestion. Hence, we recommend country-specific functional rules need to answer these issues so that the technologies can provide the anticipated services without being influenced by the suspected challenges.

Current uses of UAS in Ethiopia

Limited literature exists about the application of UAS in Ethiopia. Few reports indicate that UAS have been used in Ethiopia for various purposes. For instance, the US deployed surveillance UAS in Ethiopia to monitor the security of many African countries in 2011 (Ahmed, 2013; Sudan Tribune, 2013; UN, 2013). The US established a UAS military base in Arba Minch, a town about 500 km south of Addis Ababa (Whitlock, 2012; *The Japan Times*: 14 January 2016). However, it was also reported that the US stopped its mission at the beginning of 2016 (*The Japan Times*: 14 January 2016). A similar report indicated that UAS technologies helped the fight against tsetse fly in Ethiopia (Engadget, 2016). Drones have also been used to map and support the construction of railway systems in Eastern part of the country (Lopez, 2016).

The use of UAS in forestry in Ethiopia has not been recognized despite the huge potential that they can provide to the sector. Therefore, this study suggests that Ethiopia should learn from experiences of other countries and use the technology to supplement the efforts of enhancing its forest information system, which has suffered from the limitations of ground-based and satellite remote sensing technologies. The ground-based techniques, although excellent in terms of accuracy, require long time to collect data and are expensive. On the other hand, satellite remote sensing techniques, especially those with low and medium resolution sensor systems have limited image quality (i.e. spatial, spectral, temporal and radiometric) and are influenced by environmental conditions like the atmosphere. In addition, products of some satellite remote sensing are expensive to be used for national forest inventories (NFI) in the context of developing countries like Ethiopia.

When using UAS, the country has to make sure that there is no misuse of the technology. Hence, proper legal systems have to be set and implemented to limit the use of the technology for development endeavours only. Currently, Ethiopia does not have formalized regulation for managing the use of UAS (Jeanneret & Rambaldi, 2016) except that a permit should be applied for from the ministry of communication prior to a flight. This is valid both for commercial and private UAS use. Due to volcanic activity in many parts of the country, particularly along the rift valley system, recalibrating the flight compass is required before each flight. The maximum flight

altitude for a drone in Ethiopia is conventionally limited to be 150 m (Drone Traveller, 2016). These are the working principles in Ethiopia as far as UAS are concerned; however, the country has not yet declared a formal regulation.

Potential forestry applications of UAS in Ethiopia

The country had conducted only two NFI in its history. The older one, which was carried out from 1994 to 2004 was almost a lost opportunity. The inventory is known as the Woody Biomass Inventory and Strategic Planning Project or the woody biomass inventory for short. The data are non-existent and there is no responsible body to the sources of data. There is no officially documented data to be referred to currently. As a result, change monitoring becomes impossible. A new NFI project has been implemented since 2013 and is underway. This new NFI was initiated from scratch and has its own limitations. The field-based data collection had very few sampling sites, which are less than 650 for a country of more than 1 million square kilometres of land area. Moreover, the remote sensing data used for this NFI were Landsat 8 images, which have limited spatial resolution. The use of UAS will solve the problem of getting high-resolution images for selected resource rich hotspot areas and enhance the quality of the NFI data. The anticipated system requirements for the NFI are the remote sensing technologies that provide quality images, which in turn are less costly, flexible and frequently acquired to provide time-series imagery for change detection and growth monitoring. While medium resolution images like Landsat products provide a wall to wall coverage, UAS data will be used to get detail information about forest attributes.

On the contrary, the country needs to produce verifiable information to be reported for the international REDD+ Measurement, Reporting and Verification (MRV) systems and other conventions. Data quality is a requirement in these systems. This implies that there should be some innovative techniques to enhance the drawbacks of the conventional data acquisition techniques in terms of cost, time and accuracy.

Hence, the emerging UAS technologies have huge potential to contribute to the effort towards generating reliable forestry information in the country. This is mainly because UAS have great potential to provide high spatial resolution data at the required time. Studies show that other African countries like Zambia and Tanzania have identified UAS as potential tools for MRV of REDD+ activities (Day, Gumbo, Moombe, Wijaya, & Sunderland, 2014; Mauya et al., 2015). Thus, we are convinced that UAS can enhance the efficiency and quality of the forest information systems of Ethiopia.

We suggest that Ethiopia should adopt the UAS technologies for supporting the NFI and do its best to generate as much detail information as possible. Research institutions and universities should conduct experiments and provide evidence to support the optimal use of the system.

Conclusions

The use of UAS is critically required in Ethiopia due to the poor situation of forest information in the country. The field-based forest inventory, although accurate, has limitations of exaggerated costs of finance and time. On the other hand, local estimates using satellite remote sensing have suffered from accuracy problems and lack of coherence. Therefore, the new UAS technology will contribute to improving accuracy of estimates and reducing data collection costs.

Globally, there is ample evidence on the possible uses of UAS in forestry. Those lessons can be adopted and customized to the Ethiopian conditions and need to be used to supplement the existing methods. However, care should be taken into account when using UAS in rough topographic settings as the systems have very limited range of flight altitude. Besides, UAS regulations should also be set explicitly so that the national security is not endangered.

Disclosure statement

No potential conflict of interest was reported by the authors.

ORCID

Habitamu Taddese Berie http://orcid.org/0000-0002-0381-8874

References

Ahmed, A. (2013). The thistle and the drone: How America's war on terror became a global war on tribal Islam. *Brookings Institution Press*, 270.

Allison, R.S., Johnston, J.M., Craig, G., & Jennings, S. (2016). Airborne optical and thermal remote sensing for wildfire detection and monitoring. *Sensors (Basel, Switzerland)*, *16*(8), 1310.

Anderson, C. 2012. Here come the drones! August issue: *Wired* magazine. Accessed on 12 June 2017, http://www.wired.co.uk/article/here-come-the-drones.

Anderson, K., & Gaston, K.J. (2013). Lightweight unmanned aerial vehicles will revolutionize spatial ecology. *Frontiers in Ecology and the Environment*, *11* (3), 138–146.

Banu, T.P., Borlea, G.F., & Banu, C. (2016). The Use of Drones in Forestry. *Journal of Environmental Science and Engineering B*, *5*, 557–562.

Boon, M.A., Greenfield, R., & Tesfamichael, S. (2016). Wetland Assessment Using Unmanned Aerial Vehicle

(UAV) Photogrammetry. In *Proceedings of the International Archives of the Photogrammetry, Remote Sensing and Spatial Information Sciences, XXIII ISPRS Congress*, Prague, Czech Republic (pp. 12–19).

Boyle, M.J. (2015). The legal and ethical implications of drone warfare. *The International Journal of Human Rights*, *19*(*2*), 105–126.

Budiyono, A. (2008). Advances in unmanned aerial vehicles technologies. *International Symposium on Intelligent Unmanned System, ISIUS 2008 - Nanjing*, China.

Burchfield, D.R. (2014). *Mapping eastern redcedar (Juniperus Virginiana L.) and quantifying its biomass in Riley County, Kansas* (Doctoral dissertation, Kansas State University).

Callam, A. (2015). Drone wars: Armed unmanned aerial vehicles. *International Affairs Review*, *18*(3).

Casbeer, D.W., Beard, R.W., McLain, T.W., Li, S.M., & Mehra, R.K. (2005). Forest fire monitoring with multiple small UAVs. In *American Control Conference, 2005. Proceedings of the 2005* (pp. 3530–3535).

Caturegli, L., Corniglia, M., Gaetani, M., Grossi, N., Magni, S., Migliazzi, M., … Volterrani, M. (2016). Unmanned aerial vehicle to estimate nitrogen status of turfgrasses. *PLoS ONE*, *11*(*6*), e0158268.

Christensen, B.R. (2015). Use of UAV or remotely piloted aircraft and forward-looking infrared in forest, rural and wildland fire management: Evaluation using simple economic analysis. *New Zealand Journal of Forestry Science*, *45*, 16.

Christie, K.S., Gilbert, S.L., Brown, C.L., Hatfield, M., & Hanson, L. (2016). Unmanned aircraft systems in wildlife research: Current and future applications of a transformative technology. *Frontiers in Ecology and the Environment*, *14*(*5*), 241–251.

Colomina, I., & Molina, P. (2014). Unmanned aerial systems for photogrammetry and remote sensing: A review. *ISPRS Journal of Photogrammetry and Remote Sensing*, *92*, 9–97.

Crommelinck, S., Bennett, R., Gerke, M., Nex, F., Yang, M.Y., & Vosselman, G. (2016). Review of automatic feature extraction from high-resolution optical sensor data for UAS-based cadastral mapping. *Remote Sensing*, *8*(8). doi:10.3390/rs8080689

Cruz, H., Eckert, M., Meneses, J., & Martínez, J.F. (2016). Efficient forest fire detection index for application in unmanned aerial systems (UASs). *Sensors*, *16*(*6*), 893.

Dandois, J.P., & Ellis, E.C. (2013). High spatial resolution three-dimensional mapping of vegetation spectral dynamics using computer vision. *Remote Sensing of Environment*, *136*, 259–276.

Day, M., Gumbo, D., Moombe, K.B., Wijaya, A., & Sunderland, T. (2014). Zambia country profile: Monitoring, reporting and verification for REDD+. Occasional Paper 113. Bogor, Indonesia: CIFOR.

Drone Traveller: (2016). 'Drone Regulations in Africa'. Accessed on 01 June 2017, https://drone-traveller.com/drone-laws-africa/.

Engadget: (2016). Drones deliver sterile insects to tackle disease in Ethiopia. Accessed on 01 June 2017, https://www.engadget.com/2016/03/30/drones-tsetse-flies-combat-ethiopia/.

Felderhof, L., Gillieson, D., Zadro, P., & Van Boven, A. (2008). *Linking UAV (unmanned aerial vehicle) technology with precision agriculture.*

Feng, Q., Liu, J., & Gong, J. (2015). Urban flood mapping based on unmanned aerial vehicle remote sensing and random forest classifier—A case of Yuyao, China. *Water*, *7*, 1437.

Finn, R.L., & Wright, D. (2012). Unmanned aircraft systems: Surveillance, ethics and privacy in civil applications. *Computer Law & Security Review*, *28*, 184–194.

Gaitani, N., Burud, I., Thiis, T.K., & Santamouris, M. (2017). High-resolution spectral mapping of urban thermal properties with unmanned aerial vehicles. *Building and Environment*, *121*, 215–224.

Galarreta, J.F., Kerle, N., & Gerke, M. (2015). UAS-based urban structural damage assessment using object-based image analysis and semantic reasoning. *Natural Hazards Earth Systems Sciences*, *15*, 1087–1101.

Gatziolis, D., Lienard, J.F., Vogs, A., & Strigul, N.S. (2015). 3D tree dimensionality assessment using photogrammetry and small unmanned aerial vehicles. *PLoS ONE*, *10* (*9*), e0137765.

Getzin, S., Nuske, R.S., & Wiegand, K. (2014). Using Unmanned aerial vehicles (UAS) to quantify spatial gap patterns in forests. *Remote Sensing*, *6*(*8*), 6988–7004.

Giordan, D., Manconi, A., Remondino, F., & Nex, F. (2017). Use of Unmanned aerial vehicles in monitoring application and management of natural hazards. *Geomatics, Natural Hazards and Risk*, *8*, 1–4.

Gonzalez, L.F., Montes, G.A., Puig, E., Johnson, S., Mengersen, K., & Gaston, K.J. (2016). Unmanned aerial vehicles (UAV) and artificial intelligence revolutionizing wildlife monitoring and conservation. *Sensors*, *16*(*1*), 97.

Goodbody, T.R.H., Coops, N.C., Marshall, P.L., Tompalski, P., & Crawford, P. (2017). Unmanned aerial systems for precision forest inventory purposes: A review and case study. *The Forestry Chronicle*, *93*, 71–81.

Gregory, D. (2011). From a view to a kill: Drones and late modern war. *Theory, Culture & Society*, *28*(7–8), 188–215.

Gupta, S.G., Ghonge, M.M., & Jawandhiya, P.M. (2013). Review of unmanned aircraft system (UAS). *International Journal of Advanced Research in Computer Engineering & Technology (IJARCET)*, *2*(4), 1646–1658.

Hird, J.N., Montaghi, A., McDermid, G.J., Kariyeva, J., Moorman, B.J., Nielsen, S.E., & McIntosh, A.C.S. (2017). Use of unmanned aerial vehicles for monitoring recovery of forest vegetation on petroleum well sites. *Remote Sensing*, *9*(5), 1–20.

Hodgson, J.C., Baylis, S.M., Mott, R., Herrod, A., & Clarke, R.H. (2016). Precision wildlife monitoring using unmanned aerial vehicles. *Sciences Reports*, *6*, 22574.

Hoffmann, H., Nieto, H., Jensen, R., Guzinski, R., Zarco-Tejada, P., & Friborg, T. (2016). Estimating evaporation with thermal UAV data and two-source energy balance models. *Hydrology and Earth System Sciences*, *20*(2), 697–713.

The Japan Times: (2016). 'U.S. shuts down drone base in Ethiopia'. Accessed on 01 June 2017, http://www.japantimes.co.jp/news/2016/01/04/world/u-s-shuts-down-drone-base-in-ethiopia/#.WTAjceC0m70.

Jeanneret, C., & Rambaldi, G. (ed.) (2016). Drone governance: A scan of policies, laws and regulations governing the use of unmanned aerial vehicles (UAV) in 79 countries. CTA Working Paper.

Klemas, V.V. (2015). Coastal and environmental remote sensing from Unmanned aerial vehicles: An overview. *Journal of Coastal Research*, *31*(*5*), 1260–1267.

Klimkowska, A., Lee, I., & Choi, K. (2016). Possibilities of UAS for maritime monitoring. *The International Archives of the Photogrammetry, Remote Sensing and Spatial Information Sciences, Volume XLI-B1, 2016 XXIII ISPRS Congress*, Prague, Czech Republic.

Lehmann, J.R.K., Nieberding, F., Prinz, T., & Knoth, C. (2015). Analysis of unmanned aerial system-based CIR images in forestry - A new perspective to monitor pest infestation levels. *Forests*, *6*(3), 594–612.

Linchant, J., Lisein, J., Semeki, J., Lejeune, P., & Vermeulen, C. (2015). Are unmanned aircraft systems (UAS) the future of wildlife monitoring? A review of accomplishments and challenges. *Mammal Review*, *45*, 239–252.

Lisein, J., Pierrot-Deseilligny, M., Bonnet, S., & Lejeune, P. (2013). A photogrammetric workflow for the creation of a forest canopy height model from small-unmanned aerial system imagery. *Forests*, *4*(4), 922–944.

Lopez, A. 2016. 'Drone mapping a 447 km railway in Ethiopia'. Accessed on 01 June 2017, http://www.uashub.org/single-post/2016/07/05/Drone-mapping-a-447-km-railway-in-Ethiopia.

Luna, I., & Lobo, A. (2016). Mapping crop planting quality in sugarcane from UAV imagery: A pilot study in Nicaragua. *Remote Sensing*, *8*(*500*). doi:10.3390/rs8060500

Marcaccio, J.V., Markle, C.E., & Chow-Fraser, P. (2015). Unmanned aerial vehicles produce high-resolution, seasonally relevant imagery for classifying wetland vegetation. *The International Archives of the Photogrammetry, Remote Sensing and Spatial Information Sciences, Volume XL-1/W4*, International Conference on Unmanned aerial vehicles in Geomatics, 30 Aug–02 Sep 2015, Toronto, Canada. doi:10.5194/isprsarchives-XL-1-W4-249-2015

Martínez-De Dios, J.R., Merino, L., Caballero, F., & Ollero, A. (2011). Automatic forest-fire measuring using ground stations and unmanned aerial systems. *Sensors*, *11*(*6*), 6328–6353.

Mauya, E.W., Ene, L.T., Bollandsås, O.M., Gobakken, T., Næsset, E., Malimbwi, R.E., & Zahabu, E. (2015). Modelling aboveground forest biomass using airborne laser scanner data in the miombo woodlands of Tanzania. *Carbon Balance and Managent*, *10*(28), 1–16.

Merino, L., Caballero, F., Martínez-de-Dios, J.R., Maza, I., & Ollero, A. (2012). An unmanned aircraft system for automatic forest fire monitoring and measurement. *Journal of Intelligence and Robot Systems*, *65*(*1*), 533–548.

Michez, A., Piégay, H., Lisein, J., Claessens, H., & Lejeune, P. (2016). Classification of riparian forest species and health condition using multi-temporal and hyperspatial imagery from unmanned aerial system. *Environmental Monitoring and Assessment*, *188*(*3*), 1–19.

Muchiri, N., & Kimathi, S. (2016). A review of applications and potential applications of UAV. In *Proceedings of Sustainable Research and Innovation Conference* (pp. 280–283).

Ollero, A., & Merino, L. (2006). Unmanned aerial vehicles as tools for forest-fire fighting. *Forest Ecology and Management*, *234*(1), 263.

Paneque-Gálvez, J., McCall, M.K., Napoletano, B.M., Wich, S.A., & Koh, L.P. (2014). Small drones for community-based forest monitoring: An assessment of their feasibility and potential in tropical areas. *Forests*, *5*(*6*), 1481–1507.

Perks, M.T., Russell, A.J., & Large, A.R. (2016). Technical note: Advances in flash flood monitoring using unmanned aerial vehicles (UAV). *Hydrology and Earth System Sciences*, *20*(*10*), 4005–4015.

Popescu, D., Ichim, L., & Stoican, F. (2017). Unmanned aerial vehicle systems for remote estimation of flooded areas based on complex image processing. *Sensors*, *17*(3), 446.

Psirofonia, P., Samaritakis, V., Eliopoulos, P., & Potamitis, I. (2017). Use of unmanned aerial vehicles for agricultural applications with emphasis on crop protection: Three novel case studies. *Journal of Agricultural Science and Technology*, *5*(*1*), 30–39.

Puliti, S., Ørka, H.O., Gobakken, T., & Næsset, E. (2015). Inventory of small forest areas using an unmanned aerial system. *Remote Sensing*, *7*, 9632–9654.

Rango, A., Laliberte, A., Herrick, J.E., Winters, C., Havstad, K., Steele, C., & Browning, D. (2009). Unmanned aerial vehicle-based remote sensing for rangeland assessment, monitoring, and management. *Journal Applications Remote Sensing*, *3*(1), 033542.

Sandbrook, C. (2015). The social implications of using drones for biodiversity conservation. *Ambio*, *44*(4), 636–647.

Scholtz, A., Kaschwich, C., Krüger, A., Kufieta, K., Schnetter, P., Wilkens, C.S., … Vörsmann, P. (2011). Development of a new multi-purpose UAS for scientific application. *International Archives of the Photogrammetry, Remote Sensing and Spatial Information Sciences*, *38*, 149–154.

Shi, Y., Thomasson, J.A., Murray, S.C., Pugh, N.A., Rooney, W.L., Shafian, S., … Yang, C. (2016). Unmanned aerial vehicles for high-throughput phenotyping and agronomic research. *PLoS ONE*, *11*(*7*), e0159781.

Simelli, I., & Tsagaris, A. (2015). The Use of Unmanned Aerial Systems (UAS) in Agriculture. *In HAICTA*, 730–736.

Sudan Tribune: (2013). Ethiopia produces first military drone aircraft'. Accessed on May 31, 2017. http://www.sudantribune.com/spip.php?iframe&page=imprimable&id_article=45518.

Torresan, C., Berton, A., Carotenuto, F., Gennaro, S.F.D., Gioli, B., Matese, A., … Wallace, L. (2017). Forestry applications of UAVs in Europe: A review unmanned aerial vehicles for environmental applications. *International Journal of Remote Sensing*, *38*(8–10), 2029–2036.

UN (United Nations). (2013). The UN's use of Unmanned aerial vehicles in the democratic Republic of the Congo: U.S. Support and potential foreign policy advantages, better world campaign, accessed on 01 June 2017, http://betterworldcampaign.org/assets/pdf/bwc-white-paper-the-uns-use-of-UASs-in-th-drc-may-2013.pdf.

UNOCHA (United Nations Office for the Coordination of Humanitarian Affairs). (2014). Unmanned aerial vehicles in humanitarian response. Accessed on June 02, 2017, https://docs.unocha.org/sites/dms/Documents/Unmanned%20Aerial%20Vehicles%20in%20Humanitarian%20Response%20OCHA%20July%202014.pdf.

Wall, T., & Monahan, T. (2011). Surveillance and violence from afar: The politics of drones and liminal security-scapes. *Theoretical Criminology*, *15*(3), 239–254.

Watts, A.C., Ambrosia, V.G., & Hinkley, E.A. (2012). Unmanned aircraft systems in remote sensing and

scientific research: Classification and considerations of use. *Remote Sensing*, *4*, 1671–1692.

Watts, A.C., Kobziar, L.N., & Percival, H.F. (2010). Unmanned aircraft systems for fire and natural resource monitoring: Technology overview and future trends. In K.M. Robertson, K.E.M. Galley, & R.E. Masters (eds.), *Proceedings of the 24th tall timbers fire ecology conference: The future of prescribed fire: Public awareness, health, and safety* (pp. 86–89). Tallahassee, Florida, USA: Tall Timbers Research Station.

Whitlock, C. (2012). Remote US base at core of secret operations. *The Washington Post*.

Wich, S.A. (2015). Drones and conservation. In *Drones and aerial observation: New technologies for property rights, human rights, and global development a primer* (pp. 63–70).

Wolf, H.G. (2017). *Drones: Safety risk management for the next evolution of flight*. Routledge. ISBN:1315471396, 9781315471396.

Wolfert, S., Ge, L., Verdouw, C., & Bogaardt, M.J. (2017). Big data in smart farming – A review. *Agricultural Systems*, *153*, 69–80.

Yuan, C., Zhang, Y., & Liu, Z. (2015). A survey on technologies for automatic forest fire monitoring, detection, and fighting using unmanned aerial vehicles and remote sensing techniques. *Canadian Journal of Forest Research*, *45*, 783–792.

Zahawi, R.A., Dandois, J.P., Holl, K.D., Nadwodny, D., Reid, J.L., & Ellis, E.C. (2015). Using lightweight unmanned aerial vehicles to monitor tropical forest recovery. *Biological Conservation*, *186*, 287–295.

PAPER-II

land

MDPI

Article

Estimation of Forest Area and Canopy Cover Based on Visual Interpretation of Satellite Images in Ethiopia

Zerihun Asrat [1], Habitamu Taddese [2], Hans Ole Ørka [1], Terje Gobakken [1,*], Ingunn Burud [2] and Erik Næsset [1]

[1] Faculty of Environmental Sciences and Natural Resource Management, Norwegian University of Life Sciences, P.O. Box 5003, 1432 Ås, Norway; zerihun.asrat.kutie@nmbu.no (Z.A.); hans.ole.orka@nmbu.no (H.O.Ø.); erik.naesset@nmbu.no (E.N.)

[2] Faculty of Science and Technology, Norwegian University of Life Sciences, P.O. Box 5003, 1432 Ås, Norway; habitamu.taddese.berie@nmbu.no (H.T.); ingunn.burud@nmbu.no (I.B.)

* Correspondence: terje.gobakken@nmbu.no; Tel.: +47-67-23-17-55

Received: 23 May 2018; Accepted: 24 July 2018; Published: 30 July 2018

Abstract: Forests, particularly in the tropics, are suffering from deforestation and forest degradations. The estimation of forest area and canopy cover is an essential part of the establishment of a measurement, reporting, and verification (MRV) system that is needed for monitoring carbon stocks and the associated greenhouse gas emissions and removals. Information about forest area and canopy cover might be obtained by visual image interpretation as an alternative to expensive fieldwork. The objectives of this study were to evaluate different types of satellite images for forest area and canopy cover estimation though visual image interpretation, and assess the influence of sample sizes on the estimates. Seven sites in Ethiopia with different vegetation systems were subjectively identified, and visual interpretations were carried out in a systematical design. Bootstrapping was applied to evaluate the effects of sample sizes. The results showed that high-resolution satellite images ($\leq$5 m) (PlanetScope and RapidEye) images produced very similar estimates, while coarser resolution imagery (10 m, Sentinel-2) estimates were dependent on forest conditions. Estimates based on Sentinel-2 images varied significantly from the two other types of images in sites with denser forest cover. The estimates from PlanetScope and RapidEye were less sensitive to changes in sample size.

Keywords: land cover; land use; visual interpretation; high resolution imagery; estimation; design-based inference

1. Introduction

Forests constitute the largest terrestrial ecosystem, and they provide a variety of services and functions [1,2]. One of the services that forests offer is carbon sequestration; approximately 2.5 billion tons carbon are absorbed annually [3–5]. Despite their contributions to carbon sequestration, much of the world's forests, particularly tropical forests, are suffering from severe deforestation and degradation, contributing to increased carbon emission [5–7]. About 12% of the total anthropogenic carbon emissions come from deforestation [5,8]. The pressure from deforestation and degradation on forests is larger particularly in tropical, developing countries due to heavy dependence on the resource for livelihoods [9].

The world has been acting continuously from the Kyoto Protocol in 1992 to the recent Paris Agreement in 2015 to halt the global warming through various means, one of which is the REDD+ mechanism (Reducing Emissions from Deforestation and forest Degradation). The REDD+ mechanism gives financial incentives to countries decreasing their deforestation and forest degradation. Ethiopia is one of the tropical countries that has lost much of its forest resources in the past [10]. Historically,

the forest cover of Ethiopia was reported to be more than 30–40% of the area [10,11]. However, the origin of this number is uncertain, and the amount itself is questionable [12]. Either way, there has been severe deforestation and forest degradation in the country the last century [11–14]. The pressure to convert forests into land for food production to support the increasing human population and provide socio-economic benefits to the nature-based livelihoods of the majority of the people has been huge. The use of wood for fuel has also aggravated the rate of deforestation [10,11].

Ethiopia is currently in the process of implementing REDD+, and one of the prerequisites for implementing the REDD+ mechanism is to develop a robust measuring, reporting, and verification (MRV) system following the Intergovernmental Panel on Climate Change (IPCC) Good Practice Guidelines [15]. Information about forest area and canopy cover are required for a MRV system in the REDD+ process and sustainable forest management practices. Forest area is the proportion of an area that is covered with trees and other perennial components of a forest land. The definition of forest varies among countries, the contexts of institutions, and of course the purpose [16]. The Food and Agriculture Organization (FAO) of the United Nations defines forest as land spanning more than 0.5 hectares with trees higher than 5 m and a canopy cover of more than 10%, or trees that are able to reach these thresholds in situ [17]. In Ethiopia, the working definition of forest describes it as any land spanning at least 0.5 hectares covered by trees (including bamboo) attaining a height of at least 2 m and a canopy cover of at least 20%, or trees with the potential to reach these thresholds in situ in due course. Canopy cover is the proportion of the forest floor covered by the vertical projection of the tree crowns [15,18,19]. Canopy cover plays a significant role in forest management for various decisions related to silviculture and the utilization of the forests [20].

In REDD+, developing countries rehabilitate and preserve their forests, and in turn get paid for the extra amount of CO_2 sequestered beyond a certain agreed level following MRV after their commitment [21]. The REDD+ system, of course, requires accurate measurement and estimation methods to be carried out through a properly established MRV system [22]. In the course of quantifying the amount of CO_2 by sink and source, reliable forest area and canopy cover estimations are key attributes [15,23]. However, according to the IPCC, information on forest area and deforestation in tropical countries is highly uncertain, often up to 50% of error [24]. This is because tropical countries are constrained by a lack of technical capacity and lack of both trained human power as well as infrastructure. In such situations, when and where there are technical inefficiencies, it would be important to critically scrutinize and choose the most feasible methods and technologies [23].

Past and current practices of forest cover assessment as well as land-use and land-cover (LULC) mapping in Ethiopia, digital image classification, and mapping methods are practiced, such as supervised, unsupervised, and object-based classification (e.g., [13,14]). However, digital image classification and mapping methods in general require a high level of technical skill, and in most cases, technical software [25,26]. Furthermore, the spectral similarity of land-cover classes is also challenging. As a result, the wider application and use of such methodologies for large-scale activities such as nationwide assessment could be problematic. For instance, Ethiopia's historical data on LULC changes between 2000–2013 for forest reference level (FRL) submission to the United Nations Framework Convention on Climate Change (UNFCCC) were generated through digital image classification and mapping using Landsat data. Nevertheless, the report underlined the need for the further reduction of uncertainties of the estimates [27]. In response to the drawbacks of digital image classification and mapping mentioned above, some platforms of free and open source software such as Geo-Wiki, VIEW-IT, and Sky Truth are developed by different bodies, including academic institutions [26,28]. The software support visual satellite image interpretation and LULC map validation by non-remote sensing experts, while some of the programs can also be used for other advanced applications by professional users [26,29]. The application of these software packages is associated with the use of very high-resolution images, which are often known to have a small geographic scope and an irregular time interval of acquisition, in turn limiting its utility for large areas. On the other hand, using Landsat images will provide a global coverage with bi-monthly acquisitions; however, interpretation is limited

by its low spatial resolution. FAO designed the software system Collect Earth as an open source tool that helps to collect, analyze, and compile reports on LULC through visual image interpretation based on freely available satellite images mainly with the Google Earth platform [25]. The tool has been adopted, and many countries have used it around the world for activities such as national forest inventory, LULC mapping, and the estimation of activity data for REDD+ [25].

The mentioned software supporting visual satellite image interpretation are efficient tools for gathering reference data. Such reference data gathered using interpretation of satellite imagery with different spatial resolutions under different forest conditions has been used to provide forest area and forest cover change estimates [30,31]. However, forest conditions and properties of the imagery, such as spatial resolution and revisit times, could potentially influence estimates. Hence, it is important to evaluate different types of satellite images under different forest conditions in order to provide guidelines for using such tools at a national level.

Thus, the aim of this study was to identify and evaluate different and alternative types of satellite images to minimize the level of uncertainties of the estimation of forest area and canopy cover in different forest conditions in Ethiopia. The specific objectives of the study were to: (1) evaluate the use of PlanetScope, RapidEye, and Sentinel-2 satellite images for forest area and canopy cover estimation through visual interpretation; and (2) assess the influence of sample sizes on the estimates. Accordingly, efforts were made to see if there is variation in the pattern of the estimates and the uncertainty of estimates from the three types of satellite images over the different areas of interest (sites of the study), which are characterized by having different biomes. Thus, such efforts would provide insight on the robustness of the method when applied to different forest conditions. The time elapsed for interpretation was assessed to evaluate the effectiveness of the method. In general, the study sites were selected so that they covered the important carbon storage areas of the country. Therefore, the study is helpful for gaining knowledge and contributing to improving Ethiopia's REDD+ MRV system in practice.

2. Materials and Methods

2.1. Description of the Study Sites

Ethiopia is located in eastern Africa, geographically extending from 3° to 15° north latitude and from 33° to 48° east longitude. It is known for its topographic diversity, stretching from the lowest Danakil depression 125 m below sea level to the highest peak of the Simien Mountains, which is over 4500 m above sea level. The great East African rift valley that runs from northeast to southwest divides the country into north, northwest, and southwest highlands and the western lowlands on one side, and the eastern and southeastern highlands and the associated lowlands on the other side [32]. This topographic diversity favored the country to have a wide range of climate and a diverse flora and fauna, with a considerable amount of it being endemic [33].

For this study, seven sites were identified to represent the major biomes of the country, as well as their tree gain or loss conditions (Table 1). The selection of sites was subjective in order to have sites covering a range of forest conditions. The size of each site was 2052 km^2 (36 km × 57 km). The major biomes were used in activity data compilation for FRL submission to the UNFCCC, and stratification during the national forest inventory planning and implementation [27]. The major biomes include (1) Dry Afromontane: includes undifferentiated Afromontane forest; dry single dominant Afromontane forest of the Ethiopian highland; Afromontane woodland, wooded grassland, and grassland. In addition, transition between Afromontane vegetation and *Acacia-Commiphora* bushland on the eastern escarpment, as well as Ericaceous and Afroalpine belts, are included. (2) Moist Afromontane: comprises mainly primary or mature secondary moist evergreen Afromontane forest. Also contains edges of moist evergreen Afromontane forest, bushland, woodland, and wooded grassland, as well as transitional rain forest. (3) *Combretum-Terminalia*: *Combretum-Terminalia* woodland and wooded grassland is a major component. Furthermore, it includes wooded grassland of

the western Gambela region. (4) *Acacia-Commiphora*: *Acacia-Commiphora* woodland and bushland proper; Acacia wooded grassland of the rift valley as well as desert and semi-desert vegetation [32]. Accordingly, dry Afromontane forests cover the north, central, and eastern highlands of the country; moist Afromontane forests dominate the southwest and south-central areas. *Combretum-Terminalia* covers the northwest, west, and southwest lowlands; *Acacia-Commiphora* includes the northeast, east, and south lowlands of the country, while the rest that is categorized as others included water bodies and wetlands (Figure 1).

Table 1. Description of the study sites.

Site	Biome Type	Condition of Forest in the Area *
A	*Acacia-Commiphora* and partly dry Afromontane	Both tree gain and loss of similar magnitude
B	Moist Afromontane	Characterized by tree loss
C	Partly moist Afromontane and partly *Acacia-Commiphora*	Characterized by tree loss and very little gain
D	Moist Afromontane	Characterized by tree loss
E	Moist Afromontane	Both tree gain and loss of similar magnitude
F	Dry Afromontane	Characterized by tree gain
G	*Combretum-Terminalia*	Characterized by tree loss

* Source: Global Forest Watch (www.globalforestwatch.org).

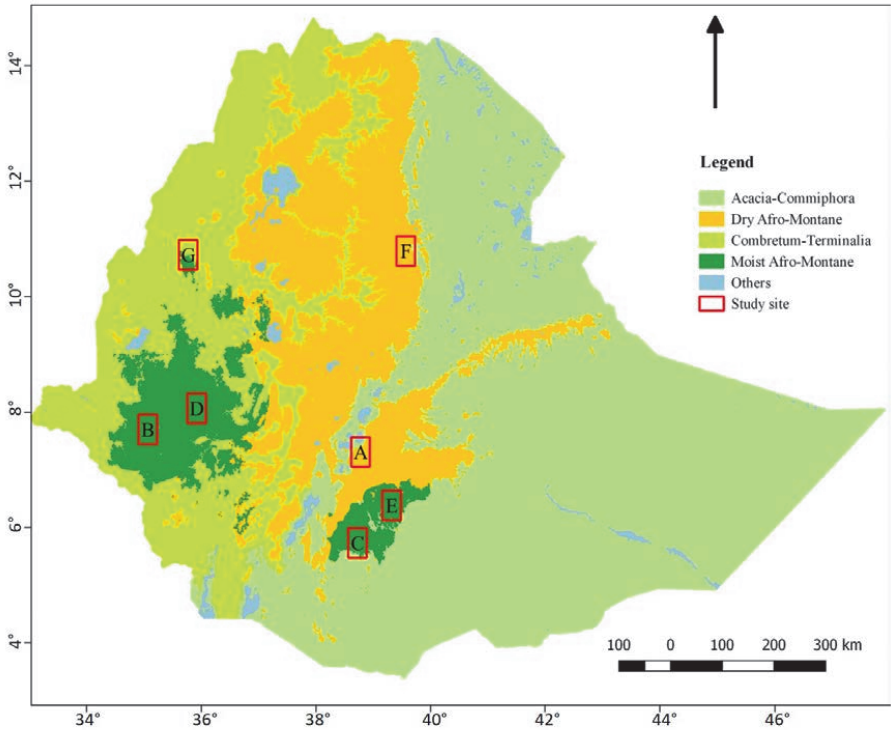

Figure 1. The major biomes in Ethiopia and the seven sites (A, B, . . . , G) selected for the study.

2.2. Satellite Imagery

Satellite images upon which the visual interpretation was based were PlanetScope, RapidEye, and Sentinel-2, which were all in their true color image (red, blue, and green).

2.2.1. PlanetScope

PlanetScope image products are available in three different forms. PlanetScope Basic Scene (1B) is a product with radiometric and sensor corrections only, which is designed for users with advanced knowledge of image processing. PlanetScope Ortho Scene (3B) is an orthorectified product that is projected to a cartographic projection. PlanetScope Ortho Tile (3A) products are orthorectified as individual 25 km × 25 km tiles, and can serve a wide range of applications that need accurate geolocation and cartographic projection. PlanetScope satellite imagery is state-of-the-art optical products with up to 3-m spatial resolution. Unlike other optical satellites, the PlanetScope satellite constellation consists of multiple launches of groups of individual satellites (also called "Doves") with continuous improvements of on-orbit capacity. The complete PlanetScope constellation of about 175 satellites (by 2 April 2018) covers the entire earth's landmass every day, and has a daily collection capacity of about 300 million km^2. PlanetScope Ortho Tile images of the study sites were downloaded from the Planet Explorer Beta website in June 2017. Only images with cloud cover <50% and images acquired between January–May 2017 were used. On average, 13.0 images were available for each location. The minimum number of images per location was four, and the maximum was 24.

2.2.2. RapidEye

RapidEye and PlanetScope imagery products are currently acquired and supplied by the same private company, Planet Labs Inc. RapidEye provides optical imagery from a constellation of five earth-imaging satellites. It has a large area coverage with frequent revisit time (one-day interval), which allows one to get cloud-free images for almost all areas. The images have high spatial (5-m pixel size) resolution. RapidEye image products can be obtained in different forms (RapidEye basic (1B): least processed product; RapidEye Ortho (3A): orthorectified and other required corrections made at individual 25 km × 25 km tiles; and RapidEye Ortho Take (3B): large-scale orthorectified product based on RapidEye Image Takes), depending on the users' needs and image processing capability (Planet, 2017). Recent RapidEye Ortho Take (product level 3B) images of the study sites were obtained from the same source as PlanetScope. Only images with a cloud cover <50% and images from December 2015 to May 2017 were used. The minimum number of images per location was one, and the maximum was 12 images; on average, 4.5 RapidEye images were available for interpretation for each location.

2.2.3. Sentinel-2

Sentinel-2 is owned by the European Space Agency (ESA); it was launched to support activities such as land monitoring, emergency management, security, and climate change issues. In order to fulfill such objectives, the mission was designed in such a way that it has high revisit frequency (five days at the equator), high spatial resolution (up to 10 m in some bands), and having wider swath (290 km). It has been providing unprecedented freely available data to the public since June 2015. The Sentinel-2 product level 2A images (Table 2) used for this study were also downloaded from the Planet Explorer Beta. Only images with a cloud cover <50% and images from December 2016 to May 2017 were used. The average number of Sentinel-2 images available for interpretation at each location was 5.6 with a range from two to 10 images.

Table 2. Satellite images used in this study.

Satellite	Spatial Resolution (m)	Product Level
Planet Scope	3	3B
RapidEye	5	3B
Sentinel-2	10	2A

2.3. Data Collection Techniques

For each of the seven sites, a 3 km × 3 km grid of systematically distributed points were prepared and overlaid the images. This resulted in 228 sample points within each site. Systematic sampling design was used because of its potential to uniformly cover the entire sites and thereby produce more precise estimates [15]. Each of the two observers interpreted a total of 4788 observation points (228 observation points per site per image type × seven sites × three image types). Having the grid point at the center, a square of 0.5 ha (about 70 m × 70 m) was created for all of the 228 grid points within each site. This cell layer was the unit of interpretation of the LULC class. This cell size was chosen to match with the minimum area of the national and FAO definitions of forest. Within these 0.5 ha cells, a systematic grid consisting of 49 squares of 2 m × 2 m in size, was arranged. These small squares were used in the visual interpretation to observe the presence/absence of tree crowns, and then used for canopy cover determination. The canopy cover of a single cell of 0.5 ha was determined using the count of points that coincided with the crowns of trees divided by 49. The images were clipped to 1 km × 1 km tiles for each of the 228 points, and centered at each point to have a better overview of the surrounding land cover during the interpretation. A package was written in R language to develop a graphical user interface that was used to display images for each point in a completely randomized manner, and record and save the results of the image interpretation. The 0.5-ha cell with 49 grid points was enabled to be zoomed in and displayed together with the clipped image (Figure 2). In addition, the land-cover type, time of acquisition for the selected image, and elapsed time (time from launching a location to saving results) were recorded.

A given LULC type within the 0.5 ha was determined visually based on the IPCC definitions of LULC categories [15] i.e., forest land, cropland, grassland, wetland, settlements, and other land; see the IPCC guidelines for details. The thresholds for forest land were 0.5 ha area and 20% canopy cover in the current study. Furthermore, interpretation decisions were made following a hierarchy of rules [34] (Figure 3). The proportions of points that fell on tree crowns (if any) were determined, regardless of the LULC class types. Among the potential images for interpretation, the newest image was used. Two persons performed the interpretation, and the average of the interpretation results was used in further analyses.

Figure 2. The graphical user interface used for visual image interpretation. (**A**) A window for opening new image and recording the interpreted data; (**B**) 1 km × 1 km image with a point at the center; (**C**) a zoomed into 0.5-ha cell with the 49 points (2 m × 2 m squares).

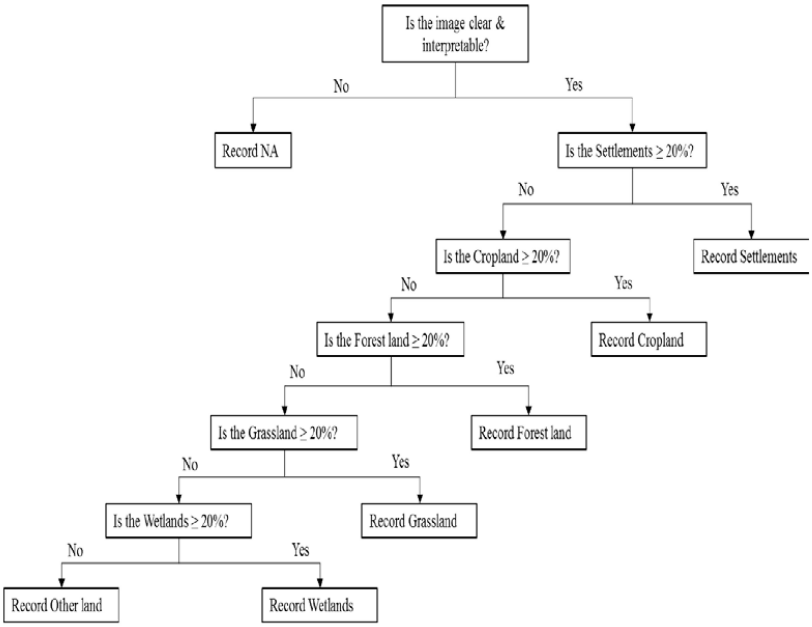

Figure 3. Decision tree based on the hierarchy of rules.

2.4. Estimation

Forest area estimates were computed for the three image types in all seven sites. Observation points were coded as 1 if they were forest and 0 otherwise, and then the mean forest area was estimated using the expression in Equation (1). Canopy cover estimates were also computed for the different image types in the seven respective sites, as well as each LULC class, applying the estimator in Equation (2):

$$\hat{\bar{X}}_i = \frac{\sum_{j=1}^{n} x_{ij}}{n}, \tag{1}$$

where $\hat{\bar{X}}_i$ is the mean forest area estimate of site i; x_{ij} is the proportion of forest area observed in site i at sample point j; and n is the number of observations in a site i.

$$\hat{\bar{Y}}_i = \frac{\sum_{j=1}^{n} y_{ij}}{n}, \tag{2}$$

where $\hat{\bar{Y}}_i$ is the estimated mean canopy cover of site i; and n is the number of observations.

The uncertainty of each estimate was computed using Equations (3) and (4) for forest area and canopy cover, respectively. The standard error (SE) of the mean of each estimate was computed by taking the square root of the error variance. An analysis of variance was then performed to assess the presence of significant differences among the forest area and canopy cover estimates from each image type.

$$\widehat{Var}\left(\hat{\bar{X}}_i\right) = \frac{\sum_{j=1}^{n}\left(x_{ij} - \hat{\bar{X}}_i\right)^2}{n(n-1)}, \tag{3}$$

where $\widehat{Var}\left(\hat{\bar{X}}_i\right)$ is the estimated error variance of the mean forest area estimate of site i.

$$\widehat{Var}\left(\hat{\bar{Y}}_i\right) = \frac{\sum_{j=1}^{n}\left(y_{ij} - \hat{\bar{Y}}_i\right)^2}{n(n-1)}, \quad (4)$$

where $\widehat{Var}\left(\hat{\bar{Y}}_i\right)$ is the error variance of the mean canopy cover estimate of site *i*.

Analysis was carried out on the data that were averaged between the two observers, as given in Table 3.

Table 3. Observation results of forest and non-forest classes from the three image types.

Observation	PlanetScope	RapidEye	Sentinel-2
Forest	819	824	602
Non-Forest	774	772	947
NA *	3	0	47
Total	1596	1596	1596

* Not recorded due to clouds or missing imagery.

In order to assess the effects of the number of observations, bootstrap sampling was carried out for each of the forest area and canopy cover estimates of the three image types and the seven respective sites. Four different resample sizes (m = 50, 100, 150, and 200) were used in the bootstrapping with replacement, and the standard deviation of the boot statistics (Equation (5)), which is an estimate of the standard error [35], was computed and compared with the standard error of the original sample:

$$SE_{boot,\,\bar{x}} = \sqrt{\frac{1}{m-1}\sum\left(\bar{x}* - \frac{1}{m}\sum\bar{x}*\right)^2} \quad (5)$$

where $SE_{boot,\,\bar{x}}$ is the standard error of an estimate, and $\bar{x}*$ is the mean of each resample.

3. Results

3.1. Dates and Time Elapsed for Interpretation

There was a substantial difference between the acquisition dates of the images selected for interpretation for the different image types. For PlanetScope imagery, 85% of the images used were from May 2017, and only 2.4% were from March and earlier. For Sentinel-2 imagery, 51% were from May and April, and only a marginal number were from pre-2017 (<1%). Meanwhile, for RapidEye, none of the images interpreted was from April and May 2017, and only 23% were acquired in 2017. However, most of the images were acquired during the dry season (December–May), except for 13% of the images from RapidEye, which were acquired in October and November. There was no identified effect of any differences in the time of acquisitions.

On average, 83 s were used for each location to record the LULC class and canopy coverage. The difference between RapidEye and Sentinel-2 was minor (68 s versus 73 s), while for PlanetScope, 107 s on average were needed to carry out the interpretation for each location. The seven sites were forming three clusters with respect to time consumption. The time consumption for the three groups were 67–75 s (sites A, F, and G), 87–89 s (sites C, D, and E) and 103 s (site B).

3.2. Forest Area Estimation

Mean forest area estimates from the three image types for all of the study sites are displayed in Figure 4. Sites B, D, and E were the three densely forested sites with estimated proportions of forest area of 0.89, 0.77, and 0.60 from PlanetScope, 0.88, 0.76, and 0.56 from RapidEye, and 0.55, 0.48, and 0.41 from Sentinel-2, respectively. On the other hand, site F has the least forest cover, with an estimated proportion of forest area of 0.03, 0.07, and 0.05 from the PlanetScope, RapidEye, and

Sentinel-2 images, respectively. Forest area estimates from PlanetScope and RapidEye images showed similarities consistently over the seven study sites, although there were marginal differences, where estimates from RapidEye image were smaller in most cases. The estimates from Sentinel-2 images differed from the other two image types in most of the study sites, and these differences in mean forest area were much larger and statistically significant ($p < 0.01$) for sites B, D, E, and G. However, the magnitude of the differences in mean forest area estimates decreased as the overall forest cover of the sites decreased. Thus, no significant differences were observed among the different image types for the three study sites A, C, and F, which had relatively smaller forest cover. It appears that when an area has a small proportion of forest such as sites A, C, and F, Sentinel-2 images, having relatively coarser resolution than PlanetScope and RapidEye images, would produce a reasonably comparable estimate.

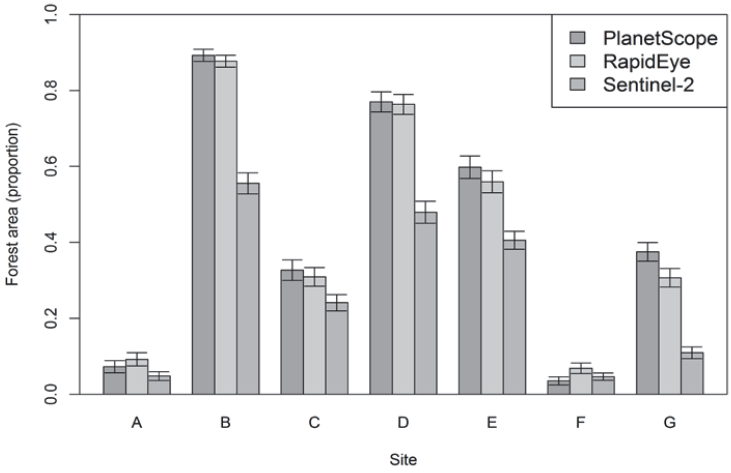

Figure 4. Forest area (proportion) estimates from PlanetScope, RapidEye, and Sentinel-2 images for each study site (A–G). Error bars represent the estimated standard error of the mean.

3.3. Canopy Cover Estimation

Estimates of proportions of canopy cover from the three image types for all of the study sites are shown in Figure 5 and for LULC classes in Figure 6. The largest canopy cover estimate was recorded for site B as 0.59, 0.56, and 0.34 using PlanetScope, RapidEye, and Sentinel-2 images, respectively. By contrast, site F showed the smallest estimates of all of the sites with canopy cover estimates of 0.05, 0.09, and 0.07 from PlanetScope, RapidEye, and Sentinel-2 images. Estimates from PlanetScope and RapidEye images again appeared to be comparable, with a slightly larger difference between them than those of the forest area estimates. Nevertheless, no statistically significant difference was seen in any site between the two software packages. In sites A, C, and F, all of which had less forest cover, Sentinel-2 produced quite similar estimates to the other image types. In contrast, in sites B, D, E, and G, which had large forest cover where one also could expect large canopy cover, the estimates from Sentinel-2 significantly varied ($p < 0.01$) from the rest. This shows that the estimates from Sentinel-2 images provided smaller canopy cover values where forests tended to be denser compared to PlanetScope and RapidEye. In terms of overall performance, when taking into account the magnitude of the standard errors of canopy cover estimates of all of the sites, although the differences were not that big, PlanetScope seemed to produce a precise estimate since it on average had the smallest value, whereas RapidEye and Sentinel-2 resulted in slightly less precise estimates (Figure 7).

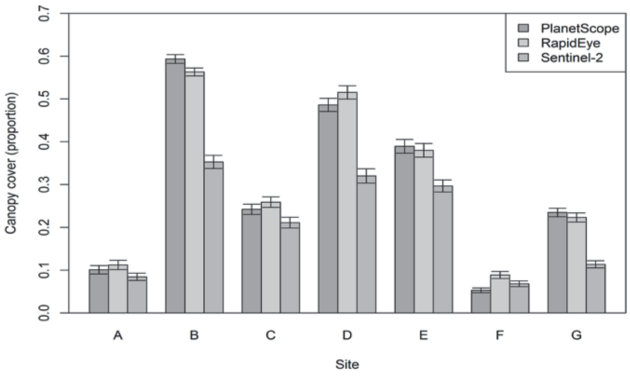

Figure 5. Canopy cover (proportion) estimates from PlanetScope, RapidEye, and Sentinel-2 images for each study site (A–G). Error bars represent the estimated standard error of the mean.

When analyses of estimates of tree canopy cover were carried out for each LULC class using the three image types (Figure 6) the largest proportion of canopy cover estimate was, as expected, obtained in the Forest land category, with a magnitude of 0.57 from PlanetScope, 0.59 from RapidEye, and 0.58 from the Sentinel-2 images. According to the estimates from PlanetScope, Settlements (0.10), Cropland (0.09), and Grassland (0.08) were the second, third, and fourth LULC classes in terms of their canopy coverage. Within each LULC class, the different image types resulted in estimates that were very similar to each other except for the Settlements, Wetlands, and Other land classes. However, even in these classes, the differences were not significant in the statistical sense. It seems that if a given LULC class is a homogenous one such as Forest land, Cropland, or Grassland, then any of these images could produce reasonably comparable estimates of canopy cover. Whereas on the contrary, in heterogeneous LULC scenarios, coarser resolution images tended to either overestimate or underestimate canopy cover as compared with estimates from finer resolution images. Considering overall standard errors for each image type, it was observed that PlanetScope resulted in a smaller overall variability, showing a better precision of estimates, whereas the largest variability of estimates was seen for RapidEye (Figure 7).

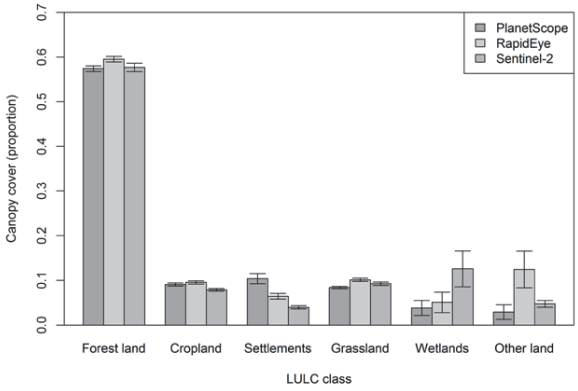

Figure 6. Canopy cover (proportion) estimates from PlanetScope, RapidEye, and Sentinel-2 images by land-use and land-cover (LULC) classes. Error bars represent the estimated standard error of the mean.

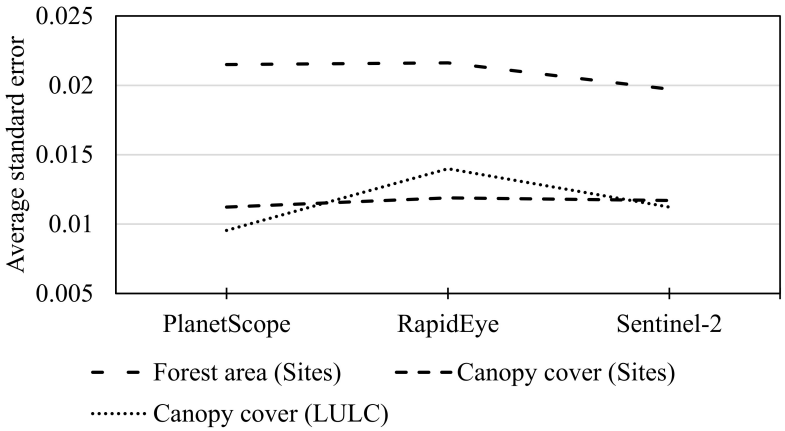

Figure 7. Average standard error for forest area and canopy cover estimates by sites as well as for canopy cover estimates by LULC classes from the three image types.

3.4. Optimal Sample Size Determination

The results from the bootstrapping showed increasing standard errors as the sample size decreased for both forest area and canopy cover estimates, regardless of site and image type (Figure 8). Resampling with a sample size of 200 observations resulted in estimates that were very close to the original sample size of 228, followed by 150, 100, and 50 as the second, third, and fourth closest estimates, respectively. On average, the increase in standard error when using 200 instead of 228 sample observations was 6.7%, 6.5%, and 4.9% for forest area and 8.7%, 6.0%, and 4.2% for canopy cover estimates from PlanetScope, RapidEye, and Sentinel-2, respectively. Similarly, samples of 150 observations on average generated estimates with a standard error inflation of less than 24.0% for all of the image types and both forest area and canopy cover estimations. Furthermore, when the sample size was reduced to 100 observations, the standard error increased almost by 50%.

The standard errors were consistently smaller for site F than for the rest of the study sites. In addition, the standard error values of sites A and F were entirely below the average curve, while those of sites D and E were constantly above the average curve for both the forest area and canopy cover estimates of the three image types (Figure 8). Reducing the sample size to only 50 observations resulted in a steeper curve and increased the standard errors by more than 100% in all of the cases. In general, considering the sample sizes, overall estimates of PlanetScope and RapidEye were found to be less sensitive to the reduction of sample size for forest area and canopy cover estimations, and the ranges of percentage increment across the sites were smaller in each respective case. Meanwhile, the Sentinel-2 estimates were highly sensitive in both cases with larger range values across the sites, regardless of having some smaller values.

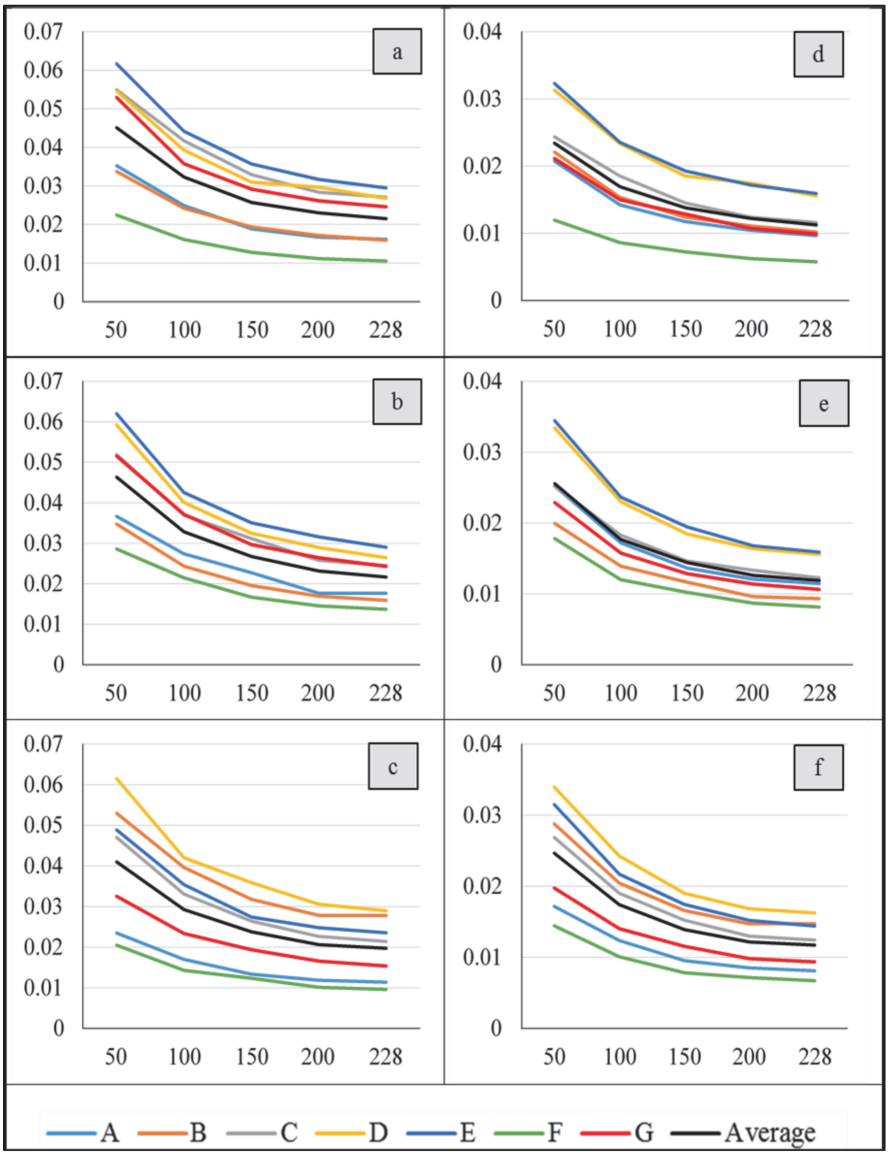

Figure 8. Standard error (*y*-axis) for forest area and canopy cover estimates in connection with sample size (*x*-axis). The results were determined through bootstrapping, except for 228 obtained from the original sample. (**a**–**c**) are for forest area; and (**d**–**f**) are for canopy cover estimates from PlanetScope, RapidEye, and Sentinel-2 images, respectively.

4. Discussion

4.1. Visual Image Interpretation in a REDD+ MRV

Visual image interpretation was adopted in this study to estimate the proportion of forest area and crown cover in seven subjectively selected sites in Ethiopia that have different forest and

vegetation types. Satellite images of PlanetScope, RapidEye, and Sentinel-2 were examined for their performance of producing estimates of forest area and canopy cover across the variety of site conditions. In addition, the study evaluated how sample size affected the uncertainty of the estimates from different image types.

The proportion of forest cover within an area of interest can be used to estimate the area of the forest by multiplying it with the total size of the area. Such information are of paramount importance for LULC change analysis as well as the quantification of emissions and removals for REDD+ activities [23,36]. Likewise, canopy cover information is used in several forest management applications. For instance, it serves as an important ecological indicator such as for habitat, microclimate, and light condition assessment [18], and it is used as a criterion in forest definitions [17].

In the current study, it was possible to record data representing 390 km^2 per hour on average. Meanwhile, for field surveys, only moving to a field plot representing 9 km^2 could be difficult within the same amount of time. Thus, the efficiency of visual interpretation is the major advantage. However, a disadvantage is the amount of subjectivity that is allowed in the interpretation. In this study, the average interpretation between two interpreters was used. However, if multiple interpreters are available, the difference between them could be calculated and thus calibrated for. Hence, multiple interpreters can mitigate systematic errors occurring due to individual decisions. In addition, it is problematic that the interpreted value could also have errors when trained and experienced interpreters are carrying out the work. Experience form Tanzania showed that tree cover and the amount of woody biomass is not necessarily a good indicator of land-use or land-cover classification in field [37]. Thus, a major confine of the current study is that we did not have any ground-measured value. However, indicating that differences between the imagery exist is important. A natural assumption is that higher resolution imageries provide a more accurate interpretation.

In this study, design-based estimates were the focus, and only the interpretations for the observation points were used to create estimates. The next step for implementing REDD+ MRV could be to include complete cover information e.g., from PlanetScope, RapidEye, or Sentinel, and combine the complete cover information with the interpretations making a wall-to-wall map that can be used in model-assisted estimation [37,38]. This will be a natural extension of the current study, as capacity building are taking place in the REDD+ countries.

4.2. Factors Influencing Estimates

Proportions of forest area estimated using PlanetScope and RapidEye images were very similar across the seven sites, regardless of their differences in spatial resolution. On the other hand, estimates from Sentinel-2 images for most of the sites differed significantly from those of both PlanetScope and RapidEye images. Exactly the same pattern of similarities and differences occurred as well for canopy cover estimates. It seemed that PlanetScope and RapidEye estimates were robust and capable of producing reliable results in different biomes with different forest types and magnitudes of forest coverage. However, the performance of Sentinel-2 images seemed to be dependent on the magnitude of forest cover. It produced similar estimates to those of PlanetScope and RapidEye for areas with less forest cover, and varied as the forest cover of the area increased. Each land-cover category has its own property that needs to be considered when selecting methods, including the images to be used for land-cover classification and mapping [39]. Accordingly, the discrepancy among estimates from these image types is perhaps due to a number of factors, one of which is the differences in the resolution of the images. Draksler [40] investigated the effect of satellite image resolution and minimum mapping unit on the accuracy of forest cover mapping in two different sites using RapidEye, Sentinel-2, and Landsat-8, and reported a declining trend in overall accuracy as the resolution got coarser. A similar trend was reported by Churches et al. [41], who compared forest cover estimates of Haiti using different satellite images.

Another factor contributing to the differences could be missing data, which will reduce the number of observations and hence affect the quality of estimates [42]. Most of the missing data during

image interpretation (NAs) were recorded for Sentinel-2 images (Table 3). Out of the total NAs in Sentinel-2, more than 70% were in sites B and D. These are the sites that are known to have denser forest cover and be accompanied by the presence of heavy cloud cover during most of the year. Therefore, its relatively coarser resolution coupled with the cloud cover might have affected the interpretation result, since it failed to sufficiently capture the existing variability within the study sites. The revisit frequency also directly influences the availability at cloudy locations. The frequent revisits of PlanetScope is highly favorable for REDD+ MRV, since 85% of the images used for the interpretations were acquired within a time period of one month, May 2017, while for RapidEye and Sentinel-2, a maximum of 34% and 40% of the images originated from one single month, respectively.

The majority of the images used for interpretation was acquired during the dry season. One reason for this is that cloud coverage is smaller in this season compared with the rainy season. It is likely that the phenology of the trees and other vegetation influences the interpretation. A tree crown with more leaves could potentially lead to a larger interpreted crown cover compared with when the tree has less or no leaves. The design of this study did not provide data to analyze the effect of seasonality in a statistical sense.

Satellite imagery used for the visual interpretation of forest area and canopy cover should be carefully selected. For low-density forest areas, say, somewhere below 30% canopy cover, Sentinel-2 images may be safely used, whereas for denser forest areas, higher resolution images such as PlanetScope and RapidEye should be considered. Of course, the choice may depend on the purpose of the study and available resources. To reduce costs, sampling instead of large-scale wall-to-wall observation could be used [43,44]. The method used in this study is such an alternative to obtain reliable estimates at a lower cost of image procurement, especially for dense forest areas where low-resolution images have deficiencies, and the quality of information pays off.

4.3. Sample Size

When resources allocated for data collection are limited, it is important also to apply appropriate sampling designs and use adequate sampling intensities [45,46]. Hence, it would be necessary to look for and determine optimal sample sizes that will result in a precise estimate with the possible minimum resource [45]. The bootstrapping technique allowed us to repeatedly sample from a given set of observations and assess the uncertainty of an estimate under certain circumstances, such as for example with different sample sizes, as in our case. As indicated in Figure 8, the precision of the estimates is sensitive to changes in the number of observations in the sample. The sensitivity also differs depending on the parameter of interest to be estimated as well as the types of images to be used. Hence, depending on the purpose of the study, the available resources, and the precisions that are required, one may decide on the number of observations accordingly. From the analysis of sample size in the current study, it seems possible to reduce the sample size slightly without substantially affecting the obtained accuracy. Perhaps a sample plot spacing of 3.5 km or 4 km between sample locations could have been considered.

5. Conclusions

Forest area and canopy cover estimates are among the most essential information in any forest management practice. One of the approaches to derive such information is through visual image interpretation techniques using satellite images. The technique is particularly quick, less costly, and helpful when the technical capacities to use digital image classification and mapping are limited. In this study, visual image interpretation was applied, and the use of PlanetScope, RapidEye, and Sentinel-2 satellite images for forest area and canopy cover estimation was evaluated. PlanetScope and RapidEye images produced similar estimates for all of the study sites and all of the LULC classes. Sentinel-2 image estimates varied significantly from the two other types of images in study sites with relatively denser forest cover, but resulted in similar estimates in sites with less dense forests. In visual image interpretation practices, very high-resolution images should be given priority. The choice of

image type can be influenced by the condition of the forest on the ground as well as the costs of the images. In case of using expensive and very high-resolution images, a sampling approach could reduce the overall costs compared to wall-to-wall acquisitions. Furthermore, the precision of the estimate is dependent on the sample size. Therefore, by taking the purpose of the assessment as well as the available resources into account, one should aim for sample sizes that balance the inventory costs and the required precision of an estimate.

Author Contributions: Z.A. and H.T. performed the experiments, analyzed the data and wrote the paper; H.O.Ø. conceived and designed the experiments, supervised all the research work that led to this paper and reviewed the manuscript; T.G. supervised the research work that led to this paper and reviewed the manuscript; I.B. reviewed the manuscript; E.N. provided inputs to the experiments and reviewed the manuscript.

Funding: The first and second authors of the study are funded as a Ph.D. student by the Norwegian Government through support of the project "National MRV capacity Building towards Climate Resilient Development in Ethiopia".

Acknowledgments: Special thanks should go to the Norwegian University of Life Sciences and Wondo Genet College of Forestry and Natural Resources (Hawassa University). The authors would also like to thank the Planet Company for allowing to freely download and use PlanetScope and RapidEye images in this study.

Conflicts of Interest: The founding sponsors had no role in the design of the study; in the collection, analyses, or interpretation of data; in the writing of the manuscript, and in the decision to publish the results.

References

1. Dudley, N.; Stolton, S. Running Pure: The Importance of Forest Protected Areas to Drinking Water. World Bank/WWF Alliance for Forest Conservation and Sustainable Use, 2003. Available online: http://d2ouvy59p0dg6k.cloudfront.net/downloads/runningpurereport.pdf (accessed 16 November 2017).
2. McMahon, P. A Burning Issue: Tropical Forests and the Health of Global Ecosystems. In *Challenges and Opportunities for the World's Forests in the 21st Century*; Fenning, T., Ed.; Springer: Dordrecht, The Netherlands, 2014; pp. 23–35.
3. Le Quéré, C.; Raupach, M.R.; Canadell, J.G.; Marland, G.; Bopp, L.; Ciais, P.; Conway, T.J.; Doney, S.C.; Feely, R.A.; Foster, P.; et al. Trends in the sources and sinks of carbon dioxide. *Nat. Geosci.* **2009**, *2*, 831–836.
4. Canadell, J.G.; Le Quéré, C.; Raupach, M.R.; Field, C.B.; Buitenhuis, E.T.; Ciais, P.; Conway, T.J.; Gillett, N.P.; Houghton, R.A.; Marland, G. Contributions to accelerating atmospheric CO_2 growth from economic activity, carbon intensity, and efficiency of natural sinks. *Proc. Natl. Acad. Sci. USA* **2007**, *104*, 18866–18870. [CrossRef] [PubMed]
5. Pan, Y.; Birdsey, R.A.; Fang, J.; Houghton, R.; Kauppi, P.E.; Kurz, W.A.; Phillips, O.L.; Shvidenko, A.; Lewis, S.L.; Canadell, J.G.; et al. A large and persistent carbon sink in the world's forests. *Science* **2011**, *333*, 988–993. [CrossRef] [PubMed]
6. Baccini, A.; Friedl, M.A.; Woodcock, C.E.; Warbington, R. Forest biomass estimation over regional scales using multisource data. *Geophys. Res. Lett.* **2004**, *31*, L10501. [CrossRef]
7. Kim, D.-H.; Sexton, J.O.; Townshend, J.R. Accelerated Deforestation in the Humid Tropics from the 1990s to the 2000s. *Geophys. Res. Lett.* **2015**. [CrossRef] [PubMed]
8. Van der Werf, G.R.; Morton, D.C.; DeFries, R.S.; Olivier, J.G.J.; Kasibhatla, P.S.; Jackson, R.B.; Collatz, G.J.; Randerson, J.T. CO_2 emissions from forest loss. *Nat. Geosci.* **2009**, *2*, 737–738. [CrossRef]
9. Noriko, H.; Martin, H.; Veronique De, S.; Ruth, S.D.F.; Maria, B.; Louis, V.; Arild, A.; Erika, R. An assessment of deforestation and forest degradation drivers in developing countries. *Environ. Res. Lett.* **2012**, *7*, 044009. [CrossRef]
10. Pohjonen, V.; Pukkala, T. Eucalyptus globulus in Ethiopian forestry. *For. Ecol. Manag.* **1990**, *36*, 19–31. [CrossRef]
11. Bishaw, B. Deforestation and Land Degradation in the Ethiopian Highlands: A Strategy for Physical Recovery. *Northeast Afr. Stud.* **2001**, *8*, 7–25. [CrossRef]
12. McCann, J.C. The Plow and the Forest: Narratives of Deforestation in Ethiopia, 1840–1992. *Environ. Hist.* **1997**, *2*, 138–159. [CrossRef]

13. Kindu, M.; Schneider, T.; Teketay, D.; Knoke, T. Land Use/Land Cover Change Analysis Using Object-Based Classification Approach in Munessa-Shashemene Landscape of the Ethiopian Highlands. *Remote Sens.* **2013**, *5*, 2411–2435. [CrossRef]
14. Hailemariam, S.N.; Soromessa, T.; Teketay, D. Land Use and Land Cover Change in the Bale Mountain Eco-Region of Ethiopia during 1985 to 2015. *Land* **2016**, *5*, 41. [CrossRef]
15. Penman, J.; Gytarsky, M.; Hiraishi, T.; Krug, T.; Kruger, D.; Pipatti, R.; Buendia, L.; Miwa, K.; Ngara, T.; Tanabe, K.; et al. *Good Practice Guidance for Land Use, Land-Use Change and Forestry*; IPCC: Geneva, Switzerland, 2003.
16. Chazdon, R.L.; Brancalion, P.H.S.; Laestadius, L.; Bennett-Curry, A.; Buckingham, K.; Kumar, C.; Moll-Rocek, J.; Vieira, I.C.L.G.E.; Wilson, S.J. When is a forest a forest? Forest concepts and definitions in the era of forest and landscape restoration. *Ambio* **2016**, *45*, 538–550. [CrossRef] [PubMed]
17. FAO. *Global Forest Resources Assessment 2000*; Forestry Paper No. 140; UN Food and Agricultural Organization: Rome, Italy, 2001.
18. Jennings, S.B.; Brown, N.D.; Sheil, D. Assessing forest canopies and understorey illumination: Canopy closure, canopy cover and other measures. *Forestry* **1999**, *72*, 59–73. [CrossRef]
19. Gschwantner, T.; Schadauer, K.; Vidal, C.; Lanz, A.; Tomppo, E.; di Cosmo, L.; Robert, N.; Duursma, D.E.; Lawrence, M. Common Tree Definitions for National Forest Inventories in Europe. *Silva Fenn.* **2009**, *43*, 303–321. [CrossRef]
20. Korhonen, L.; Korhonen, K.T.; Rautiainen, M.; Stenberg, P. Estimation of forest canopy cover: A comparison of field measurement techniques. *Silva Fenn.* **2006**, *40*, 577–588. [CrossRef]
21. Mbow, C.; Skole, D.; Dieng, M.; Justice, C.; Kwesha, D.; Mane, L.; El Gamri, M.; Von Vordzogbe, V.; Virji, H. *Challenges and Prospects for REDD+ in Africa: Desk Review of REDD+ Implementation in Africa*; Global Land Project Reports; GLP International Project Office: Copenhagen, Denmark, 2012; Volume 5.
22. Herold, M.; Skutsch, M. Monitoring, reporting and verification for national REDD + programmes: Two proposals. *Environ. Res. Lett.* **2011**, *6*, 014002. [CrossRef]
23. IPCC. *2006 IPCC Guidelines for National Greenhouse Gas Inventories*; IGES: Berlin, Germay, 2006.
24. IPCC. *Land Use, Land Use Change, and Forestry*; Cambridge University Press: Cambridge, UK, 2000.
25. Bey, A.; Díaz, A.S.-P.; Maniatis, D.; Marchi, G.; Mollicone, D.; Ricci, S.; Bastin, J.-F.O.; Moore, R.; Federici, S.; Rezende, M.; et al. Collect Earth: Land Use and Land Cover Assessment through Augmented Visual Interpretation. *Remote Sens.* **2016**, *8*, 807. [CrossRef]
26. Clark, M.L.; Aide, T.M. Virtual Interpretation of Earth Web-Interface Tool (VIEW-IT) for Collecting Land-Use/Land-Cover Reference Data. *Remote Sens.* **2011**, *3*, 601–620. [CrossRef]
27. MEFCC. *Ethiopia's Forest Reference Level Submittssion to the UNFCCC*; Ministry of Environment, Forestry and Climate Change: Addis Ababa, Ethiopia, 2017.
28. Fritz, S.; McCallum, I.; Schill, C.; Perger, C.; See, L.; Schepaschenko, D.; van der Velde, M.; Kraxner, F.; Obersteiner, M. Geo-Wiki: An online platform for improving global land cover. *Environ. Model. Softw.* **2012**, *31*, 110–123. [CrossRef]
29. Fritz, S.; McCallum, I.; Schill, C.; Perger, C.; Grillmayer, R.; Achard, F.; Kraxner, F.; Obersteiner, M. Geo-Wiki.Org: The Use of Crowdsourcing to Improve Global Land Cover. *Remote Sens.* **2009**, *1*, 345–354. [CrossRef]
30. Sannier, C.; McRoberts, R.E.; Fichet, L.-V.; Makaga, E.M.K. Using the regression estimator with Landsat data to estimate proportion forest cover and net proportion deforestation in Gabon. *Remote Sens. Environ.* **2014**, *151*, 138–148. [CrossRef]
31. Potapov, P.V.; Dempewolf, J.; Talero, Y.; Hansen, M.C.; Stehman, S.V.; Vargas, C.; Rojas, E.J.; Castillo, D.; Mendoza, E.; Calderón, A.; et al. National satellite-based humid tropical forest change assessment in Peru in support of REDD+ implementation. *Environ. Res. Lett.* **2014**, *9*, 124012. [CrossRef]
32. Ib, F.; Sebsebe, D.; Breugel, P.V. *Atlas of the Potential Vegetation of Ethiopia*; The Royal Danish Academy of Science and Letters: Copenhagen, Denmark, 2010; Volume 58.
33. Egziabher, T.B.G. Diversity of Ethiopian flora. In *Plant Genetic Resources of Ethiopia*; Engles, J., Hawkes, J.G., Worede, M., Eds.; Cambridge University Press: Cambridge, UK, 1991; pp. 75–81.
34. Martínez, S.; Mollicone, D. From Land Cover to Land Use: A Methodology to Assess Land Use from Remote Sensing Data. *Remote Sens.* **2012**, *4*, 1024–1045. [CrossRef]

35. Hesterberg, T.; Moore, D.S.; Monaghan, S.; Clipson, A.; Epstein, R. Bootstrap methods and permutation tests. In *Introduction to the Practice of Statistics*; W.H. Freeman & Company: New York, NY, USA, 2003.
36. Köhl, M.; Magnussen, S.; Marchetti, M. *Sampling Methods, Remote Sensing and GIS Multiresource Forest Inventory*; Springer: Berlin/Heidelberg, Germany, 2006.
37. Næsset, E.; Ørka, H.O.; Solberg, S.; Bollandsås, O.M.; Hansen, E.H.; Mauya, E.; Zahabu, E.; Malimbwi, R.; Chamuya, N.; Olsson, H.; et al. Mapping and estimating forest area and aboveground biomass in miombo woodlands in Tanzania using data from airborne laser scanning, TanDEM-X, RapidEye, and global forest maps: A comparison of estimated precision. *Remote Sens. Environ.* **2016**, *175*, 282–300. [CrossRef]
38. McRoberts, R.E. Probability- and model-based approaches to inference for proportion forest using satellite imagery as ancillary data. *Remote Sens. Environ.* **2010**, *114*, 1017–1025. [CrossRef]
39. King, R.B. Land cover mapping principles: A return to interpretation fundamentals. *Int. J. Remote Sens.* **2002**, *23*, 3525–3545. [CrossRef]
40. Draksler, A. *The Effect of Satellite Image Resolution and Minimum Mapping Unit on the Accuracy of Forest Cover Maps*; Technische Universität München: Munich, Germany, 2017.
41. Churches, C.E.; Wampler, P.J.; Sun, W.; Smith, A.J. Evaluation of forest cover estimates for Haiti using supervised classification of Landsat data. *Int. J. Appl. Earth Obs. Geoinf.* **2014**, *30*, 203–216. [CrossRef]
42. Lohr, S. *Sampling: Design and Analysis*; Nelson Education: Scarborough, ON, Canada, 2009.
43. Böttcher, H.; Eisbrenner, K.; Fritz, S.; Kindermann, G.; Kraxner, F.; McCallum, I.; Obersteiner, M. An assessment of monitoring requirements and costs of 'Reduced Emissions from Deforestation and Degradation'. *Carbon Balanc. Manag.* **2009**, *4*, 14. [CrossRef] [PubMed]
44. Falkowski, M.J.; Wulder, M.A.; White, J.C.; Gillis, M.D. Supporting large-area, sample-based forest inventories with very high spatial resolution satellite imagery. *Prog. Phys. Geogr.* **2009**, *33*, 403–423. [CrossRef]
45. Jayaraman, K. A Statistical Manual for Forestry Research. FORSPA, 2000. Available online: http://www.fao.org/3/a-x6831e.pdf (accessed on 10 November 2017).
46. Lenth, R.V. Some Practical Guidelines for Effective Sample Size Determination. *Am. Stat.* **2001**, *55*, 187–193. [CrossRef]

PAPER-III

remote sensing

MDPI

Article

Use of Remotely Sensed Data to Enhance Estimation of Aboveground Biomass for the Dry Afromontane Forest in South-Central Ethiopia

Habitamu Taddese [1,2,*], Zerihun Asrat [2,3], Ingunn Burud [1], Terje Gobakken [3], Hans Ole Ørka [3], Øystein B. Dick [1] and Erik Næsset [3]

1 Faculty of Science and Technology, Norwegian University of Life Sciences, P.O. Box 5003, 1432 Ås, Norway; ingunn.burud@nmbu.no (I.B.); oystein.dick@nmbu.no (Ø.B.D.)
2 Wondo Genet College of Forestry and Natural Resources, Hawassa University, P.O. Box 128, Shashemene 3870006, Ethiopia; zerihun.asrat.kutie@nmbu.no
3 Faculty Environmental Sciences and Natural Resource Management, Norwegian University of Life Sciences, P.O. Box 5003, 1432 Ås, Norway; terje.gobakken@nmbu.no (T.G.); hansole.orka@nmbu.no (H.O.Ø.); erik.naesset@nmbu.no (E.N.)
* Correspondence: habitamu.taddese.berie@nmbu.no; Tel.: +47-4671-8534

Received: 31 July 2020; Accepted: 11 October 2020; Published: 13 October 2020

Abstract: Periodic assessment of forest aboveground biomass (AGB) is essential to regulate the impacts of the changing climate. However, AGB estimation using field-based sample survey (FBSS) has limited precision due to cost and accessibility constraints. Fortunately, remote sensing technologies assist to improve AGB estimation precisions. Thus, this study assessed the role of remotely sensed (RS) data in improving the precision of AGB estimation in an Afromontane forest in south-central Ethiopia. The research objectives were to identify RS variables that are useful for estimating AGB and evaluate the extent of improvement in the precision of the remote sensing-assisted AGB estimates beyond the precision of a pure FBSS. Reference AGB data for model calibration and estimation were collected from 111 systematically distributed circular sample plots (SPs) of 1000 m^2 area. Independent variables were derived from Landsat-8, Sentinel-2 and PlanetScope images acquired in January 2019. The area-weighted mean and standard deviation of the spectral reflectance, spectral index and texture (only for PlanetScope) variables were extracted for each SP. A maximum of two independent variables from each image type was fitted to a generalized linear model for AGB estimation using model-assisted estimators. The results of this study revealed that the Landsat-8 model with the predictor variable of shortwave infrared band reflectance and the PlanetScope model with the predictor variable of green band reflectance had estimation efficiency of 1.40 and 1.37, respectively. Similarly, the Sentinel-2 model, which had predictor variables of shortwave infrared reflectance and standard deviation of green leaf index, improved AGB estimation with the relative efficiency of 1.68. Utilizing freely available Sentinel-2 data seems to enhance the AGB estimation efficiency and reduce cost and extensive fieldwork in inaccessible areas.

Keywords: aboveground biomass; Sentinel-2; generalized linear model; model-assisted estimation; relative efficiency

1. Introduction

Forests are paramount in regulating the global environment, mainly through sequestering carbon [1]. They are particularly important these days to combat the changing climate, which affects people's lives in many aspects. Due to the multiple significance of forest resources, information about the resource base, its spatial distribution and spatio-temporal changes have become a global

concern. The information is a basis to make decisions when planning and assessing impacts regarding mitigation and adaptation to global climate change [2–4]. Following a series of international dialogues, the conference of the parties to the United Nations Framework Convention on Climate Change (UNFCCC) has passed several decisions to combat the impacts of climate change through sequestering carbon in the living biomass, which mainly includes forests. Incentivizing the REDD+ (Reducing Emission from Deforestation and Forest Degradation, Sustainable Forest Management and Conservation) programs was one of the main issues in the Paris agreement in 2015 [4]. All these programs, initiatives and treaties require information about the resource stock and trends of changes over time.

Many forest types, which the dry Afromontane forest type is one of them, contribute to the REDD+ programs through storing carbon for mitigating the impacts of climate change. The dry Afromontane forests in Ethiopia are attributed to areas with an altitude range from 1500 to 3400 m above sea level; mean annual temperature of 14–25 °C; and mean annual precipitation of 400–1700 mm [5]. These forests are of great ecological and economic importance [6,7]. They contribute to the national and international initiatives towards biodiversity conservation, soil erosion control and the mitigation of the global climate change [6]. Although these forests are important forest types in Ethiopia and have various benefits [8], they are under pressure from the local community for expansion of agriculture, settlement and fuelwood collection [7,9].

Among the forest variables, aboveground biomass (AGB) estimation is of great importance due to its multiple uses. AGB of trees is the weight of all living materials of trees above the soil surface including the stem, stump, branches, bark, seeds and leaves. A change in AGB stock can be used to monitor forest dynamics. AGB estimates, which can be converted to carbon stock estimates, are required in forest management, particularly in the implementation of the REDD+ programs that are underway in Ethiopia. Despite growing requirements for a precise estimation and timely reporting, the current tradition of measurement, monitoring and change estimation for forest resources in Ethiopia relies mainly on field-based sample surveys (FBSSs). These methods are not suitable for biomass monitoring in large areas. The FBSS methods are constrained by high costs, logistical challenges and limited field access [10]. As a result, many of the national forest inventory programs in developing countries including Ethiopia are dependent on field inventories conducted with relatively small sample sizes and thus, have high uncertainties in the estimates [11]. Studies about uncertainties of emission reduction in Ethiopia indicated that the estimates based on FBSSs with small sample size are not sufficiently precise to support decision-making [12]. The sources of uncertainties for biomass estimation using remotely sensed (RS) data can be tree measurement, allometric models or RS-based model predictions. Therefore, it is important to look for alternative approaches that can reduce costs and contribute to improving the precision of estimates from pure FBSSs.

In recent years, RS data and associated estimation techniques have become viable options to support quantification of resource stocks cost-effectively in areas inaccessible for FBSS [13–15]. Previous research has shown that RS data can help reducing FBSS efforts without loss of precision of estimates [16]. Following the improvements in RS data and technologies, there are many sources of useful satellite RS data for estimation of forest variables including AGB. Landsat and Sentinel are examples of such satellite programs, which provide freely available data [17,18]. Images of Landsat-8 (L8) and Sentinel-2 (S2) are useful for AGB estimation in various forest ecosystems [19–23]. However, data with higher spatial resolution are often considered better [24,25]. PlanetScope (PS) images are among potentially applicable commercial satellite RS data, which have 3 m spatial resolution and been acquired daily. These image characteristics make the PS data suitable for REDD+ MRV (measurement, reporting and verification) systems [25]. Compared to the L8 and S2 images, fewer studies have been carried out on biomass estimation using the PS images [26].

Various studies used either spectral band (SB) reflectance, spectral indices (SIs) or texture variables solely or in combination for AGB modelling. For example, a study by [27] on AGB estimation using Landsat TM data in the Brazilian Amazon indicated that a combination of SB and texture variables

improved AGB estimation. The study showed the importance of texture information particularly in primary forests, which have complex canopy structures. The most commonly used SBs that correlate strongly with AGB, particularly in forests with simple stand structure, are the visible, near-infrared and shortwave infrared bands (e.g., [27,28]).

Existing scientific works found that some types of SIs contribute greatly to AGB estimation in different forest types. A study of AGB estimation using Landsat images in Northwestern Turkey revealed that SIs were better in estimating AGB in that forest type as compared to SB reflectance [29]. However, the sensitivity of SIs to biomass vary between environments and forest types [30–33]. According to the research findings by [30] in India, a significant correlation was observed between AGB and simple ratio (SR), difference vegetation index (DVI), normalized difference vegetation index (NDVI), soil adjusted vegetation index (SAVI) and modified soil adjusted vegetation index (MSAVI). Gizachew et al. [19] found that NDVI, enhance vegetation index (EVI), SAVI, MSAVI, and normalized difference moisture index (NDMI) had significant correlations with total AGB in the Miombo woodlands of Tanzania. Furthermore, atmospherically resistant vegetation index (ARVI) of L8 imagery was used for AGB estimation in Mount Tai, China [22]. A similar study in southern Portugal indicated that SIs are useful as predictors of AGB [34]. Imran et al. [35] in their study in Pakistan found that red-edge normalized difference vegetation index (RENDVI) had greater correlation with AGB than the individual SBs. Together with other SIs mentioned above, the red-edge simple ratio (SRRE) index was used for estimating AGB of mangrove forest in the Philippines [26]. Motohka et al. [36] studied the normalized difference green index (NDGI) as a good phenological indicator of various ecosystems in Japan. According to the study by [37], data collected using unmanned aerial vehicles for monitoring the post-fire recovery of pine forests in the Mediterranean areas indicated excessive green index (ExGI) as a useful variable for estimating diameter at breast height (DBH), which is a default predictor of AGB allometry. In another study, ExGI was used for discriminating vegetation types in the USA and Canada [38]. Furthermore, SIs that are indicators of leaf greenness and used in different applications including crop monitoring and discriminating vegetation types, like the green leaf index (GLI) and vegetation index (VI), were included in the current list of potential predictor variables to test if they relate to AGB. See Table 2 for detailed descriptions of the SIs explored in this study.

The other group of potentially useful variables for AGB estimation are the texture data derived from the high-resolution PS images. These variables describe the role of pixel resolution in identifying spatial variations of image values. The texture information of L8 and S2 images were not used due to the coarser resolution of these images as compared to the PS images. Several studies indicated that image texture variables could improve AGB estimation, especially in dense tropical forests [22,27,39]. The most common method of calculating image texture variables is the grey level co-occurrence matrix (GLCM). Table 3 shows how the GLCM variables were calculated.

Some studies (e.g., [16,19,40]) evaluated the use of RS data for biomass estimation in small study areas in the region of east Africa. However, to the best of our knowledge, except some efforts related to the use of Landsat images for land cover classification and mapping, data from the mentioned satellite missions subject to analysis in the current study have never been used to assess AGB of the dry Afromontane forests in Ethiopia.

Because there is little current experience with what types of variables extracted from the satellite systems in question that would be useful for AGB modelling in this forest type, the first objective of this study was to explore what kind of variables extracted from the different satellite programs might be useful for AGB modelling in the dry Afromontane forest. The second objective was to evaluate to what extent such RS data could help improving the precision of AGB estimates beyond the precision of a pure FBSS in these forests.

2. Materials and Methods

2.1. Description of the Study Area

The study was conducted in the Degaga-Gambo forest in south-central Ethiopia. It belongs to a state-owned enterprise, Oromia Forest and Wildlife. The study area is located on the eastern escarpment of the central rift valley of Ethiopia, in the Horn of Africa (Figure 1). It extends geographically from 38°45′ to 38°56′ E longitude and from 7°13′ to 7°33′ N latitude. The forest has an area of 14,176 ha. The altitude of the study area ranges from 2100 to 2730 m above sea level. The study area has a bimodal rainfall distribution. The main rainy season is from July to September while the short rainy season is from March to May [41]. The mean annual precipitation and temperature in the area are 1245 mm and 14.9 °C, respectively.

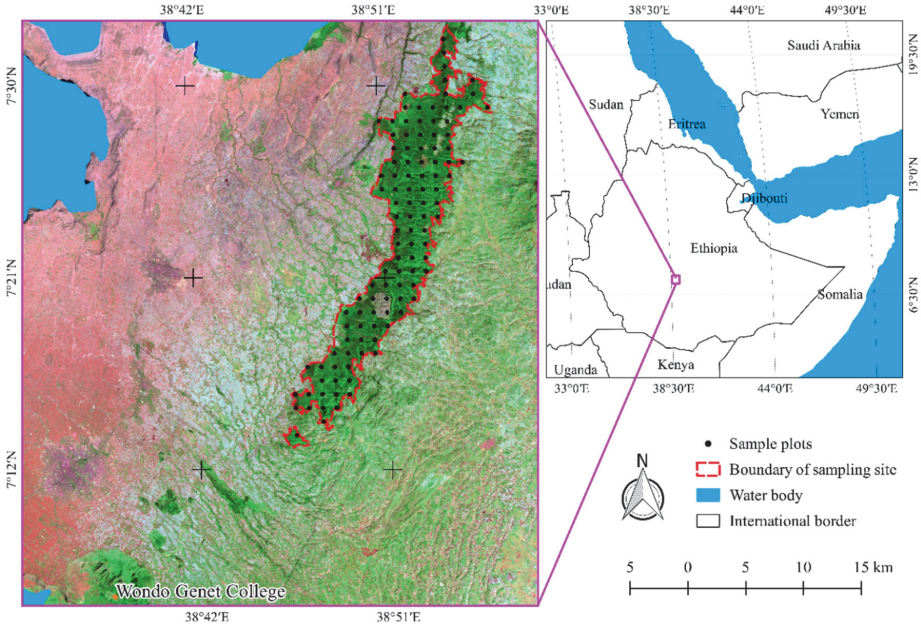

Figure 1. Location of the study area and distribution of the field sample plots (SPs). A band combination of SWIR-NIR-R (in the order of R-G-B) of L8 image was used to enhance the appearance of vegetated areas (in green).

The forest area has both natural and plantation forest types. The major species of plantation forest compartments, which are mostly found in the lower elevations, are *Cupressus lucitanica*, *Pinus patula*, *Grevillea robusta* and different *Eucalyptus* species. The natural forest has high tree species diversity. The dominant tree species observed in the natural forest include *Syzygium guineense*, *Afrocarpus falcatus*, *Juniperus procera*, *Pitosporum viridiflorum*, *Maesa lanceolate*, *Millettia ferruginea*, *Croton macrostachyus* and *Maytenus arbutifolia*. The objectives of the enterprise are the production of lumber and poles from the plantations and conserving the natural forests. The natural forests are home to a wide range of wildlife species and are sources of water for the downstream areas. Nevertheless, the forests are under severe pressure. Illegal cutting of trees and land-use change for settlement and farmland expansion are the common problems in the area.

The forest has complex vertical and horizontal structures. Besides the species diversity, there is large variability in tree height and wood basic density of the study forest. The mean (and range) of

observed tree height was 13.90 m (4.90–40.10 m); while the mean (and range) of wood basic density (g cm^{-3}) for tree species in the forest was 0.59 (0.43–0.98) [42].

2.2. Field Data Collection

The sampling frame was defined to include the Degaga-Gambo forest territory, which contains both the natural and plantation forest types. Circular sample plots (SPs) of 17.85 m radius aligned in a systematic grid at an interval of 1.18 km were used for field data collection (Figure 1). One hundred and eleven plots (from the natural forests, plantation forests and other categories like clear-cut, cropland, settlement and grassland cover types) were sampled from February 2018 to January 2019. Handheld global positioning system (GPS) receiver was used to navigate to the pre-defined locations of the SPs. Then, the precise coordinates of the plot centers were determined using differential GPS and global navigation satellite system (GLONASS) measurements. Two Topcon legacy-E + 40 dual-frequency receivers were used for this purpose [43]; one serving as a base station and the other as a rover field unit. The receivers record pseudo-range and carrier phase of GPS and GLONASS.

The base station was set up at Wondo Genet College of Forestry and Natural Resources campus. The Euclidean distance between the base station and the plot centers ranged between 21.70 and 57.20 km with an average distance of 41.80 km. To determine the position of the base station using precise point positioning, the GPS and GLONASS data were recorded continuously for 24 h [44]. At the plot centers, the rover was mounted on a 2.98 m carbon rod and recorded for 41.50 min on average using a one-second logging rate. The recordings were post-processed using the Magnet tools software [45]. The standard error of the post-processed planimetric plot coordinates ranged from 0.02 to 1.11 m with a mean of 0.23 m.

In each of the SPs, we recorded species names and measured DBH, i.e., the diameter of trees at 1.3 m above the ground, for all the trees with DBH ≥ 5 cm. Caliper or diameter tape was used for DBH measurement depending on tree size. Tree height measurements were carried out for 10 trees selected systematically in each of the plots using a Haglöf vertex laser 5 instrument [46]. Heights of the trees for which height was not measured were predicted using height-diameter models developed based on the sample trees [16,19,47].

2.3. Plot-Level AGB Estimation

Plot-level AGB was estimated by aggregating the predicted individual tree AGB in the respective plots. For predicting tree AGB in the natural forests, the allometric model constructed by [42] was used. This model has DBH, height and wood basic density as predictor variables. Wood basic density values were obtained from [48]. For plantation forests, tree AGB was estimated using species-specific allometric models. Accordingly, for *Cupressus lusitanica,* we used the model by [49] with DBH and height as predictor variables. For *Eucalyptus* species and *Grevillea robusta*, models by [50,51] were used, respectively, having DBH and height as predictor variables. The plot-level AGB data in units of kg m^{-2} were converted to Mg ha^{-1} (megagrams per hectare) since the data were collected from large plots (1000 m^2). The plot-level AGB values ranged from 0 to 845.70 Mg ha^{-1} with a mean and standard deviation of 184.35 Mg ha^{-1} and 155.10 Mg ha^{-1}, respectively.

2.4. Satellite Image Acquisition

Satellite images acquired in January 2019 were considered since this is the dry season when most of the undergrowth vegetation dries up and is easier to distinguish from the trees. This time window was also within the field inventory period. Additionally, selected images were restricted to those with cloud cover < 5%. A detail description of the images used in this study is given in Table 1.

Single tiles of each of the L8 and S2 products were downloaded from the USGS Earth Explorer website [52]. Both images were Level-1C products, which means that the images were corrected for any possible topographic and geometric errors. The processing level of the L8 image used in this study was L1-TP, which is a Level-1 precision and terrain corrected product. Besides terrain and topographic

correction, radiometric correction has already been done for S2 products before delivery. The SBs used in this study (i.e., blue (B), green (G), red (R), near-infrared (NIR), shortwave infrared-1 (SWIR1) (for both L8 and S2), red-edge (RE) (only for S2)) have spatial resolutions of 30 m for L8 and 10 or 20 m for S2 (see Table 1 for details of the resolutions of individual bands).

We downloaded the PS Ortho Scene Product (Level-3B) from the Planet Explorer website [53]. Six scenes of orthorectified scaled Top of Atmosphere Radiance (at sensor) images were downloaded to cover the study area. These images contain information about the B, G, R and NIR SBs.

Table 1. Major characteristics of Landsat-8 (L8), Sentinel-2 (S2) and PlanetScope (PS) systems and properties of images used in this study.

Satellite	Sensor [a]	Path/Row or Tile Number	Date of Acquisition	Cloud Cover (%)	Product Processing Level	Spectral Bands [b]	Spatial Resolution
L8	OLI	168/055	16 January 2019	0	L1-TP	B, G, R, NIR, SWIR1	30 m: all SB
S2	MSI	T37NDJ	14 January 2019	3	Level-1C	B, G, R, RE, NIR, SWIR1	10 m: visible, NIR; 20 m: RE, SWIR1
PS	4-band frame imager; NIR filter	Scene-based frames	27 January 2019	0	3B-Analytic-MS	B, G, R, NIR	3 m: all SB

Source: USGS Earth Explorer [52] for L8 and S2; Planet Explorer [53] for PS. [a] OLI and MSI stand for operational land imager and multispectral instrument sensors of L8 and S2, respectively. [b] B, G, R, NIR, SWIR1 and RE represent the blue, green, red, near-infrared, shortwave infrared-1 and red-edge spectral bands (SBs), respectively.

2.5. Image Processing and Independent Variable Definition

In the current study, we first evaluated a great number of potential candidate variables that could be useful for AGB modelling. A series of image processing techniques were applied to the satellite images to get the independent variables. First, atmospheric correction was done using the QGIS software version 3.1.0 [54] and python codes. For L8 and S2 images, the semi-automatic classification plugin (SCP) of QGIS was used for running the dark-object subtraction (DOS-1) algorithm, which removes the dark pixels that result from atmospheric scattering. The satellite images were transformed from spectral radiance to top of atmosphere reflectance values based on the conversion factors in the metadata file that comes along with the image files. However, the PS images were processed using the empirical line correction for conversion of radiance to reflectance values indicated in Equation (1):

$$\text{Reflectance} = \text{coefficient} \times \text{Radiance (Input data)} \quad (1)$$

The radiances of the input images were converted to reflectance values and atmospheric correction applied since variables from multiple images were compared. In addition to variation in the sensors, the three sets of images were acquired on different dates although within 13 days of maximum gap among them. Furthermore, six scenes of the PS imagery covered the area of interest. After atmospheric correction, all the images became Level-2A products, which have pixels with surface reflectance values suitable for calculating SIs and texture variables used in this study. Atmospherically corrected SBs, which were used for creating SIs and texture variables shown in Table 2 and Table 3, respectively, were selected for this study.

Table 2. Description of spectral indices (SIs) used as candidate independent variables for aboveground biomass (AGB) modelling in this research.

SI	Expression [c]	Reference(s)	
		General	Relationship with AGB
NDVI	$\frac{(NIR-R)}{(NIR+R)}$	[55,56]	[19,30]
SR	NIR/R	[57]	[30,34]
VI	G/R	[58]	
DVI	$NIR-R$	[59]	[30]
ExGI	$2\times G-(B+R)$		
GLI	$\frac{(G-R)+(G-B)}{2\times G+R+B}$	[60]	
EVI	$2.5\times\frac{(NIR-R)}{(NIR+6\times R-7.5\times B+1)}$	[61]	[19]
SAVI	$\frac{(NIR-R)}{(NIR+R+0.5)}\times(1.5)$	[62]	[30]
MSAVI	$\frac{2\times NIR+1-\left(\sqrt{(2(NIR)+1)^2-8(NIR-R)}\right)}{2}$	[63]	[30]
NDMI	$\frac{(NIR-SWIR1)}{(NIR+SWIR1)}$	[64]	[19]
NDGI	$\frac{(G-R)}{(G+R)}$	[36]	
ARVI	$\frac{(NIR-(2\times R-B))}{(NIR+(2\times R-B))}$	[65]	[22]
SRRE	NIR/RE	[66,67]	[26]
RENDVI	$\frac{(NIR-RE)}{(NIR+RE)}$	[68]	[35]

[c] See Table 1 for description of the acronyms of the SBs used in the expressions of the SIs in this table.

Table 3. General description of the grey level co-occurrence matrix (GLCM) texture features used in this study.

GLCM Texture [d]	Expression [e]	Description
Contrast	$\sum_{i,j=0}^{N-1} p_{i,j}\times(i-j)^2$	Contrast and dissimilarity indicate the amount of local grey level (GL) variation in an image. Large values indicate the presence of edges, noise or wrinkled features.
Dissimilarity	$\sum_{i,j=0}^{N-1} p_{i,j}\times\lvert i-j\rvert$	
Homogeneity (IDM)	$\sum_{i,j=0}^{N-1}\frac{p_{i,j}}{1+(i-j)^2}$	Measures the smoothness (homogeneity) of the GL distribution of an image.
ASM	$\sum_{i,j=0}^{N-1}(p_{i,j})^2$	ASM measures the degree of orderliness of pixel values in an image.
Energy	$\sqrt{ASM}$	Energy is a measure of uniformity.
Maximum probability	$\text{maximum}\left(p_{i,j}\right)$	Maximum probability of the GL values.
Entropy	$\sum_{i,j=0}^{N-1} p_{i,j}\times\left(-\ln^{p_{i,j}}\right)$	It measures the degree of randomness of pixel values in an image. Entropy is inversely related to uniformity.
GLCM mean	$\mu_i=\sum_{i,j=0}^{N-1} i\times\left(p_{i,j}\right);\ \mu_j=\sum_{i,j=0}^{N-1} j\times\left(p_{i,j}\right)$	Mean of GL distribution of the image.
GLCM variance	$s^2{}_i=\sum_{i,j=0}^{N-1} p_{i,j}\times(i-\mu_i)^2;$ $s^2{}_j=\sum_{i,j=0}^{N-1} p_{i,j}\times\left(j-\mu_j\right)^2$	GLCM variance is a measure of the dispersion of GL distribution.
Correlation	$\sum_{i,j=0}^{N-1} p_{i,j}\times\left[\frac{(i-\mu_i)\times(j-\mu_j)}{\sqrt{s^2{}_i\times s^2{}_j}}\right]$	Correlation indicates the linear dependency of GL on their neighboring pixels.

[d] IDM and ASM stand for inverse difference moment and angular second moment, respectively. [e] Where $p_{i,j}$ is the probability of finding the GLCM relationship at cell (i, j) and is calculated as $p_{i,j}=\frac{V_{i,j}}{\sum_{i,j=0}^{N-1} V_{i,j}}$; such that $\sum_{i,j=0}^{N-1}\left(p_{i,j}\right)=1$, N = Number of grey levels in the image as specified by the number of levels in the quantization, $V_{i,j}$ = grey level value in a cell (i, j) of the image window.

Table 2 shows the expressions used to derive spectral index values from each satellite image type used in this study and references to scientific evidences on the use of the indices in general and for biomass estimation in particular.

Descriptions of the GLCM image texture data derived from the PS images are presented in Table 3. Texture information of the L8 and S2 images were not used due to the coarse spatial resolutions. Sentinel Application Platform (SNAP) software version 7.0.0 [69] was used for calculating the texture variables. Processing parameters of window size of 11 × 11 pixels, angle in all directions,

probability quantization with level of 128 were set to obtain the texture data used in the current study. This processing window size was set to provide an equivalent area to the field SPs.

Area-weighted mean and standard deviation (hereafter referred to as mean and standard deviation, respectively) of all the variables were extracted to each SP using QGIS. These were used as independent variables of the models constructed from each RS data type, the details of which are explained in the following sections.

2.6. Variable Selection and Model Fitting

The purpose of the AGB regression modelling was to construct models with variables from the RS data as predictors and which could be used to enhance the precision of the overall AGB estimates for the study area. For the AGB estimation, we used a model-assisted approach to inference (see details in Section 2.8) because that would allow a direct comparison of the uncertainty of the AGB estimate with similar uncertainty estimates obtained for the pure field-based estimate. In model-assisted estimation, the model form and the predictors selected for the model should be determined independent of the sample at hand [70]. In model-assisted inference, no claim of a true model is necessary. A poor choice of model form and predictors would have negative consequences in terms of efficiency [71] (p. 238), but would not invalidate the unbiasedness of the estimator. If, however, the choice of model form and the choice of predictors were sample-based, e.g., by choosing predictors by optimizing the predictive power of the model for the sample at hand, there would be a risk of overfitting and underreporting of uncertainty [72].

On this background, we found ourselves in a dilemma in this study. On one hand, we had no prior information about useful variables derived from the given RS data for AGB modelling for the particular forest types under study. Neither had we any experience with suitable model forms for the study area. On the other hand, if model selection and variable selection were optimized for the given sample, overfitting would be a likely consequence.

To balance these conflicting requirements, we first did a screening of the variables mentioned above to gain first-hand experience with the three types of satellite data for the current forest types. We then chose a model-form a priori, and allowed only a small number of predictors to be included in the model. In the modelling phase, we paid special attention to any sign of overfitting.

Thus, in the first phase of the analysis, Pearson's correlation coefficient was used to explore the relationships of individual independent variables with AGB. Those variables that had a significant correlation with AGB were used as potential variables for the AGB model fitting. Furthermore, correlation analysis was done for each pair of independent variables within each satellite data source to evaluate the level of intercorrelation between them. Results of the correlation analysis indicated that most of the variables were strongly intercorrelated (Figure 2). Hence, variable screening was employed to reduce the redundant information emanating from those strongly intercorrelated variables. Results of the initial analysis using more complex models showed overfitting problems, which was manifested in precision difference between training and validation results for each model. Such severe overfitting was observed for models with more than two variables. Because of the risk of overfitting, we restricted the selection of independent variables in the models to a maximum of two variables only. The results from the analysis of models with more than two variables are not documented any further.

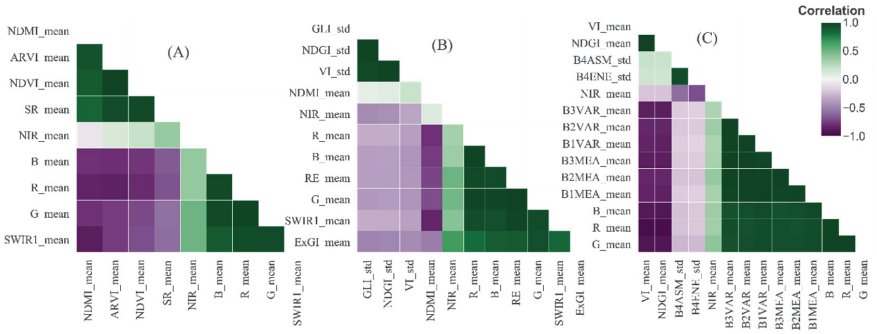

Figure 2. Intercorrelation among independent variables derived from (**A**) L8, (**B**) S2, and (**C**) PS images. See Table 4 for the descriptions of the notations used to represent the independent variables.

Table 4. Correlation of relevant independent variables (see Tables 1–3 for definitions) derived from L8, S2 and PS images with AGB. The notations for SB and SI variables of all the image types are MMM_mean or MMM_std representing the mean and standard deviation of the variable MMM, in respective order. For texture variables of the PS data, BnXXX_mean is the mean of the mentioned (XXX) texture variable of the SB Bn where n = 1, 2, 3, 4 for B, G, R, NIR, respectively. Similarly, BnXXX_std is the standard deviation of the texture variable as described above for the BnXXX_mean, except replacing 'mean' by 'std'. VAR and MEA stand for the GLCM variance and mean, respectively.

L8		S2		PS	
Variable	**Correlation**	**Variable**	**Correlation**	**Variable**	**Correlation**
NDMI_mean	0.39 ***	GLI_std	0.44 ***	VI_mean	0.44 ***
ARVI_mean	0.27 **	NDGI_std	0.43 ***	NDGI_mean	0.44 ***
NDVI_mean	0.23 *	VI_std	0.43 ***	B4ASM_std	0.37 ***
SR_mean	0.19 *	NDMI_mean	0.31 ***	B4ENE_std	0.35 ***
NIR_mean	−0.38 ***	NIR_mean	−0.42 ***	NIR_mean	−0.38 ***
B_mean	−0.41 ***	R_mean	−0.43 ***	B3VAR_mean	−0.39 ***
R_mean	−0.42 ***	B_mean	−0.46 ***	B2VAR_mean	−0.39 ***
G_mean	−0.45 ***	RE_mean	−0.48 ***	B1VAR_mean	−0.39 ***
SWIR1_mean	−0.48 ***	G_mean	−0.49 ***	B3MEA_mean	−0.40 ***
		SWIR1_mean	−0.49 ***	B2MEA_mean	−0.40 ***
		ExGI_mean	−0.51 ***	B1MEA_mean	−0.40 ***
				B_mean	−0.46 ***
				R_mean	−0.46 ***
				G_mean	−0.48 ***

* p-Value < 0.05; ** p-value < 0.01; *** p-value < 0.001.

The relevant variables of each satellite data source were related to plot-level AGB using the logarithmic link function in a generalized linear model (GLM) of the form:

$$\ln(y_i) = \beta_0 + \sum_{i=1}^{i} \beta_i X_i \quad (2)$$

where y_i is ground reference AGB (Mg ha^{-1}), β_0 is intercept, β_i is the coefficient of the independent variable (X_i), and i is the index of an individual independent variable.

This model form was chosen since it provides valid estimates where true zeroes are included in the estimate of AGB, which has positive continuous numerical values. A study of AGB prediction using topographic variables in human-impacted tropical dry forest landscapes of Mexico indicated that GLM estimation technique improved predictions [73]. Thus, the mean of SBs and SIs of L8 image were candidate independent variables for the L8 model. The mean and standard deviation of the SBs and SIs of the S2 image were candidate independent variables for the S2 model. The mean and standard

deviation of SBs, SIs and texture features of PS bands were used as candidate independent variables for the PS model.

2.7. Model Validation

We evaluated the performance of the models using a leave-one-out-cross validation technique. The cross-validation was used to assess overfitting. Each model was validated in terms of coefficient of determination (R^2), root mean squared error (RMSE, %), mean deviation (MD, %), and Akaike Information Criterion (AIC) as determined by Equations (3)–(8). The AIC was used to evaluate the maximum likelihood of the model parameters. The maximum likelihood estimation enables choosing the parameter that makes the likelihood of having the observed data a maximum fit with the dependent variable (AGB) without causing an overfitting issue. When comparing models, the model with a smaller AIC is better than the one with a higher AIC.

$$R^2 = 1 - \frac{\text{Residual deviance}}{\text{Null deviance}} \tag{3}$$

$$\text{RMSE} = \sqrt{\frac{1}{n}\sum_{i=1}^{n}\left(y_i - \hat{y}_i\right)^2} \tag{4}$$

$$\text{RMSE\%} = \frac{\text{RMSE}}{\overline{y}} \times 100 \tag{5}$$

$$\text{MD} = \frac{1}{n}\sum_{i=1}^{n}\left(y_i - \hat{y}_i\right) \tag{6}$$

$$\text{MD\%} = \frac{\text{MD}}{\overline{y}} \times 100 \tag{7}$$

$$\text{AIC} = -2\ln L\left[\hat{\beta}(k)\right] + 2k \tag{8}$$

where y_i and $\hat{y}_i$ are the ground reference and predicted AGB (Mg ha^{-1}) in the ith SP; $\overline{y}$ is the mean of ground reference AGB (Mg ha^{-1}) of all SPs; n is the sample size; $L\left[\hat{\beta}(k)\right]$ is the likelihood function of the observations, $\hat{\beta}(k)$ is the maximum likelihood estimation of the parameter β given the number of parameters of k within the model.

In addition to the validation metrics indicated above, we did qualitative evaluation based on a visual comparison between the predictions using the selected models in each satellite data source and false-color composite (i.e., band combination of NIR-R-G in the R-G-B channels) depiction of the S2 image.

2.8. Population-Level Estimation and Efficiency Assessment

Based on the SP inventory data, for the sample size of 111 plots of about 1000 m^2 area, the estimators of the mean AGB for the population and its variance were calculated by Equation (9) and Equation (10), respectively [71]:

$$\hat{\mu}_{\text{field}} = \frac{1}{n}\sum_{i=1}^{n} y_i \tag{9}$$

$$\hat{\text{var}}(\hat{\mu}_{\text{field}}) = \frac{1}{n(n-1)}\sum_{i=1}^{n}\left(y_i - \hat{\mu}_{\text{field}}\right)^2 \tag{10}$$

where y_i is AGB (Mg ha^{-1}) of the ith SP in the sample and n is the sample size.

The 95% confidence interval (CI) of $\hat{\mu}_{\text{field}}$ was calculated using Equation (11):

$$\text{CI} = \hat{\mu}_{\text{field}} \pm t \times \text{SE}(\hat{\mu}_{\text{field}}) \tag{11}$$

where $SE(\hat{\mu}_{field}) = \sqrt{\hat{var}(\hat{\mu}_{field})}$ is the standard error (SE) of $\hat{\mu}_{field}$ and t is student's t at a significance level of 0.05.

Similarly, we estimated the mean AGB for the entire study area using the selected regression model for each satellite data source. For this purpose, the study area was tessellated into grid cells of 31.64 × 31.64 m providing a total of N (141,604) population units. The size of the grid cells was chosen to be equivalent to that of the SPs. Area-weighted mean and standard deviation of the variables used in the regression models were extracted for each grid cell using QGIS. AGB was predicted for each population unit (i) in the map of the tessellated granules using the selected regression models for each satellite data source and is represented by $\hat{y}_i$. Because the prediction relied on field data collected based on probability sampling inside the population of interest, we adopted generalized model-assisted regression estimators. The mean and the variance estimates were computed using Equation (12) and Equation (13), respectively [71] (p. 231):

$$\hat{\mu}_{image} = \frac{1}{N}\sum_{i=1}^{N}\hat{y}_i + \frac{1}{n}\sum_{i=1}^{n}\left(y_i - \hat{y}_i\right) \quad (12)$$

where $\hat{\mu}_{image}$ is the mean remote sensing-assisted estimate of AGB (either L8, S2 or PS). The first term in this estimator ($\frac{1}{N}\sum_{i=1}^{N}\hat{y}_i$) is the mean of the model predictions ($\hat{y}_i$) for all population units, and the second term ($\frac{1}{n}\sum_{i=1}^{n}\left(\hat{y}_i - y_i\right)$) is an estimate of the mean error calculated over the sample units and compensates for systematic model prediction errors.

$$\hat{var}\left(\hat{\mu}_{image}\right) = \frac{1}{n(n-1)}\sum_{i=1}^{n}(\varepsilon_i - \bar{\varepsilon})^2 \quad (13)$$

where ε_i and $\bar{\varepsilon}$ are the estimates of error at each data point (i) and the average, respectively.

The SE of the mean AGB estimators (i.e., $SE(\hat{\mu}_{field})$ and $SE\left(\hat{\mu}_{image}\right)$) were calculated by taking the square root of the respective variance estimators $\hat{var}(\hat{\mu}_{field})$ and $\hat{var}\left(\hat{\mu}_{image}\right)$.

The study assessed the gain in precision of AGB estimation with the use of the three types of RS data. The measure of quantifying such a gain in precision of using RS data over the pure field-based estimates was expressed using relative efficiency (REf). REf quantifies the magnitude of estimated variance of a remote sensing-assisted estimate of mean AGB to a field-based estimate. It was computed by Equation (14) as the ratio of the variance of the field-based estimates to the remote sensing-assisted estimates:

$$REf = \frac{\hat{var}(\hat{\mu}_{field})}{\hat{var}\left(\hat{\mu}_{image}\right)} \quad (14)$$

When REf is greater than one, it is interpreted as the amount of additional precision gained due to the use of the RS data for estimating mean AGB.

3. Results

3.1. Relationship of Independent Variables with AGB

Statistical test for significance of correlation coefficients of the relationship of individual RS variables with AGB demonstrated that many of the candidate variables were reasonably related to AGB. Correlation coefficients were translated to descriptors like 'weak', 'moderate' and 'strong' relationships according to the scheme used by [74]. The mean SB reflectance values of the three satellite data sources had negative moderate correlation with AGB (Table 4). On the other hand, the mean values of most SIs tend to show moderate positive relationships with AGB with some exceptions (for instance, mean ExGI of S2). It was revealed from the exploratory analysis that standard deviation of SIs of S2 and PS images and texture variables of PS images had moderate relationships with AGB.

For the L8 category of independent variables, the mean SIs were less correlated with AGB as compared to those of the SBs. Table 4 shows that from the SIs, the mean NDMI had considerable relationship while that of ARVI, NDVI and SR have weaker performance. The mean values of all SBs were moderately related to AGB with correlation coefficients ranging from −0.38 (NIR_mean) to −0.48 (SWIR1_mean). The strength of the association of AGB with NIR_mean was equivalent to that observed with the strongly correlated SI (i.e., the NDMI_mean), which was 0.39.

From the S2 variables, the mean of both SBs and SIs showed reasonable association with AGB. Similar to the L8 variables, the mean of SBs had a stronger relationship than that of the SIs except the mean ExGI, which had the strongest relationship. The peculiar behavior of ExGI comes from the fact that it is just a difference of SBs. Likewise; the standard deviation of the SIs (namely GLI, NDGI and VI) had strong positive associations with the dependent variable.

Similarly, for the PS variables, the mean of SBs of G, R and B showed the strongest relationship with AGB followed by that of VI and NDGI SIs. The mean and standard deviation of the texture data had moderate relationships with AGB (Table 4).

3.2. Variable Selection for the Prediction Models

Correlation analysis indicated that independent variables of each satellite data source were strongly intercorrelated (Figure 2). Therefore, the variables that fit well with AGB in the GLM, and which had no significant collinearity problem, were selected for the AGB prediction models. As a result, the means of NDMI and NIR variables were less intercorrelated and became predictor variables for one of the L8 models. Besides, a simple model with the most strongly correlated variable (SWIR1) with AGB was considered as another candidate model in this category.

Similarly, the mean of SWIR1 and standard deviation of GLI were selected as predictor variables for the two-variable S2 model. The standard deviation of GLI had a strong positive correlation with AGB (Table 4) and was less correlated with the mean of SWIR1 variable (Figure 2), which was already in the model. Moreover, the single variable model with a predictor variable of mean of ExGI and another one with the mean of SWIR1 SB were other candidate models of the S2 category.

From the PS data, the mean of G reflectance had the strongest correlation with AGB. Thus, one of the PS models contains independent variables composed of the mean reflectance of G SB and the standard deviation of the ASM texture variable of the NIR SB. The mean of B4ASM was the least intercorrelated with the mean of G SB. The other simple model was the model with a predictor variable of the mean of G SB reflectance only.

3.3. Selected AGB Models for Each Image Type

Table 5 shows a detailed description of the candidate AGB models for each image type. Two candidate models were obtained from the L8 data. There was a marginal difference between the single and two-variable models with AIC of 1403.31 and 1402.68, respectively. The model calibration RMSE of the single and two-variable models were 70.22% and 71.06% of the mean AGB, respectively. Likewise, the respective model validation RMSE values were 73.23% and 73.31% of the mean AGB. As clearly revealed in these model metrics, there is concern of less responsiveness of the selected variables for the AGB estimates in the two-variable model. The presence of two variables in the model did not significantly improve the model performance. Therefore, the model with the mean of SWIR1 reflectance as the only predictor variable was selected for AGB estimation.

Three models were selected as candidates from the S2 variables. Two of them were with a single predictor variable while the third has two variables (Table 5). The model with the mean of ExGI as a predictor variable had a larger validation RMSE (73.80%) than the other models. The model with the predictor variable of the mean of SWIR1 was better than the one with the mean of ExGI. However, the two-variable model had even greater performance among the S2 category of models. The two-variable S2 model with predictor variables of the mean of SWIR1 and standard deviation of GLI had the least AIC value among the models (1385.06) and minimal overfitting problem (Table 5).

Additional indicators of the model fit and validation results of this model were better than the other models in the category. This model explained 40.96% of the variability in the ground reference AGB unlike the selected L8 and PS models, each of which explained less than 30%.

Two candidate models were obtained from the PS data. The two-variable PS model contains the mean of G reflectance and the standard deviation of B4ASM texture as predictor variables. However, this model revealed a severe overfitting problem. The model RMSE and validation RMSE were 70.19% and 79.48%, respectively. Thus, the single-variable model with the mean of G reflectance was selected for AGB estimation in this category. It had model calibration and validation RMSE of 71.79% and 75.17%, respectively. Overall performance of the selected PS model was slightly lower than the selected S2 model but similar to that of the selected L8 model (Table 5).

The validation results of all the three selected models for AGB estimation indicated that the models have sensible performance in predicting AGB for the data with which they were not trained. The scatter plot of fitted versus ground reference AGB values shown in Figure 3 indicates a reasonable predictive power of the models given the complex settings of the study area. Pearson's correlation coefficients of the model predicted and ground reference AGB in the SPs revealed that the S2 model predictions were more correlated with the ground reference AGB than the other two models. The S2 model predictions had a correlation coefficient of 0.64 with the ground reference AGB.

The L8 and PS models had equivalent performance and explained a considerable amount of the variation in the FBSS estimate of mean AGB with R^2 of 29% and 27%, respectively, given the complex forest structure and topography in the study area.

Although the general trend of the error distribution of the three selected models looks similar, prediction errors of the L8 and PS models spread out at small and large AGB more than the S2 model did (Figure 3). The extents of deviation of predicted values from the ground reference AGB differ for each model especially at the smaller and larger AGB values. With this variability maintained, the selected models of all the three-image data inflated predictions of small AGB, particularly those below approximately 300 Mg ha^{-1}. For SPs with large AGB, the predictions using all the three models were smaller than the ground reference values.

The L8 and S2 models had smaller prediction error at the small AGB end than at the large AGB levels. Generally, the predictive power of the S2 model prevailed over that of the other models.

3.4. Estimation and Mapping of AGB Using the Selected Models

Table 6 shows the estimated mean AGB, estimates of mean deviation, SE of the mean AGB estimates and REf for the selected models of the three image categories presented in Table 5. The estimates of mean AGB were 179.67 Mg ha^{-1}, 177.79 Mg ha^{-1} and 184.27 Mg ha^{-1} when using the L8, S2 and PS model predictions, respectively. The model-assisted estimates of the mean AGB for all the three categories of models were within 95% CI of the mean AGB estimate based on the field data only (i.e., 155.15–213.76 Mg ha^{-1}). The estimated mean AGB using the PS model was closer to the field-estimated mean AGB (i.e., 184.35 Mg ha^{-1}) than the estimates using the other models. The estimated mean AGB using the L8 and PS models had the largest and smallest MDs, respectively. The AGB estimate based on the PS model was relatively less precise followed by the L8 model. The estimation results revealed that the L8 and PS models resulted in equivalent estimation efficiencies (i.e., 1.40 and 1.37, respectively).

Table 5. Models and performance indicators for mean AGB estimation in the Degaga-Gambo forest using independent variables from L8, S2 and PS images.

Image	Model [f]	AIC	Calibration	Validation	Prediction
			RMSE (%)	RMSE (%)	Correlation [g]
L8	$\hat{AGB} = \exp(6.0703 - 9.3781 \times NIR\_mean + 3.5489 \times NDMI\_mean)$	1402.68	129.46 (70.22)	135.20 (73.31)	0.55
	$\hat{AGB}^{@} = \exp(6.9967 - 16.1492 \times SWIR1\_mean)$	1403.31	131.00 (71.06)	135.00 (73.23)	0.54
S2	$\hat{AGB}^{@} = \exp(6.1310 - 11.4874 \times SWIR1\_mean + 12.7865 \times GLI\_std)$	1385.06	119.58 (64.87)	123.70 (67.12)	0.64
	$\hat{AGB} = \exp(7.1200 - 51.3576 \times ExGI\_mean)$	1400.00	128.97 (69.96)	136.01 (73.80)	0.56
	$\hat{AGB} = \exp(6.9968 - 15.2480 \times SWIR1\_mean)$	1402.00	130.33 (70.69)	134.70 (73.06)	0.54
PS	$\hat{AGB} = \exp(10.0593 - 56.0248 \times G\_mean + 1.1545 \times B4ASM\_std)$	1402.55	129.40 (70.19)	147.30 (79.48)	0.55
	$\hat{AGB}^{@} = \exp(11.7696 - 75.2766 \times G\_mean)$	1406.00	132.34 (71.79)	138.58 (75.17)	0.52

[f] Mean and std refer to the area-weighted mean and standard deviation of the image-derived variables within the grid cells. [@] Selected model for AGB prediction (from each image type). [g] Pearson correlation coefficient between ground reference and model-predicted values of AGB for the models in each image type. The square of these coefficients is the same as the R^2 of the models, which was determined using Equation (3).

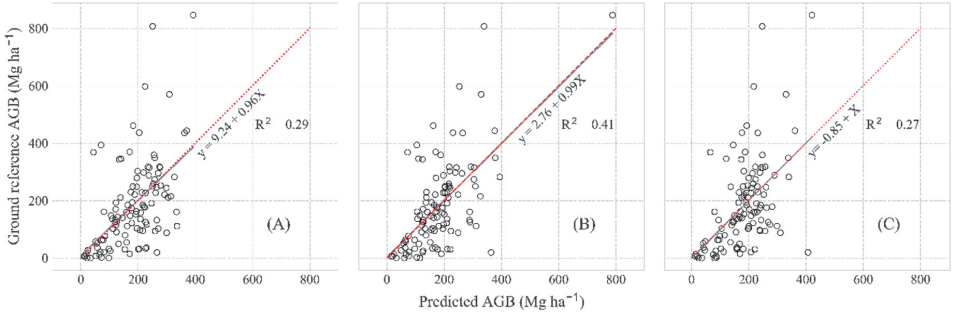

Figure 3. Relationship of ground reference versus predicted AGB using selected models of (**A**) L8, (**B**) S2, and (**C**) PS data. The dashed red and grey solid lines (overlapping) represent the identity (1:1) and the correlation functions, respectively.

Table 6. Estimated mean AGB (Mg ha^{-1}), mean deviation (MD) in Mg ha^{-1}, standard error (SE) of the mean estimates (Mg ha^{-1}) and relative efficiency (REf) when using the selected models to assist in the estimation.

Estimator Data Source	Estimated Mean AGB	Estimated MD	SE	Ref
Model-assisted; L8-model	179.67	1.71	12.49	1.40
Model-assisted; S2-model	177.79	0.62	11.40	1.68
Model-assisted; PS-model	184.27	-0.13	12.62	1.37
Field-based	184.35	—	14.79	—

The estimate based on the S2 model was the most precise among the three model-assisted AGB estimates with SE of 11.40 Mg ha^{-1}. As a result, the REf of the mean AGB estimate using the S2 model (i.e., 1.68) was greater than what we obtained by using the other two models.

Visual inspection of the predicted AGB using the three selected models and the false-color composite of the S2 image shows convincing AGB distribution across the landscape. As expected, the patches of bare land (non-forest areas) in the study area (shown in different shades of grey in Figure 4D) have small AGB predictions using all the models (shades of yellow in Figure 4A–C) while the dense forest areas (colored red in Figure 4D) yielded greater predicted AGB values (shades of green in Figure 4A–C). The map revealed that AGB predictions using the selected models of the three satellite image types had many similarities, which also was confirmed by similarities in the estimated uncertainties (Table 6). The distribution patterns of AGB predictions in the maps (Figure 4A–C) indicated the spatial consistency of AGB predictions across the area for the selected models.

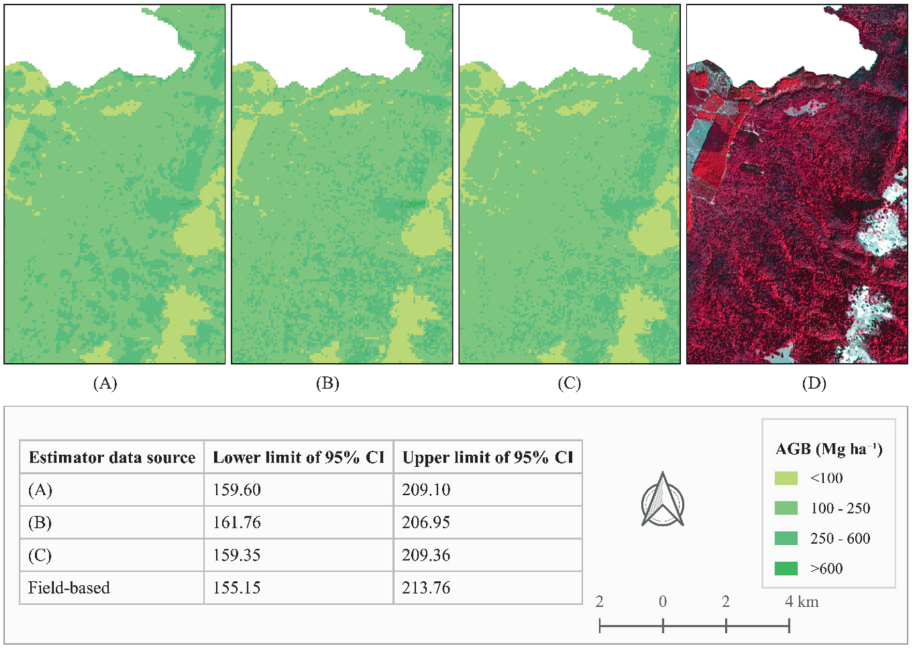

Figure 4. Visual representation of a portion of the predicted AGB using the selected models of (**A**) L8, (**B**) S2, (**C**) PS and (**D**) false-color composite (NIR-R-G in the R-G-B channels) of the S2 image of the study area acquired on 14 January 2019. The 95% CI for the mean AGB estimates of the respective model predictions for the population are shown in the table.

4. Discussion

4.1. Variable Exploration for Estimating AGB and Model Selection

The observed moderate relationships of independent variables of the RS data with AGB demonstrated the potential of optical RS data for developing models to enhance AGB estimation. The observed negative correlation coefficients between the mean of SB reflectance and AGB agree with results of similar studies conducted in various forest types [19,75,76]. The negative correlation coefficients indicate the inverse relationship between reflectance values from the SBs and AGB. This relationship in the current study could be explained by a shadow effect within the complex forest stands where AGB is large [77,78]. The presence of scattered big trees in SPs with large AGB results in large shadows. Additionally, such an effect might be related to large canopy water content, which is directly linked to photosynthetic efficiency [79]. The reflectance of the SBs from uniform forest stands like young plantations is large but they have relatively small AGB.

The positive relationship of most of the SIs with AGB found in this study is in accordance with previous research findings [19,34,76]. Besides the mean of SIs, the standard deviation of some SIs had also remarkable potential to relate with AGB. Næsset et al. [16] got similar results in Tanzania. Reviewed literature indicated that application of some of the SIs like the GLI, ExGI and NDGI have been limited to assessing grass biomass and crop cover or yield estimation. However, the current study showed that they had great potential to predict AGB in this type of forest. Thus, an in-depth study is required to understand the potential of such SIs for AGB estimation in different forest types.

It was revealed from the correlation analysis that most of the predictor variables in each satellite data type were intercorrelated. Lu et al. [80] found a similar result for estimation of AGB in wheat using an unmanned aerial vehicle. Among the different SBs the visible and SWIR bands, which are affected by atmospheric interference and shadow, were more strongly intercorrelated [78]. Besides, the SIs and texture variables were derived from these interrelated SBs. Therefore, the observed intercorrelation among the independent variables was likely to happen. This suggests the importance of a careful screening of RS variables for AGB modelling.

Furthermore, inter-resolution comparison of SBs showed that the limited spectral properties of the PS images might have restricted their potential to characterize AGB. For example, AGB correlated similarly with the G SB from each of the three image sources regardless of the differences in spatial resolution. The study results showed that the same SB across the resolution gradient characterized AGB similarly, indicating only a minor impact of pixel resolution on the quality of the AGB models if only SBs are related to AGB (Table 4). We observed that the S2 data contain a range of SBs that were more sensitive to AGB than the PS data, which have a higher spatial resolution.

Based on the relationship of the independent variables with AGB, we identified useful variables and models for each satellite data source. For example, exploration of the L8 data revealed that the NDMI showed a stronger correlation with AGB than other SI variables including the NDVI. This might be due to the improvements in the NDMI to detect leaf water content at the canopy level [7]. Previous research indicated that NDMI is useful for predicting forest attributes, including biomass [35,81]. The NDVI, which is the most popular SI for AGB modelling mostly in the temperate and boreal forests, was not a good predictor of AGB in the current study. Sader et al. [32] got similar results indicating unsuitability of NDVI for estimating AGB in tropical dense forests.

However, for the L8 data, AGB had a stronger correlation with SBs than the SIs mentioned above. Even among the SBs, AGB strongly correlated with the mean of SWIR1. The significance of the SWIR1 variable for AGB modelling was according to the results of other studies [23]. A study of biomass estimation using RS data in India indicated that biomass models using the SWIR bands were more reliable than those using short-wavelength SBs like the visible bands, which are more sensitive to atmospheric effects [82,83]. For green vegetation, reflectance in the SWIR spectral regions is controlled by the amount of water in the leaf biomass of the canopy. There is low diffuse of light at the SWIR wavelengths, and hence shadows are contrasted. The presence of thick layers of fragmented tree

canopy and shadows in SPs with large AGB yielded low reflectance in the SBs, including the SWIR1 SB as indicated with the negative coefficient in the selected model.

The S2 model used for AGB estimation was the two-variable model with the independent variables of the mean of SWIR1 and standard deviation of GLI. Inclusion of the standard deviation of the GLI variable in the S2 model indicates the ability to capture spatial variation in canopy structure in the forest as the GLI can identify green leaves and stems from the background soil surface [60]. This variable may reflect the level of disturbance, terrain variation or presence of very big scattered trees in the natural forest. This variable signifies the importance of using measures of variability derived from higher resolution images in AGB modelling. The mean of ExGI was also another variable from the S2 data sensitive to AGB variability.

Besides the SBs and SIs, texture variables of the PS images had considerable potential for AGB modelling. The standard deviation of B4ASM that was included in one of the PS models, indicating the importance of high-resolution images for AGB modelling. Image texture variables like the ASM, describe the spatial arrangement of pixels with varying intensities that resulted in different AGB. The texture variables were able to differentiate between heterogeneous and homogenous surfaces, which prevailed in the disturbed natural forest patches and young plantation forests, respectively. This might be the reason for the observed strong positive relationship of the standard deviation of B4ASM with AGB. Improvement in the model performance by including this texture variable was in line with the findings of other studies [24,39,84]. Nevertheless, the two-variable model containing the standard deviation of B4ASM was subject to overfitting as compared to the reduced model with the mean of the G reflectance variable (Table 5).

4.2. Model Characteristics and Their Contribution to Enhance AGB Estimation

Generally, the selected L8 and PS models explained some proportion of the variability in the ground reference AGB that was better than the results from [16] although the nature of the current forest and terrain configuration was complex. The calibration RMSEs of the L8 and PS models were 71.06% and 71.79% of the mean of the ground reference AGB, respectively. This was comparable with the results of other studies conducted even in intermediate vegetation cover conditions where it is easier to get a stronger relationship between image data and AGB [70]. The REf of the AGB estimates based on the selected L8 and PS models were 1.40 and 1.37, respectively. That means the selected L8 and PS models could reduce sample sizes to 71% and 73%, respectively, of the field sample size to get the same precision with the FBSS estimates. These amounts (or proportions) of the variability in the field estimates remained unexplained when the model-assisted estimation was applied. Consequently, there was a similarity in improving the mean AGB estimates based on the L8 and PS models. The REf when using the L8 model in this study was slightly larger than the findings by Næsset et al. [16] for Miombo woodlands in Tanzania using the global Landsat products.

The selected S2 model contributed more strongly to improve the precision of the AGB estimates than the L8 and PS models. This improvement in estimation efficiency contributes to reducing the number of field SPs required to attain the same precision, to approximately 59% of the sample size required for a pure FBSS estimate. The REf when using the S2 model was smaller than that of the RapidEye images used for AGB estimation in the Miombo woodlands in Tanzania [16]. This might be attributed to the heterogeneity of the forest in the current study or the interaction effect of forest types and spatial resolution of the images. Besides, [16] stated that the small study area covered in their study might have resulted in overly optimistic results because the RS data were very homogenous since they came from only a single scene. On the other hand, the results of the current study were similar to the findings by Navarro et al. [21] who studied AGB of mangrove plantations using S2 images in Senegal. Thus, the findings of the current study are reasonable given the heterogeneity of the terrain and forest conditions, which influence the relationship of image data and AGB [83].

Although there might be some variations between the models in this regard, they were able to predict only to a limited range of the ground reference AGB. This shows a saturation problem for

which canopy shadow is mainly responsible in the SPs with large AGB. Similar studies in primary and successional forests in Brazil indicated that shadows were among the main factors resulting in data saturation, particularly in natural forests with large AGB [77]. Modelling of tree heights might also contribute to the low/moderate estimation efficiencies in these models. There is uncertainty inherent in the field measurements of AGB, which could be caused by the AGB estimation procedure (e.g., errors in measurement and in the allometric models). The error in the height-DBH models could increase the uncertainties and limit performance of the models. Therefore, future efforts should focus on synchronizing other auxiliary variables like canopy density and canopy height from airborne laser scanning data with the identified variables to improve the model performances.

During the fieldwork, understory vegetation was observed in SPs (see Figure 5). The inflated predictions at SPs with small AGB might be attributed to this phenomenon. The field inventory was limited to trees with DBH $\geq$ 5 cm and did not account for the understory vegetation. Dense understory vegetation composed of saplings, shrubs, lianas and herbaceous species covered most of these SPs and challenged our movement during the fieldwork. The biomass in the understory vegetation, which was not accounted for in the ground reference AGB, could have had a major influence on the SB reflectance values and hence in all the RS variables. This might partly explain the moderate improvement in the precision of the model-assisted estimates of AGB compared to the pure field-based estimate. As shown in Table 6, the PS model-assisted estimates had negative MD indicating the greater effect of the inflated predictions at SPs with small AGB than the reduced predictions at the SPs with large AGB. Thus, the effect of understory vegetation on the relationship between image-derived variables and AGB was more obvious when using the high-resolution PS images. A greater compliance of the RS data with AGB would happen for homogeneous forests in which the understory vegetation cover is minimal and the forest canopy cover is uniform. Therefore, further studies are needed in pure plantation forests to attain an optimum efficiency of RS data for AGB estimation beyond the ones we got in this study.

Figure 5. Understory vegetation in a forest SP. The understory vegetation that was not measured during the forest inventory could have influenced the image values and thus their relationship with AGB.

Generally, the findings of the current study were encouraging. We identified relevant variables extracted from RS data for AGB estimation. The selected models of each satellite data source based on

the identified variables provided reasonable improvements in AGB estimations, which were reinforced by other research findings. The freely available S2 data were particularly useful. The research results revealed that S2 images possess sensible spectral and spatial properties for AGB estimation. The results of this study will help to satisfy the existing demand for forest carbon stock assessment by the national REDD+ program in Ethiopia. Enhanced forest information using the freely available data sources like the S2 would help to improve sustainable forest management and encourage results-based payments for those who properly manage their forest resources according to established principles like the REDD+ schemes.

5. Conclusions

Optical RS images from L8, S2 and PS satellites were studied to identify relevant RS predictor variables that could be used to enhance AGB estimation in a dry Afromontane forest. Most of the SBs, some SIs and texture variables (listed in Table 4) were found to be promising variables for predicting AGB. Although some of them were not selected in the models used for assisting AGB estimation, we identified variables including the mean of GLI, ExGI and NDGI that were seldom used for AGB modelling but are highly correlated with AGB. We recommend a detailed investigation of the importance of these variables for AGB assessment in various forest conditions.

The simple models selected for each satellite data source enhanced AGB estimation. Of the variables used in the models, the SWIR1 SB, which lacks in the PS data, was a useful variable of the L8 and S2 images for AGB estimation in this forest type despite the huge differences in pixel resolution among the image types. The study suggested that the additional spectral information of L8 and S2 images was more determinant of AGB estimation than the small pixel size of the PS images.

The use of RS data for AGB estimation improved the precision of estimates. Thus, the remote sensing-assisted estimation techniques used in this study will complement the FBSS estimates of AGB by improving precision. The model-assisted estimation will reduce sample sizes to obtain a similar estimation efficiency with the field survey. However, the models used for AGB estimation in this study revealed saturation problem. Therefore, future studies should focus on refining these limitations using a synergy of different data sources to enhance the estimation efficiency of AGB models beyond the ones achieved in the current study.

The methods used in this study could be adopted to similar conditions in forests that have limited application of RS data. The potential predictor variables derived from optical satellite images for biomass estimation were identified from studies showing global experiences. Exploratory data analysis was used to identify relevant predictor variables for biomass estimation in the current study site. Choice of a model form that is important for biomass required understanding the characteristics of data types. The selected models for each image type predicted biomass with estimation efficiencies comparable with those obtained in other forest types. These methods contain a unique mix of techniques capable of using satellite images for biomass estimation in a data scarce forest type.

Author Contributions: H.T. proposed the research idea. H.T., Z.A., T.G., I.B., H.O.Ø., E.N. and Ø.B.D. designed the field sampling protocols. H.T. carried out the RS data processing and analysis. H.T. and Z.A. implemented the field data collection, did data analysis and wrote the manuscript. T.G., H.O.Ø., I.B., E.N. and Ø.B.D. supervised the data analysis. All authors have read and agreed to the published version of the manuscript.

Funding: 'National MRV Capacity Building towards Climate Resilient Development in Ethiopia' Project: ETH 14/0002.

Acknowledgments: The Norwegian government funded this study through the "National MRV Capacity Building towards Climate Resilient Development in Ethiopia" program for which we have a profound gratitude. We appreciate the support we got from Wondo Genet College of Forestry and Natural Resources—Hawassa University, Ethiopia and Norwegian University of Life Sciences, Norway. We are grateful for the support we got from the Planet Company for offering free access to its high-resolution satellite images. We would like to thank Marie-Claude Jutras-Perreault for processing the GNSS data. We are indebted to both headquarter and Arsi branch offices of the Oromia forest and wildlife enterprise, local government and all members of the field crew for their cooperation during the data collection.

Conflicts of Interest: The authors declare no conflict of interest.

References

1. Bonan, G.B. Forests and climate change: Forcings, feedbacks, and the climate benefits of forests. *Science* **2008**, *320*, 1444–1449. [CrossRef] [PubMed]
2. Anderson, J.W. *The Kyoto Protocol on Climate Change*; Resources for the Future: Washington, DC, USA, 1998; pp. 1–21. Available online: https://media.rff.org/documents/RFF-RPT-kyotoprot.pdf (accessed on 17 September 2019).
3. UNFCCC. Decisions adopted by the Conference of the Parties. In Proceedings of the Conference of the Parties on Its Fifteenth Session, Copenhagen, Denmark, 7–19 December 2009; pp. 1–43. Available online: https://unfccc.int/resource/docs/2009/cop15/eng/11a01.pdf (accessed on 17 September 2019).
4. UNFCCC. Adoption of the Paris Agreement Proposal by the President. In Proceedings of the Paris Climate Change Conference—COP 21, Paris, France, 21 December 2015; pp. 1–31. Available online: https://unfccc.int/resource/docs/2015/cop21/eng/l09.pdf (accessed on 16 September 2019).
5. Gerhardt, K.; Hytteborn, H. Natural dynamics and regeneration methods in tropical dry forests—An introduction. *J. Veg. Sci.* **1992**, *3*, 361–364. [CrossRef]
6. Price, M.; Gratzer, G.; Alemayehu Duguma, L.; Kohler, T.; Maselli, D. *Mountain Forests in a Changing World: Realizing Values, Addressing Challenges*; Food and Agriculture Organization of the United Nations (FAO) and Centre of Development and Environment (CDE): Rome, Italy, 2011; ISBN 978-92-5-107076-5. Available online: http://www.fao.org/3/a-i2481e.pdf (accessed on 29 November 2019).
7. Solomon, N.; Segnon, A.C.; Birhane, E. Ecosystem Service Values Changes in Response to Land-Use/Land-Cover Dynamics in Dry Afromontane Forest in Northern Ethiopia. *Int. J. Environ. Res. Public Health* **2019**, *16*, 4653. [CrossRef] [PubMed]
8. Lemenih, M.; Bongers, F. Dry Forests of Ethiopia and Their Silviculture. In *Silviculture in the Tropics*; Günter, S., Weber, M., Stimm, B., Mosandl, R., Eds.; Springer: Berlin/Heidelberg, Germany, 2011; Volume 8, pp. 261–272. [CrossRef]
9. Nguon, P.; Kulakowski, D. Natural forest disturbances and the design of REDD+ initiatives. *Environ. Sci. Policy* **2013**, *33*, 332–345. [CrossRef]
10. Kebede, B.; Soromessa, T. Allometric equations for aboveground biomass estimation of *Olea europaea* L. subsp.cuspidatain Mana Angetu Forest. *Ecosyst. Health Sustain.* **2018**, *4*, 1–12. [CrossRef]
11. Duncanson, L.; Rourke, O.; Dubayah, R. Small Sample Sizes Yield Biased Allometric Equations in Temperate Forests. *Sci. Rep.* **2015**, *5*, 1–13. [CrossRef]
12. Watson, C.; Mourato, S.; Milner-Gulland, E.J. Uncertain Emission Reductions from Forest Conservation: REDD in the Bale Mountains, Ethiopia. *Ecol. Soc.* **2013**, *18*, 1–16. [CrossRef]
13. Hashim, M.; Pour, A.B.; Chong, K.W. Tropical forest degradation monitoring using ETM+ and MODIS remote sensing data in the Peninsular Malaysia. *IOP Conf. Ser. Earth Environ. Sci.* **2014**, *18*, 1–6. [CrossRef]
14. Ingole, N.A.; Ram, R.N.; Ranjan, R.; Shankhwar, A.K. Advance application of geospatial technology for fisheries perspective in Tarai region of Himalayan state of Uttarakhand. *Sustain. Water Resour. Manag.* **2015**, *1*, 181–187. [CrossRef]
15. Koch, B. Remote Sensing supporting national forest inventories NFA. In *FAO Knowledge Reference for National Forest Assessments*; FAO: Rome, Italy, 2015; pp. 77–92. Available online: http://www.fao.org/3/a-i4822e.pdf (accessed on 16 December 2019).
16. Næsset, E.; Ørka, H.O.; Solberg, S.; Bollandsås, O.M.; Hansen, E.H.; Mauya, E.; Zahabu, E.; Malimbwi, R.; Chamuya, N.; Olsson, H.; et al. Mapping and estimating forest area and aboveground biomass in miombo woodlands in Tanzania using data from airborne laser scanning, TanDEM-X, RapidEye, and global forest maps: A comparison of estimated precision. *Remote Sens. Environ.* **2016**, *175*, 282–300. [CrossRef]
17. Malenovský, Z.; Rott, H.; Cihlar, J.; Schaepman, M.E.; García-Santos, G.; Fernandes, R.; Berger, M. Sentinels for science: Potential of Sentinel-1, -2, and -3 missions for scientific observations of ocean, cryosphere, and land. *Remote Sens. Environ.* **2012**, *120*, 91–101. [CrossRef]
18. Woodcock, C.E.; Allen, R.; Anderson, M.; Belward, A.; Bindschadler, R.; Cohen, W.; Gao, F.; Goward, S.N.; Helder, D.; Helmer, E.; et al. Free access to Landsat imagery. *Sci. Lett.* **2008**, *320*, 1011–1012. [CrossRef] [PubMed]
19. Gizachew, B.; Solberg, S.; Naesset, E.; Gobakken, T.; Bollandsas, O.M.; Breidenbach, J.; Zahabu, E.; Mauya, E.W. Mapping and estimating the total living biomass and carbon in low-biomass woodlands using Landsat 8 CDR data. *Carbon Balance Manag.* **2016**, *11*, 1–14. [CrossRef] [PubMed]

20. Li, C.; Li, Y.; Li, M. Improving Forest Aboveground Biomass (AGB) Estimation by Incorporating Crown Density and Using Landsat 8 OLI Images of a Subtropical Forest in Western Hunan in Central China. *Forests* **2019**, *10*, 104. [CrossRef]
21. Navarro, J.A.; Algeet, N.; Fernández-Landa, A.; Esteban, J.; Rodríguez-Noriega, P.; Guillén-Climent, M.L. Integration of UAV, Sentinel-1, and Sentinel-2 Data for Mangrove Plantation Aboveground Biomass Monitoring in Senegal. *Remote Sens.* **2019**, *11*, 77. [CrossRef]
22. Qiu, A.; Yang, Y.; Wang, D.; Xu, S.; Wang, X. Exploring parameter selection for carbon monitoring based on Landsat-8 imagery of the aboveground forest biomass on Mount Tai. *Eur. J. Remote Sens.* **2019**, *52*, 1–12. [CrossRef]
23. Risdiyanto, I.; Fakhrul, M. Examination of Multi-Spectral Radiance of the Landsat 8 Satellite Data for Estimating Biomass Carbon Stock at Wetland Ecosystem. *Preprints* **2017**, 1–14. [CrossRef]
24. Sousa, A.M.O.; Gonçalves, A.C.; da Silva, J.R.M. Above-Ground Biomass Estimation with High Spatial Resolution Satellite Images. In *Biomass Volume Estimation and Valorization for Energy*; Tumuluru, J.S., Ed.; InTech: Rijeka, Croatia, 2017; Volume 2017, pp. 47–70. [CrossRef]
25. Sousa, A.M.O.; Gonçalves, A.C.; Mesquita, P.; Marques da Silva, J.R. Biomass estimation with high resolution satellite images: A case study of Quercus rotundifolia. *ISPRS J. Photogramm. Remote Sens.* **2015**, *101*, 69–79. [CrossRef]
26. Baloloy, A.B.; Blanco, A.C.; Candido, C.G.; Argamosa, R.J.L.; Dumalag, J.B.L.C.; Dimapilis, L.L.C.; Paringit, E.C. Estimation of Mangrove Forest Aboveground Biomass Using Multispectral Bands, Vegetation Indices and Biophysical Variables Derived from Optical Satellite Imageries: Rapideye, Planetscope and Sentinel-2. *ISPRS Ann. Photogramm. Remote Sens. Spat. Inf. Sci.* **2018**, *IV-3*, 29–36. [CrossRef]
27. Lu, D. Aboveground biomass estimation using Landsat TM data in the Brazilian Amazon. *Int. J. Remote Sens.* **2007**, *26*, 2509–2525. [CrossRef]
28. López-Serrano, P.M.; López-Sánchez, C.A.; Álvarez-González, J.G.; García-Gutiérrez, J. A Comparison of Machine Learning Techniques Applied to Landsat-5 TM Spectral Data for Biomass Estimation. *Can. J. Remote Sens.* **2016**, *42*, 690–705. [CrossRef]
29. Günlü, A.; Ercanli, I.; Başkent, E.Z.; Çakır, G. Estimating aboveground biomass using Landsat TM imagery: A case study of Anatolian Crimean pine forests in Turkey. *Ann. For. Res.* **2014**, *57*, 289–298. [CrossRef]
30. Das, S.; Singh, T.P. Correlation analysis between biomass and spectral vegetation indices of forest ecosystem. *Int. J. Eng. Res. Technol.* **2012**, *1*, 1–13.
31. Ringrose, S.; Matheson, W.; Matlala, C.J.S.S.; O'Neill, T.; Werner, P.A. Vegetation spectral reflectance along a north-south vegetation gradient in northern Australia. *J. Biogeogr.* **1994**, *21*, 33–47. [CrossRef]
32. Sader, S.A.; Waide, R.B.; Lawrence, W.T.; Joyce, A.T. Tropical forest biomass and successional age class relationships to a vegetation index derived from Landsat TM data. *Remote Sens. Environ.* **1989**, *28*, 143–156. [CrossRef]
33. Viña, A.; Gitelson, A.A.; Nguy-Robertson, A.L.; Peng, Y. Comparison of different vegetation indices for the remote assessment of green leaf area index of crops. *Remote Sens. Environ.* **2011**, *115*, 3468–3478. [CrossRef]
34. Macedo, F.L.; Sousa, A.M.O.; Gonçalves, A.C.; Marques da Silva, J.R.; Mesquita, P.A.; Rodrigues, R.A.F. Above-ground biomass estimation for *Quercus rotundifolia* using vegetation indices derived from high spatial resolution satellite images. *Eur. J. Remote Sens.* **2018**, *51*, 932–944. [CrossRef]
35. Imran, A.B.; Khan, K.; Ali, N.; Ahmad, N.; Ali, A.; Shah, K. Narrow band based and broadband derived vegetation indices using Sentinel-2 Imagery to estimate vegetation biomass. *Glob. J. Environ. Sci. Manag.* **2020**, *6*, 97–108. [CrossRef]
36. Motohka, T.; Nasahara, K.N.; Oguma, H.; Tsuchida, S. Applicability of Green-Red Vegetation Index for Remote Sensing of Vegetation Phenology. *Remote Sens.* **2010**, *2*, 2369. [CrossRef]
37. Larrinaga, A.R.; Brotons, L. Greenness Indices from a Low-Cost UAV Imagery as Tools for Monitoring Post-Fire Forest Recovery. *Drones* **2019**, *3*, 6. [CrossRef]
38. Sonnentag, O.; Hufkens, K.; Teshera-Sterne, C.; Young, A.M.; Friedl, M.; Braswell, B.H.; Milliman, T.; O'Keefe, J.; Richardson, A.D. Digital repeat photography for phenological research in forest ecosystems. *Agric. For. Meteorol.* **2012**, *152*, 159–177. [CrossRef]
39. Kelsey, K.; Neff, J. Estimates of Aboveground Biomass from Texture Analysis of Landsat Imagery. *Remote Sens.* **2014**, *6*, 6407–6422. [CrossRef]

40. Otukei, J.R.; Emanuel, M. Estimation and mapping of above ground biomass and carbon of Bwindi impenetrable National Park using ALOS PALSAR data. *S. Afr. J. Geomat.* **2015**, *4*, 1–13. [CrossRef]
41. Duriaux, J.Y.; Baudron, F. Understanding people and forest interrelations along an intensification gradient in Arsi-Negele, Ethiopia. In *Agrarian Change in Tropical Landscapes*; Deakin, L., Kshatriya, M., Sunderland, T., Eds.; Center for International Forestry Research (CIFOR): Bogor, Indonesia, 2016; pp. 14–53.
42. Asrat, Z.; Eid, T.; Gobakken, T.; Negash, M. Aboveground tree biomass prediction options for the Dry Afromontane forests in south-central Ethiopia. *For. Ecol. Manag.* **2020**, *473*, 1–14. [CrossRef]
43. Topcon Positioning Systems Inc. Available online: https://www.topconpositioning.com/gb/gnss-network-solutions (accessed on 16 September 2019).
44. Kouba, J. A Guide to Using International GNSS Service (IGS) Products. 2009, p. 34. Available online: https://www.researchgate.net/profile/Jan_Kouba/publication/228663800_A_guide_to_using_International_GNSS_Service_IGS_products/links/54fcc30c0cf270426d102cd3.pdf (accessed on 18 May 2020).
45. *MAGNET Tools 1.0*; Topcon Positioning Systems Inc.: Livermore, CA, USA, 2012; Available online: https://www.tigersupplies.com/files/bcf31975-d2e6-44c2-ba66-7bad3a95cdb3HLP_MAGNET_Office_Tools_v1_0_EN.pdf (accessed on 21 September 2019).
46. Haglöf Company Group. Available online: http://www.haglofsweden.com/index.php/en/products/instruments/height/541-the-vertex-laser-geo-all-you-need-in-a-rangefinder-hypsometer (accessed on 12 November 2019).
47. Sullivan, M.J.P.; Lewis, S.L.; Hubau, W.; Qie, L.; Baker, T.R.; Banin, L.F.; Chave, J.; Cuni-Sanchez, A.; Feldpausch, T.R.; Lopez-Gonzalez, G.; et al. Field methods for sampling tree height for tropical forest biomass estimation. *Methods Ecol. Evol.* **2018**, *9*, 1179–1189. [CrossRef] [PubMed]
48. Asrat, Z.; Eid, T.; Gobakken, T.; Negash, M. Modeling and quantifying tree biometric properties of Dry Afromontane forests of South-central Ethiopia. *Trees* **2020**. under review. [CrossRef]
49. Berhe, L.; Assefa, G.; Teklay, T. Models for estimation of carbon sequestered by *Cupressus lusitanica* plantation stands at Wondo Genet, Ethiopia. *South For.* **2013**, *75*, 113–122. [CrossRef]
50. Ounban, W.; Puangchit, L.; Diloksumpun, S. Development of general biomass allometric equations for Tectona grandis Linn. f. and Eucalyptus camaldulensis Dehnh. plantations in Thailand. *Agric. Nat. Resour.* **2016**, *50*, 48–53. [CrossRef]
51. Owate, O.A.; Mware, M.J.; Kinyanjui, M.J. Allometric Equations for Estimating Silk Oak (*Grevillea robusta*) Biomass in Agricultural Landscapes of Maragua Subcounty, Kenya. *Int. J. For. Res.* **2018**, 1–14. [CrossRef]
52. USGS. USGS Earth Explorer. Available online: https://earthexplorer.usgs.gov/ (accessed on 23 August 2019).
53. Planet. Planet Explorer. Available online: https://www.planet.com/explorer/ (accessed on 3 September 2019).
54. QGIS Development Team. QGIS—A Free and Open Source Geographic Information System. Available online: https://www.qgis.org/en/site/ (accessed on 23 November 2019).
55. Huete, A.; Justice, C.; Van Leeuwen, W. MODIS Vegetation Index (MOD13). Algorithm Theoretical Basis Document. p. 129. 1999. Available online: https://modis.gsfc.nasa.gov/data/atbd/atbd_mod13.pdf (accessed on 16 October 2019).
56. Rouse, J.W.; Hass, R.H.; Schell, J.A.; Deering, D.W.; Harlan, J.C. *Monitoring the Vernal Advancement and Netrogradation (Greenwave Effect) of Natural Vegetation*; Texas A&M University: College Station, TX, USA, 1974; p. 390.
57. Jordan, C.F. Derivation of leaf-area index from quality of light on the forest floor. *Ecology* **1969**, *5*, 663–666. [CrossRef]
58. Adamsen, F.J.; Pinter, P.J.; Barnes, E.M.; LaMorte, R.L.; Wall, G.W.; Leavitt, S.W.; Kimball, B.A. Measuring wheat senescence with a digital camera. *Crop Sci.* **1999**, *39*, 719–724. [CrossRef]
59. Richardson, A.J.; Wiegand, C.L. Distinguishing vegetation from soil background information. *Photogramm. Eng. Remote Sens.* **1977**, *43*, 1541–1552.
60. Louhaichi, M.; Borman, M.M.; Johnson, D.E. Spatially Located Platform and Aerial Photography for Documentation of Grazing Impacts on Wheat. *Geocarto Int.* **2001**, *16*, 65–70. [CrossRef]
61. Liu, H.Q.; Huete, A. A feedback based modification of the NDVI to minimize canopy background and atmospheric noise. *IEEE Trans. Geosci. Remote Sens.* **1995**, *33*, 457–465. [CrossRef]
62. Huete, A.R. A soil-adjusted vegetation index (SAVI). *Remote Sens. Environ.* **1988**, *25*, 295–309. [CrossRef]
63. Qi, J.; Kerr, Y.; Chehbouni, A. External factor consideration in vegetation index development. In Proceedings of the 6th International Symposium on Physical Measurements and Signatures in Remote Sensing, Val d'lsère, France, 17–21 January 1994; pp. 723–730.

64. Gao, B.C. NDWI—A normalized difference water index for remote sensing of vegetation liquid water from space. *Remote Sens. Environ.* **1996**, *58*, 257–266. [CrossRef]
65. Kaufman, Y.J.; Tanre, D. Atmospherically resistant vegetation index (ARVI) for EOS-MODIS. *IEEE Trans. Geosci. Remote Sens.* **1992**, *30*, 261–270. [CrossRef]
66. Rajah, P.; Odindi, J.; Mutanga, O.; Kiala, Z. The utility of Sentinel-2 Vegetation Indices (VIs) and Sentinel-1 Synthetic Aperture Radar (SAR) for invasive alien species detection and mapping. *Nat. Conserv.* **2019**, *35*, 41–61. [CrossRef]
67. Torino, M.S.; Ortiz, B.V.; Fulton, J.P.; Balkcom, K.S.; Wood, C.W. Evaluation of Vegetation Indices for Early Assessment of Corn Status and Yield Potential in the Southeastern United States. *Agron. J.* **2014**, *106*, 1389–1401. [CrossRef]
68. Gitelson, A.; Merzlyak, M.N. Quantitative estimation of chlorophyll-a using reflectance spectra: Experiments with autumn chestnut and maple leaves. *J. Photochem. Photobiol. B Biol.* **1994**, *22*, 247–252. [CrossRef]
69. ESA. SNAP Version 7.0.0. Available online: http://step.esa.int/main/download/snap-download/ (accessed on 28 August 2019).
70. Magnussen, S.; Næsset, E.; Gobakken, T. An application niche for finite mixture models in forest resource surveys. *Can. J. For. Res.* **2019**, *49*, 1453–1462. [CrossRef]
71. Särndal, C.E.; Swensson, B.; Wretman, J. *Model Assisted Survey Sampling*; Springer: New York, NY, USA, 1992; p. 694.
72. Magnussen, S.; Næsset, E.; Kändler, G.; Adler, P.; Renaud, J.P.; Gobakken, T. A functional regression model for inventories supported by aerial laser scanner data or photogrammetric point clouds. *Remote Sens. Environ.* **2016**, *184*, 496–505. [CrossRef]
73. Salinas-Melgoza, M.A.; Skutsch, M.; Lovett, J.C. Predicting aboveground forest biomass with topographic variables in human-impacted tropical dry forest landscapes. *Ecosphere* **2018**, *9*, 1–20. [CrossRef]
74. Schober, P.; Boer, C.; Schwarte, L.A. Correlation Coefficients: Appropriate Use and Interpretation. *Anesth. Analg.* **2018**, *126*, 1763–1768. [CrossRef] [PubMed]
75. Bao, N.; Li, W.; Gu, X.; Liu, Y. Biomass Estimation for Semiarid Vegetation and Mine Rehabilitation Using Worldview-3 and Sentinel-1 SAR Imagery. *Remote Sens.* **2019**, *11*, 2855. [CrossRef]
76. Lorenzen, B.; Jensen, A. Reflectance of blue, green, red and near infrared radiation from wetland vegetation used in a model discriminating live and dead above ground biomass. *New Phytol.* **1988**, *108*, 345–355. [CrossRef]
77. Lu, D.; Batistella, M.; Moran, E. Satellite estimation of aboveground biomass and impacts of forest stand structure. *Photogramm. Eng. Remote Sens.* **2005**, *71*, 967–974. [CrossRef]
78. Wang, Q.; Pang, Y.; Li, Z.; Sun, G.; Chen, E.; Ni-Meister, W. The Potential of Forest Biomass Inversion Based on Vegetation Indices Using Multi-Angle CHRIS/PROBA Data. *Remote Sens.* **2016**, *8*, 891. [CrossRef]
79. Prasad, B.; Babar, M.A.; Carver, B.F.; Raun, W.R.; Klatt, A.R. Association of biomass production and canopy spectral reflectance indices in winter wheat. *Can. J. Plant. Sci.* **2009**, *89*, 485–496. [CrossRef]
80. Lu, N.; Zhou, J.; Han, Z.; Li, D.; Cao, Q.; Yao, X.; Tian, Y.; Zhu, Y.; Cao, W.; Cheng, T. Improved estimation of aboveground biomass in wheat from RGB imagery and point cloud data acquired with a low-cost unmanned aerial vehicle system. *Plant Methods* **2019**, *15*, 1–16. [CrossRef]
81. Uyeda, K.A.; Stow, D.A.; Roberts, D.A.; Riggan, P.J. Combining ground-based measurements and MODIS-based spectral vegetation indices to track biomass accumulation in post-fire chaparral. *Int. J. Remote Sens.* **2016**, *38*, 728–741. [CrossRef]
82. Horler, D.N.H.; Ahern, F.J. Forestry information content of Thematic Mapper data. *Int. J. Remote Sens.* **1986**, *7*, 405–428. [CrossRef]
83. Roy, P.S.; Ravan, S.A. Biomass estimation using satellite remote sensing data—an investigation on possible approaches for natural forest. *J. Biosci.* **1996**, *21*, 535–561. [CrossRef]
84. Nichol, J.E.; Sarker, M.L.R. Improved Biomass Estimation Using the Texture Parameters of Two High-Resolution Optical Sensors. *IEEE Trans. Geosci. Remote Sens.* **2011**, *49*, 930–948. [CrossRef]

PAPER-IV

Digital Photography for Estimating Canopy Cover in an Afromontane Forest

Habitamu Taddese [1, 2, *], Terje Gobakken [3], Daniel Ayalew Mengistu [4], Hans Ole Ørka [3] and Ingunn Burud [1]

1 Norwegian University of Life Sciences, Faculty of Science and Technology, P. O. Box 5003, 1432, Ås, Norway; ingunn.burud@nmbu.no (I.B.)

2 Hawassa University, Wondo Genet College of Forestry and Natural Resources, Department of Geographic Information Science, P. O. Box 128, Shashemene, Ethiopia

3 Norwegian University of Life Sciences, Faculty of Environmental Sciences and Natural Resource Management, P. O. Box 5003, 1432, Ås, Norway; terje.gobakken@nmbu.no (T.G.); hans.ole.orka@nmbu.no (H.O.Ø.)

4 Bahir Dar University, Geospatial Data & Technology Center, Department of Geography and Environmental Studies, P. O. Box 1398, Bahir Dar, Ethiopia; dan952003@yahoo.com (D.A.M.)

* Correspondence: habitamu.taddese.berie@nmbu.no or habtu1976@gmail.com

Abstract

Canopy cover (CC), which is one of the attributes of the horizontal forest structure, has multiple ecological significances. Although data about forest CC provides multiple uses, its measurement has remained a time-consuming process or vulnerable to subjectivity and is seldom included in forest inventories. Recent advances in digital technology have brought opportunities for objective measurement of CC. This study was initiated to develop a methodology for analysing near-vertical digital photos for quick and precise estimation of forest CC. A photo processing routine was developed to derive CC data from digital photos. Otsu thresholding was used to segment the blue band digital photos. Then, the segmented photos were sliced radially inward into different sizes of concentric square sections to test the effect of field of view on the precision of CC estimates. The canopy fractions of the resulting photos were further classified into canopy and non-canopy classes based on different thresholds. The effects of photo size, thresholds and their interactions on the CC estimation were compared. The precision and mean difference of the photo-based estimates using the optimum criteria were evaluated against that of the point-based data. The results of this study indicated that digital photography offered ample flexibility for controlling photo sizes and thresholds that optimizes the precision of CC estimates. The central 1-3% of the photos classified with 10% and 20% thresholds gave CC estimates that had correlation coefficients of more than 92% compared with the point-based data. Therefore, a narrow-angle camera lens is recommended for canopy photography. The use of smallest threshold (i.e., 10%) improved the precision of the estimates. The new method is suitable for large-scale forest monitoring and inventory.

Keywords: photography; canopy cover; Afromontane forest; Otsu thresholding; classification threshold; photo size

1. Introduction

Description of forest canopy structure is of great importance in forest ecology and management. The descriptions of forest canopy structure encompass analyses of the vertical and horizontal arrangement of the tree crowns. While the vertical canopy structure emphasises the arrangement of tree crown heights, the horizontal canopy structure deals with the spatial arrangement of tree crowns and gaps on a horizontal plane. Canopy cover (CC), which is one of the descriptors of the horizontal forest canopy structure, is the proportion of the ground surface covered by the vertical projection of tree canopy (Jennings et al., 1999). The term CC has often been confused with crown cover and canopy closure in the literature (Gonsamo et al., 2013). Jennings et al. (1999) and Gonsamo et al. (2013) distinguished crown cover as a non-transparent crown envelope of the forest crown elements above the forest floor, and canopy closure (canopy density), which is the proportion of the sky hemisphere obscured by vegetation when viewed from a single point. Canopy closure is a perspective projection of the crown from a point whereas CC is a parallel projection of tree crowns and canopy gaps from respective point locations. Crown cover does not account for the gaps within a crown. It only assumes the gaps between crown envelopes. However, observation of within-crown gaps is useful for estimating the lighting conditions at the point of observation (Anderson, 1964; Rich, 1990; Jennings et al., 1999). In reality, the crown has both foliage fraction and gap fraction when viewed upward to the zenith. Thus, this research tried to align with the concept of CC that accounts for the distinction of foliage and gap fractions in a tree crown. The foliage component is the aerial layer of branches, stems, reproductive structures (i.e., seeds, pods and flowers) and leaves of trees in a forest.

Forest CC is one of the most important variables in forest characterization and is a basis for the definition of the forest entity itself. The united nations' food and agriculture organization (FAO) defines forest as "land spanning more than 0.5 hectares with trees higher than 5 meters and a CC of more than 10%, or trees able to reach these thresholds in situ" (FAO, 2000). Countries around the world have adopted different thresholds of minimum CC for forest ranging between 10% and 30% (UNFCCC, 2001). CC is also a useful criterion for land cover classification using remotely sensed data (Pratt et al., 1966; Korhonen, et al., 2015).

Information about the density and distribution of forest canopy has many environmental benefits. As an outer envelope of the forest, characteristics of a forest canopy determine the amount of solar radiation that reaches the forest floor and affect the local microhabitat conditions (Rich, 1990).

This, in turn, influences the forest ecosystem functions and the nature of interaction among the ecosystem components. Particularly, the heterogeneous canopy structure in tropical forests influences the understory light availability, which affects photosynthesis, plant morphology and fluxes of carbon, water, and energy between the atmosphere, pedosphere, and biosphere (Calder, 2001; Ligot et al., 2014). Interaction of the forest canopy with solar radiation makes it one of the determinants of forest reflectance from optical passive remotely sensed data (Dawson et al., 1999). Thus, field estimates of canopy structure using digital photos are useful for validating remotely sensed information (Gemmell, 1999; Korhonen et al., 2006).

Information on CC helps to support sustainable forest and land management (Akike and Samanta, 2016; Ćosović et al., 2020). Agroforestry practices including for example the traditional coffee production systems in Ethiopia require information about the amount and spatial arrangement of CC to determine the availability of adequate shade trees. CC has also a profound importance for setting forest management prescriptions (Kern et al., 2017; Vilanova, 2020), upon which canopy manipulation silvicultural methods are undertaken to enhance forest productivity by improving light penetration to the understory vegetation. Monitoring of CC can be used to evaluate the impact of forest use manipulations (e.g. thinning, forest degradation, regeneration, forestation, deforestation, and forest fire). It helps to plan pruning activities for controlling the spread of forest fires and assess its effects (Fitzgerald, 2005; Bellows et al., 2016). Some studies indicated that CC is also a useful variable for estimating timber volume (Næsset, 1997; Zhang et al., 2017). Furthermore, recent research results indicated CC is a better predictor of aboveground biomass than tree height in some tropical forests (Singh et al., 2016). The importance of trees for watershed management is mainly attributed to the contribution of tree canopies for replenishing groundwater and reducing soil erosion (Calder et al., 2008; Cao et al., 2017).

Although CC is a good indicator of forest ecosystem stability and is a critical factor of the formal forest definitions, this variable is not included in many national forest inventories (NFI) in tropical countries (e.g. Ethiopia), maybe due to practical reasons related to attaining a balance between the financial cost, time for fieldwork, and precision using the existing measurement techniques. Measurement of CC is difficult particularly in tropical forests that are composed of several species with structurally complex canopies (Taubert et al., 2015; Palace et al., 2016; Hofhansl et al., 2020).

A precise estimate of CC is of paramount importance to improve the quality of forest information. Several methods, which range from using simple handheld mirrors to sophisticated analysis of digital photos captured using smartphones and other digital devices, have been used to estimate CC (Johansson, 1985; Tichý, 2016; Bianchi et al., 2017). Many of the field estimation techniques like the use of the Cajanus tube are too expensive requiring a substantial amount of fieldwork, particularly difficult to implement over a large area (Korhonen et al., 2006). Large-scale forest monitoring like the NFI requires methods that ensure consistency between measurements made by different people at different times and in different forest types. Ocular (visual) estimation is a simple and quick technique but it measures canopy closure (Goldsmith, 1991; Jennings et al., 1999; Paletto and Tosi, 2009; Goodenough and Goodenough, 2012). There is also high interobserver variability and a lack of precision with the use of this method (Paletto and Tosi, 2009). The CC estimates can be more objective by running the observation at many points in systematic grid locations within the boundary of the plot and estimating plot CC as the average of the observations made for each point (Jennings et al., 1999; Korhonen et al., 2006). However, this incurs an increased time in fieldwork. Remote sensing technologies like the airborne LiDAR (light detection and ranging) provide precise CC data but they are slightly biased that require calibration for wide scan angles (Korhonen et al., 2011). Following the recent advances in mobile technology, new smartphone applications like HabitApp, GLAMA (gap light analysis mobile application) and CanopyApp allow a quick estimation of CC but with limited processing options (Landert, 2016; MacDonald & MacDonald, 2016; Tichý, 2016; Bianchi et al., 2017; Deichmann, et al., 2017).

Besides maintaining high precision, large-scale forest monitoring demands fast and cheap retrieval of CC data. Indirect methods such as the use of digital photography with a narrow field of view increase objectivity and precision (Chianucci, 2016; FVC, 2020). Previous studies in this regard focused on the use of hemispherical and digital cover photography for assessing forest canopy. Hemispherical photography (HP) or the fisheye method has been the most widely used photographic method. It has the advantage of sampling large areas that helps to minimize the time and labour requirements. However, parts of the hemispherical photo close to the edges suffer from distortion, coarse pixel resolution, and blurring problems (Brown et al., 2000; Gonsamo et al., 2010; Gonsamo et al., 2013; FVC, 2020). HP is used to estimate canopy closure, not CC. Therefore, the use of an ordinary digital camera is more useful for CC estimation than that of the HP. In addition, there is flexibility in the photo processing techniques used for analysing digital

photographs (Goodenough and Goodenough, 2012). Furthermore, digital cameras are becoming cheaper, have a high image resolution, and help to collect archival records that can be stored and reanalysed later for change detection. This method has huge potential combining different advantages since the data capture is fast, easy, and requires less human judgement to get an objective, reliable, and replicable estimate that is needed for forest monitoring (Chianucci, et al., 2014; Alivernini et al., 2018). However, the feasibility of the photo processing methods to get a good estimate of CC has not been investigated in the forest type under this study. Hence, it is important to test a method that is faster, cheaper, and operationally easier for multipurpose forest inventory. Developing a photo processing routine and automating its implementation are believed to enhance CC estimation efficiency, which then improves its practicability for large-area forest monitoring. Therefore, the aims of this study were: 1) to determine optimum photo processing techniques for CC estimation, and 2) to evaluate the performance of the selected optimum photo-based methods for estimating CC.

2. Materials and methods

2.1. Study area description

The study was carried out in the Degaga-Gambo forest, which is found in the eastern escarpment of the central rift valley of Ethiopia. Geographically, the forest lies between 38°45' and 38°56' E longitude and between 7°13' and 7°33' N latitude (Figure 1). The study area has a natural forest in the upland rugged topography and plantation compartments in the lower elevations where access is relatively easier. The CC data were collected from both the plantation and natural forests. The study forests in general, particularly the natural forest, is under pressure due to the increasing human population. The main economic activity of the local people relies on crop production, animal husbandry, and ecotourism activities. Rural villages and small townships are surrounding the forest. The main source of household energy in these settlements comes from the wood collected in the forest illegally. People are regularly encroaching into the forest territory for collecting wood, expanding farmlands and establishing illegal settlements inside the forest. As a result, some of the sample plot (SP) locations fell inside farmlands, harvested compartments, and home gardens with no CC or with potential risk of accessing them.

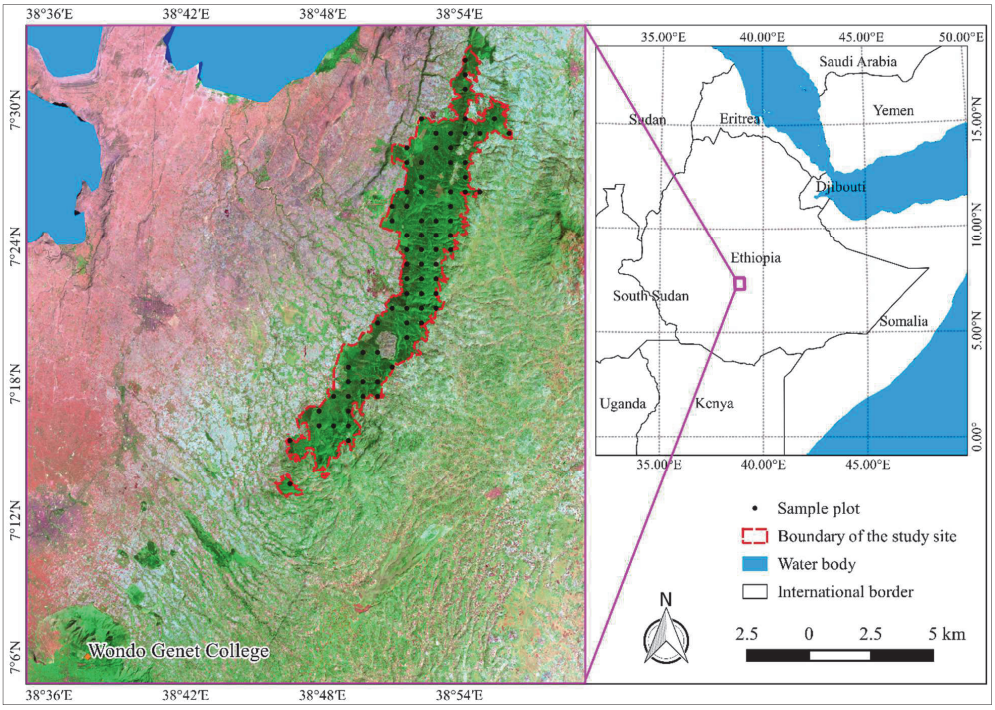

Figure 1. Location of the sample plots (SPs) in the study area. The background satellite image in the map is the false-colour composite (SWIR-NIR-R band combination) of L8 image in the order of R-G-B band rendering for enhancing the visualization of vegetation cover. (Note: SWIR, NIR, R, G and B are shortwave infrared, near-infrared, red, green and blue bands, respectively).

2.2. Forest canopy cover data collection

A spatially aligned systematic sampling design was used for locating the centre of the circular SPs in this study. The systematic sampling design was chosen due to its simplicity. It keeps a spatial balance of the samples making them representative of the entire population (Penman et al., 2003). It minimizes the spatial correlation among observations and hence increases the statistical efficiency of estimates as compared to other sampling designs (Mello et al., 2015). Furthermore, a systematic sampling design has the advantage to optimize the precision of estimates for multiple variables simultaneously (McRoberts et al., 2015). Thus, we adopted the systematic sampling design in this study since we are interested in optimising the estimation efficiency of two

measurement methods. The shape of the SPs was circular with a requirement of only one control point, which is the plot centre. A circular plot has a small perimeter compared to other shapes that demand a few number of decisions to include or exclude a tree during measurement. The field SPs were positioned at intervals of 1.18 km in both east-west and north-south directions to optimise the requirements of fieldwork and precision of the estimates. The spatial correlation of measurements is very weak at these distances. We used handheld Garmin 78 GPS to navigate to the location of the SPs. Precise positions of the plot centres were measured using differential GNSS with rover and base units of Topcon legacy-E dual-frequency receivers (Topcon Positioning Systems Inc.). The standard error of the post-processed planimetric plot coordinates ranged between 0.02 and 1.11 m with a mean of 0.23 m.

Not all of the systematically distributed point locations were sampled since some of the locations did not represent the forest. The CC data were gathered at SPs that fell in the forest. At each of the SP locations, a systematic line network of 3 m interval was created in the east-west and north-south directions. This distance provided more than 102 data points within the circular plot that offered similar estimates with a sample size of 195 in the study by Korhonen et al. (2006). The 3 m spacing gave 109 observations per SP of 1000 m^2. Canopy observation points were located at the intersections of the line networks within a radius of 17.85 m from the SP (Figure 2). The point count sampling (or simply, point-based) method of canopy cover estimation combines the advantages of the grid (line transect) method, ocular estimation, and the use of point sampling instruments like the Cajanus tube. The use of several sampling points enhances the precision of estimates (Korhonen et al., 2006) while the use of a level gauge for supporting the visual judgement reduces the inherent bias in visual estimation (FVC, 2020).

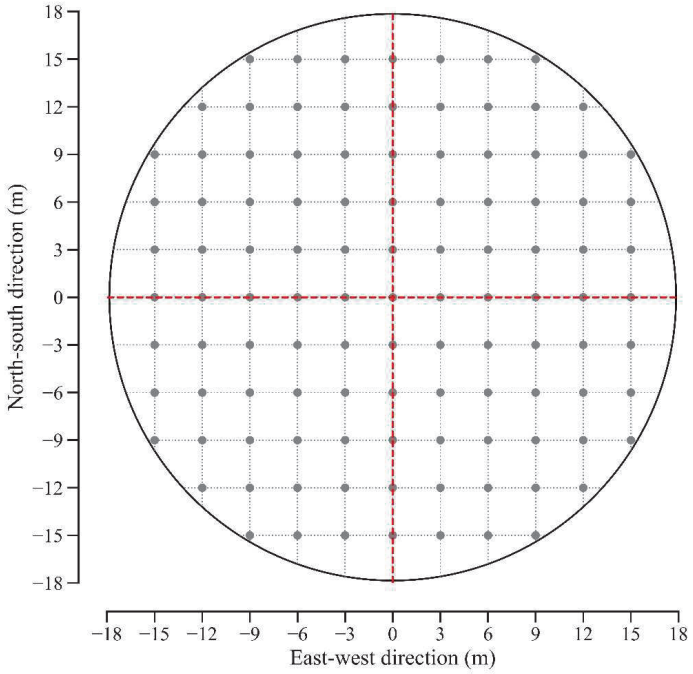

Figure 2. Design of the sampling locations (dots) within a circular SP of 17.85 m radius. The canopy cover (CC) data were gathered at the intersections of the broken lines within the circular plot at an interval of 3 m in both north-south (north is upwards) and east-west (east is rightwards) directions from the centre of the SP, which is represented by the intersection of the broken red lines.

As one of the direct methods of canopy measurement, point count sampling has limitations of efficiency since it is a time-consuming data collection method (Chianucci, 2016). Taking several observations (with a sample size of 109, in this case) in a plot yields a high precision (Jennings et al. 1999; Korhonen et al., 2006). In this method, at each of the point count sampling locations, an experienced forestry professional observed if the sky vertically above the point was obscured by forest canopy (1) or not (0). The method is a modification of the systematic point sampling technique using the Cajanus tube by Korhonen et al. (2006). Instead of the Cajanus tube, we used visual observation assisted with the level gauge of a digital camera that we used for photo capture (see section 2.3). The level gauge was used to keep the sighting angles within a very small deviation from the vertical. Leaves, twigs, and branches that obscured the sky in the zenith direction from

the observation point characterised the cover components while the clear sky or clouds formed the gap component. The binary count data (i.e. counts of 1 or 0) of the point observations were converted to CC, which is the proportion of obscured (1) counts to the total (109), using Equations 1 and 2.

$$x_{j,k} = \begin{cases} 1, & \text{if the sky above point j in plot k is canopy obscured} \\ 0, & \text{otherwise} \end{cases} \quad (1)$$

where $x_{j,k}$ is the binary variable representing the occurrence of canopy element above the point location j (1, 2, 3, …, 109) in SP k (1, 2, 3, …, 76).

The occurrences of canopy components were used for calculating the plot-level CC estimates using the point count sampling method (x_k, in %).

$$x_k = \frac{\sum_{j=1}^{m} x_{j,k}}{m} \times 100 \quad (2)$$

where m is the number of observation points in each SP (i.e., m=109 in this case).

The variance for the point estimates of the point-based CC was also calculated as:

$$\mathrm{var}(x_k) = \frac{x_k(1 - x_k)}{m} \quad (3)$$

where $\mathrm{var}(x_k)$ is the variance estimator of the binary data for each SP. This same equation was also used to compute the variance of the binary output of the photo-based method, $var(y_{j,k,m})$, which is described in section 2.5.

The distribution of the point-based CC data is skewed to the small values (Figure 3). There is a maximum CC (100%) for most SPs but a few observations skewed the mean CC to the left.

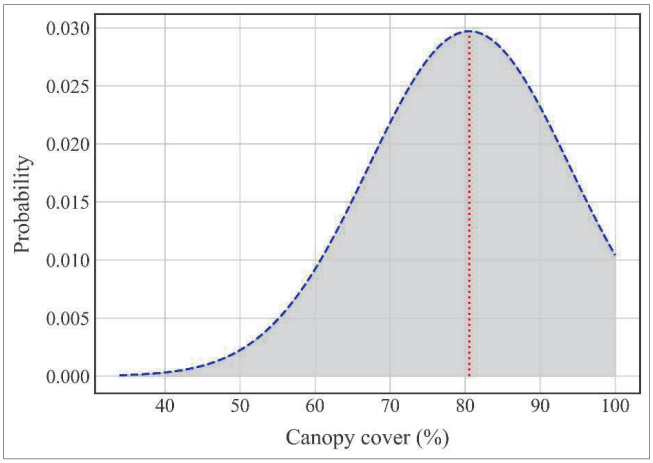

Figure 3. Distribution of point-based CC (n=76) fitted to the normal curve (dashed blue line) with centre at the mean (red broken vertical line), which was 80.55%.

2.3. Digital photo acquisition and processing

Vertical photos were captured at point locations where count data were collected. The camera was held at a constant height (at about 2m above the ground) since two persons of equivalent height captured the photos and the level of the camera was consistent by holding it as straight as possible. The camera was oriented upwards to the zenith to be able to acquire near-vertical photos. The level gauge display was used to control the vertical orientation of the optical axis. Automatic exposure and shutter speed were set throughout the photo capture as suggested by Paletto and Tosi (2009). The camera flash was turned off since there was enough light at the time of exposure. To avoid potentially confounding variables, both techniques of CC data collection (i.e., the point-based and photo-based) were done simultaneously to ensure the presence of comparable light and weather conditions.

The digital photos were captured with an Olympus Tough TG-5 camera, which has a lens with an actual focal length of 4.5 mm (which is equivalent to 25 mm of a 35 mm lens focal length). A focal length of 4.5 mm in this camera lens provides the same field of view as 25 mm compared to a 35 mm camera, which is the field of view for a full-frame sensor (Bosiers *et al*., 2003; Piper and Pelc, 2020). Thus, the camera used in this study has a wide-angle lens. Such a wide-angle lens was used to assess canopy fractions in different land-use types (Hwang et al., 2020). The Tough TG-5 camera

has an aspect ratio of 1.33 and captures photos with dimensions of 4000 × 3000 pixels (i.e., it has a 12 megapixels sensor) when taken without zooming. Since the photo periphery is prone to be obscured (i.e., radial inward distortion), the photos were cropped to 3000 × 3000 pixels before any further processing. Python programming language version 3.7 (Python Software Foundation) was used for photo processing and data analysis. Different python libraries were used in this study. Photo processing was undertaken using the OpenCV library. NumPy, SciPy, pandas, and statsmodels libraries were used for data analysis and statistical testing while matplotlib and seaborn libraries were used for data visualization.

The digital camera provides RGB (red-green-blue) colour images. The blue band was thresholded into canopy and sky since it gives a relatively higher contrast between the canopy elements and the sky even in the presence of clouds (Frazer et al., 2001; Nobis and Hunziker, 2005, Paletto and Tosi, 2009). This enhanced colour contrast in the blue band is because a clear sky tends to scatter blue light while the tree canopy absorbs most of it. Hence, there is a low level of blue scattering from leaves (Cescatti, 2007; Chianucci, 2020). Light passing through the forest canopy gaps was dominated either by blue in the clear sky or by equal intensities of red, green, and blue wavelengths in an evenly overcast sky (Frazer et al., 2001). The background noise is relatively smaller for the blue band because the brightness difference between the blue sky and white clouds is small (Korhonen and Heikkinen, 2009).

The photo processing procedure had two phases; i.e., the determination and the quantification phases as highlighted in section 2.5. The determination phase dealt with photo pre-processing and identifying atypical photos that would incur wrong results due to abnormally segmented outputs because of cloud cover, sunlight flecks or photos without tree canopy components that resulted in wrong canopy segments. The photo pre-processing included filtering the original photos with a 5×5 Gaussian kernel to remove noise and enhance the structure of the canopy and sky elements. Gaussian filtering was applied as a guarantee to remove any potential errors related to photo acquisition, which might be caused by poor or uneven illumination. Assessment of the results of the median and Gaussian filtering with 5 pixels dimension revealed only slight changes in the segmented photos from the unfiltered ones.

The second phase of photo processing implemented in this study was the quantification of canopy fraction from the photos in the selected plots. These photos used for quantification were not

severely affected by cloud cover and flecks of sunlight problems. Quantification of CC required segmenting the photos into the canopy and non-canopy classes for which the Otsu thresholding algorithm was used (Otsu, 1979). Previous studies indicated that Otsu thresholding is an effective technique for segmenting a bimodal distribution of pixel values, as it happens in the canopy photos (Otsu, 1979; Sezgin and Sankur, 2004; Zhang and Hu, 2008; Makkar and Pundir, 2014; Borlaf-Mena et al., 2019). It automatically searches for a threshold value for each photo that minimizes intra-class variance (Otsu, 1979). An automatic selection of thresholds in the Otsu method enables objective photo processing and eliminates bias (Nobis and Hunziker, 2005).

Otsu thresholding was compared with other methods like the simple binary thresholding and adaptive thresholding to identify an appropriate photo segmentation method. The visual comparison of the results of segmentation with the original photos indicated that the Otsu thresholding gave better results in differentiating the canopy and sky segments. The simple binary thresholding was not easy to apply for all the photos since it requires exploring the distribution of pixel values of individual photos for defining the optimal global threshold values. Besides, this process suffers from subjectivity. The adaptive thresholding was able to offer automatic local thresholds, which might contribute to misclassifications. The various intensities of cloud in a photo were segmented into either of the classes during adaptive thresholding, indicating the lack of appropriateness of local thresholds for such data. Therefore, Otsu thresholding, which objectively sets a photo-specific global threshold, was chosen to segment the photos into canopy and sky.

Preliminary test results showed that correctness of the results of Otsu thresholding into the canopy and background classes varied according to the presence of tree crowns in the photo, cloud cover, and flecks of sunlight, of which the latter is mainly influenced by the time of the day (Rich, 1990). Such segmentation errors were examined manually by comparing the results of segmentation with the original photos. Sometimes the dark blue sky was misclassified to the canopy class while at another time due to sun flecks on the vegetation, some canopy components were misclassified to the sky. Based on these preliminary test results, restrictions were made to exclude atypical photos in the selection of plots for the quantification of CC. The plots containing photos contaminated by the above sources of misclassification were identified and removed. Some photos of the 14 SPs out of the total 90 SPs measured in the field had such defects. Thus, only the remaining 76 SPs were selected for the final analysis.

2.4. Analysis of the effect of photo size on canopy cover estimates

Canopy fraction was calculated from each of the segmented photos. Analysing the entire photo size could not be effective for the precise estimation of canopy fraction. Existing literature suggested the use of narrow-angle of view digital photos if the focus is on CC estimation (Korhonen et al. 2006; Paletto and Tosi, 2009). Therefore, the canopy fractions were calculated for photos with concentric squares sliced inward with side lengths of 3000 pixels (full size), 2000 pixels, 1000 pixels, 500 pixels, 400 pixels, 300 pixels, 200 pixels, and 100 pixels to get the central parts, which are getting less distorted and closer to the sampling location (Figure 4). In terms of area, the resulting segmented photos represented 100%, 44.4%, 11.1%, 2.8%, 1.8%, 1.0%, 0.4%, and 0.1%, respectively, of the full size (3000 × 3000 pixels) photos. A comparison of these photo sizes was needed to determine an appropriate view angle for canopy photography.

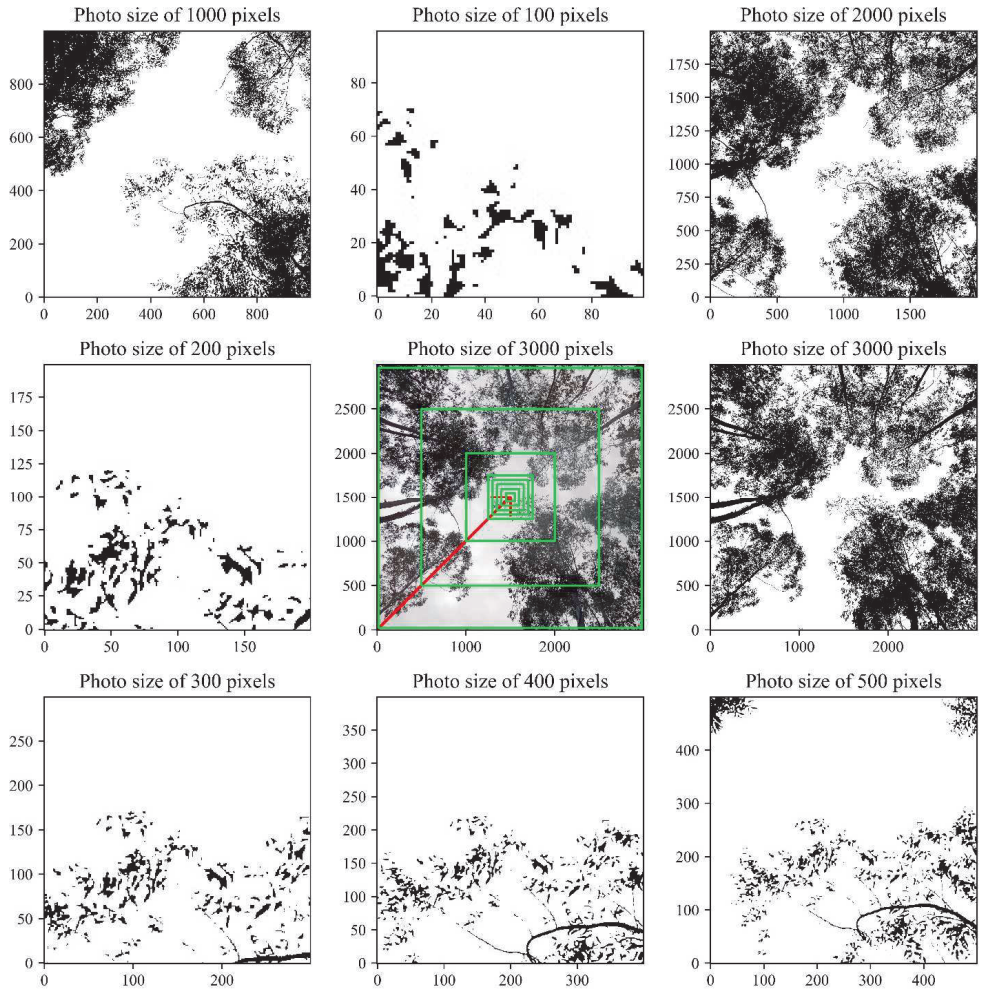

Figure 4: An example of the original RGB photo (at the centre of the subplot) and segmented photos with different sizes (border subplots). The green concentric squares in the central subplot indicate the extents to which the original image was sliced. The red line indicates the direction of change in the size of the photos.

2.5. Threshold sensitivity analysis for classifying the canopy fractions

Different canopy variables can be estimated from the segmented photos. In this study, we were interested in comparing the photo-based estimates of CC with the labour-intensive and time-consuming point-based data. We had a count of either 1's or 0's in the point-based data at each of

the photo capture locations. However, the canopy fraction values determined above could not be directly translated to CC estimates and compared with the point-based data because the canopy fractions underestimated the plot level CC for all the photo sizes.

Figure 5 indicates that most of the extreme low-density and high-density forest plots had canopy fraction estimates beyond the 95% prediction interval limits compared with the point-based data. This result suggested that these ranges of values are less likely to contain the mean CC at a 95% confidence interval. It was also observed that the canopy fractions from all the photo sizes underestimated CC. While the point-based CC ranged from 33.9 to 100% with a mean of 80.6%, the canopy fraction values fell between 29.7 and 75.2% and mean of only 56.5%.

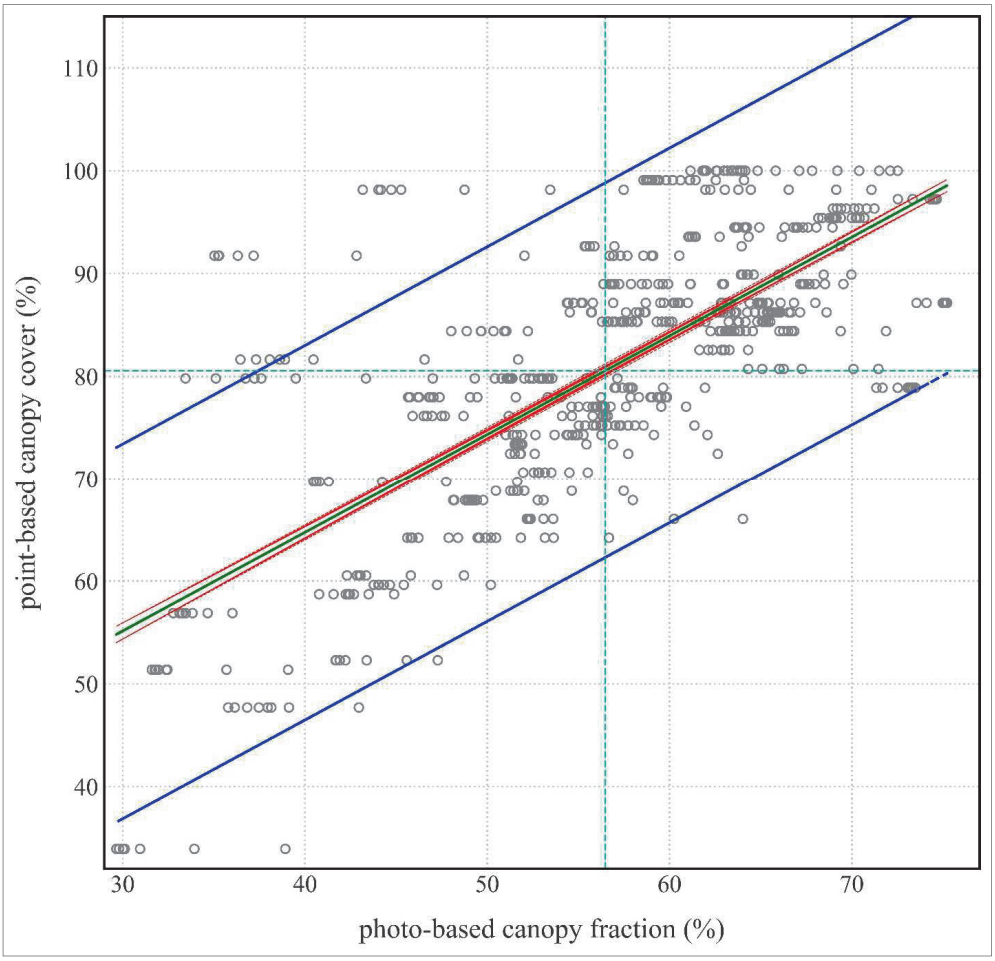

Figure 5: confidence interval (red lines) and prediction interval (blue lines) limits of predicting point-based CC from the photo-based canopy fraction. The green line shows the linear model fit. The vertical and horizontal dashed cyan lines represent the means.

Thus, the canopy fraction values of each photo underwent binary classification (classification for simplicity) into 1's or 0's, as shown in Equation 4. This classification resulted in the same data as the point-based data to make a direct comparison. To determine the effect of a classification thresholds on the resultant CC estimates, the canopy fractions of the photos in each photo size were reclassified using seven canopy fraction thresholds (i.e. 10%, 20%, 30%, 40%, 50%, 60%, and 70%). These thresholds were set to vary at intervals of the threshold of CC in the formal forest

definitions by the FAO and Ethiopia (FAO, 2000; FDRE, 2016). We tested a broader range of thresholds even beyond 50% to examine their effects on the resultant CC estimates.

$$y_{i,j,k,m} = \begin{cases} 1, & \text{if } cf_{i,j,k} \geq m \\ 0, & \text{otherwise} \end{cases} \quad (4)$$

where $y_{i,j,k,m}$ is the classified value of photo i (1, 2, 3, …, 109) within size class j (100 × 100 pixels, 200 × 200 pixels, …, 3000 × 3000 pixels) in SP k (1, 2, 3, …, 76) classified with a threshold of m (10%, 20%, …, 70%); $cf_{i,j,k}$ (which was obtained in section 2.4) is the canopy fraction of photo i of size class j in plot k.

The resulting values ($y_{i,j,k,m}$) of the classified of the canopy fraction represent absence or presence of canopy component at the zenith of the photo acquisition locations. These new values were in agreement with the point-based data, with which we made the comparison. The results of the classification were used for calculating photo-based CC at the plot level as shown in Equation 5.

$$y_{j,k,m} = \frac{\sum_{i=1}^{n} y_{i,j,k,m}}{n} \times 100 \quad (5)$$

where $y_{j,k,m}$is the photo-based CC estimate (in %) of photo size j and threshold k in plot m; n is the number of photos of respective photo size and threshold combinations in each plot m (i.e., 109).

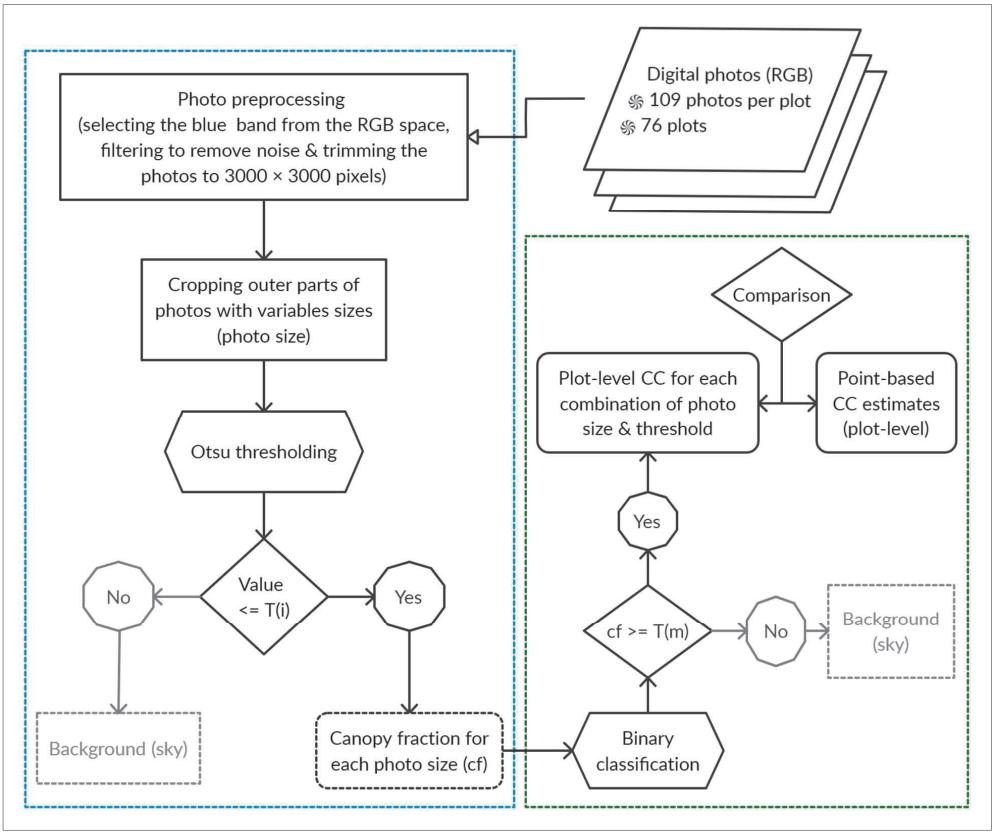

Figure 6. Flowchart for CC estimation using digital photo processing. The steps within the blue box (left side) gave canopy fraction for each photo size. The steps in the green box (right side) are for classification of the canopy fraction to get the plot-level estimates of CC for the combinations of photo sizes and classification thresholds. Otsu thresholding uses automatic threshold T(i) to segment each photo (i) in the SP into canopy and sky segments while T(m) in the classification refers to the use of m (i.e., 10%, 20%, …, 70%) thresholds to further classify the canopy fractions. See section 2.4 for detail descriptions of the photo sizes and the above paragraphs in section 2.5 for the classification thresholds.

2.6. Statistical analysis

The Chi-squared test was used to test the relationship between the two methods for detecting the presence of canopy at the observation points. To determine if there were significant effects of the photo sizes and thresholds on the estimates, the two categorical variables (i.e., the 8 factors of photo

size and 7 factors of threshold; see sections 2.4 and 2.5 for details) were compared using analysis of variance. This helped to assess the importance of these variables and their interaction effects for processing digital photos to get relatively more precise and less biased CC estimates.

The plot-level estimates of the point-based method were used to evaluate the performance of that of the photo-based method. The combinations of the different levels of photo size and classification threshold that yielded the closest estimates of plot-level CC with the point-based data were evaluated based on the Pearson's correlation coefficient (r), relative root mean square difference (RMSD%) and relative mean difference (MD%) estimates (Willmott, C.J., 1981; Curran-Everett, 2010; Rex et al., 2020). Pearson's correlation analysis was used to determine whether there was a statistically significant relationship between the methods. Evaluation of the sample variances using Levene's test indicated the appropriateness of the use of the two-sample t-test with equal variances to determine whether statistically significant differences existed in the mean CC between the two methods used for measurement at every SP. The extent of deviation of data points from the mean CC estimates derived from the different combinations of photo sizes and thresholds was evaluated using the estimated coefficient of variation (Brown, 1998). In all the statistical analyses, a confidence level of 95% was used for testing the statistical significances.

3. Results

3.1. Photo-based methods for canopy cover estimation

The photo-based estimates of CC rely on correct segmentation of the photo pixel values into the canopy and sky segments. Determination of an appropriate threshold for segmentation is vital. Figure 7 shows the optimal thresholds of photo segmentation using Otsu thresholding in the SPs. The appropriate thresholds for segmenting the pixel values of 109 photos in each SP ranged between 111.9 and 145.6 with a median of 128.1.

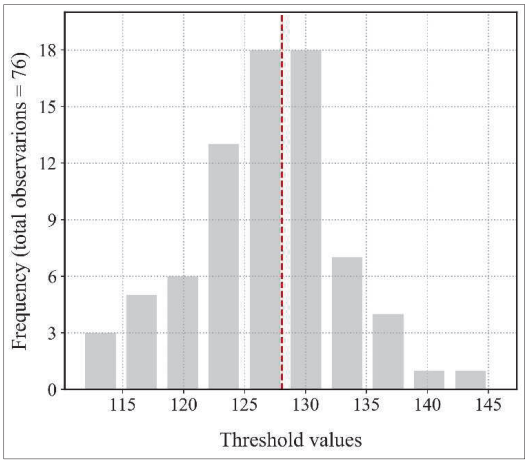

Figure 7. Distribution of the Otsu thresholds for segmenting the photos in the SPs. The dashed red vertical line represents the median of the thresholds (i.e., 128.1).

This study was conducted in a dense canopy cover condition where the minimum and average CC estimates using the point-based method were 33.9 and 80.6%, respectively (Table 1). The variances for the point-based estimates for each SP ranged between 0 and 22.9%. However, the range of variances of the photo-based estimates for individual SPs varied based on the specific combination of photo sizes and thresholds. All of the photo-based variances for each SP estimate were within the range of the point-based variances for the SPs. The CC estimates using the photo-based method were compared with the point-based data to identify the appropriate photo processing techniques for estimating CC. A summary of the statistics of the estimates of CC in the study area for each of the photo size and threshold variables is shown in Table 1. The results indicated that the mean CC estimates using digital photos increased with photo size, ranging from 64.3 to 77.9%. The standard deviation of the CC estimates increased with photo size from 16.4 to 26.9%. Despite the increase in the mean CC with an increase in photo size, all of the estimates were smaller than the mean CC using the point-based method.

The CC estimates based on the threshold classes (regardless of the photo size) indicated that they decreased by more than 50% (from 85.3 to 41.6%) with the increase in thresholds while their standard deviations increased (from 13.5 to 17.4%).

Table 1. The plot-level minimum, maximum, mean, and standard deviation (SD) of the canopy cover (CC, in %) estimates from digital photo processing using different photo sizes and thresholds and the estimates of the point-based method. Analysis of variance of the effects of the photo size, classification threshold, and their interactions is also shown for the photo-based method.

Variable	Factor	Minimum CC	Maximum CC	Mean CC	SD	F-score [b]	p-value
Photo size [a] (pixels)	100	13.8	99.1	64.3	16.4	56.2	<0.001
	200	8.3	99.1	65.4	17.4		
	300	6.4	100.0	66.2	18.2		
	400	2.8	100.0	66.8	18.8		
	500	2.8	100.0	67.2	19.4		
	1000	0.9	100.0	69.3	22.0		
	2000	0.0	100.0	74.0	25.6		
	3000	0.0	100.0	77.9	26.9		
Threshold of classification (%)	10	36.7	100.0	85.3	13.5	721.8	<0.001
	20	35.8	100.0	82.2	14.2		
	30	34.9	100.0	78.3	14.9		
	40	33.0	100.0	73.4	15.7		
	50	24.8	100.0	66.0	16.5		
	60	1.8	100.0	55.4	17.4		
	70	0.0	86.2	41.6	16.5		
Interactions [c]	---			---	---	8.0	< 0.001
Point-based estimation	---	33.9	100.0	80.6	13.4	---	---

[a] *photo size refers to the length of one side of the square-shaped photos (in number of pixels).*
[b] *significant at 95% confidence level.*
[c] *details of estimated CC for the interaction of photo size and threshold variables are presented in Table 2.*

The observed differences in the rates of change in mean CC estimates for the photo size and threshold variables encouraged us to test the interaction effect, which was significant at 95% confidence level (Table 2 and Figure 8). Table 2 indicated that the mean CC estimates ranged

between 34.8 and 98.5% for the different combinations of the photo sizes and thresholds considered in this study. The photo-based CC estimates that strongly correlated with the point-based estimates originated from only a few combinations of the photo sizes and thresholds. Photos with sizes of 300 × 300 pixels, 400 × 400 pixels, and 500 × 500 pixels (which represented 1, 1.8, and 2.8% of the original photo size) offered better estimates of CC at 10% and 20% thresholds.

Table 2. Effect of photo size and classification threshold on mean CC estimates from digital photos.

Photo size	Threshold						
	10%	**20%**	**30%**	**40%**	**50%**	**60%**	**70%**
100 × 100 pixels	76.9	74.0	70.4	66.5	61.2	54.5	46.6
200 × 200 pixels	78.9	76.0	72.6	68.1	62.1	54.8	45.5
300 × 300 pixels	80.4*	77.3*	73.8	69.3	63.0	54.8	44.5
400 × 400 pixels	81.5*	78.6*	74.8	70.4	63.8	54.8	43.6
500 × 500 pixels	82.5*	79.6*	75.7	71.0	64.1	54.6	42.9
1000 × 1000 pixels	88.0	83.7	79.6**	73.8	66.0	54.3	39.8
2000 × 2000 pixels	95.9	92.0	87.1	80.7**	71.0	55.9	35.4
3000 × 3000 pixels	98.5	96.2	92.7	86.9	76.6	59.4	34.8

* *These values, which are at the logical thresholds of CC for forest definition (FAO, 2000; FDRE, 2016), are very close to the point-based mean CC (i.e., 80.6%). Therefore, the combinations of photo sizes and thresholds that gave these estimates were discussed in detail in this paper.*

** *These estimates are also closer to the point-based CC but they had large standard deviations compared to the previous group (section 3.2. for more details). Therefore, these were not the focus of discussion.*

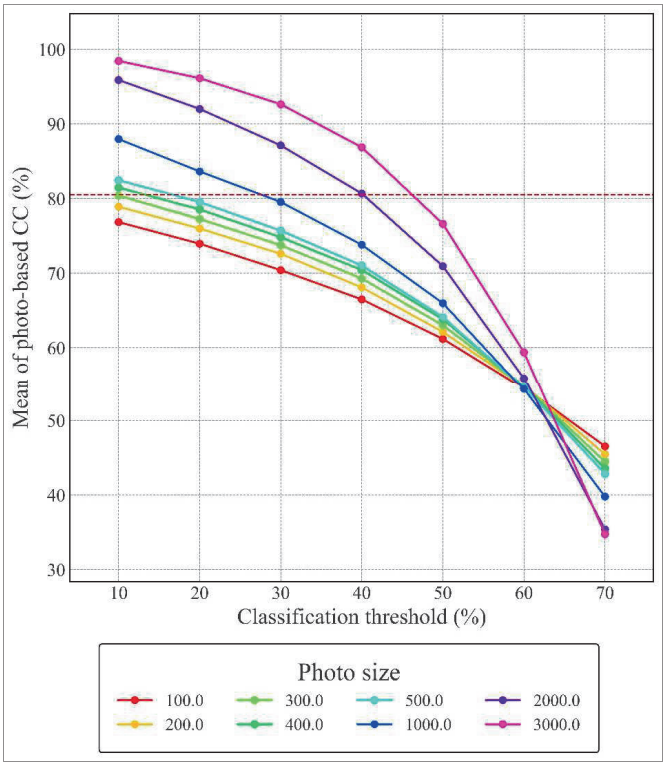

Figure 8. Interaction effect of photo size and classification threshold on the photo-based mean CC. The dashed red horizontal line is the overall mean of the point-based CC.

3.2. Evaluation of the photo-based estimates of canopy cover

Figure 9 shows the patterns of RMSD% and MD% of the photo-based estimates of CC from the point-based estimate. The combinations of the three photo sizes (i.e., 300 × 300 pixels, 400 × 400 pixels, and 500 × 500 pixels) with 10% and 20% thresholds yielded the smallest deviation in terms of RMSD% and MD%. With an increase in the thresholds, both the RMSD% and MD% values deviated from zero, which is the ideal minimum for both indicators. The figure shows the negative effect of very large photos at very small and larger classification thresholds. The larger photos tend to perform better at medium thresholds. For, instance, at 30% and 40% thresholds, estimates were better for the photo sizes of 1000 × 1000 pixels and 2000 × 2000 pixels, respectively. However, we did not emphasize these since the standard errors of these estimates were too large to consider them (i.e. greater than that of the point-based data).

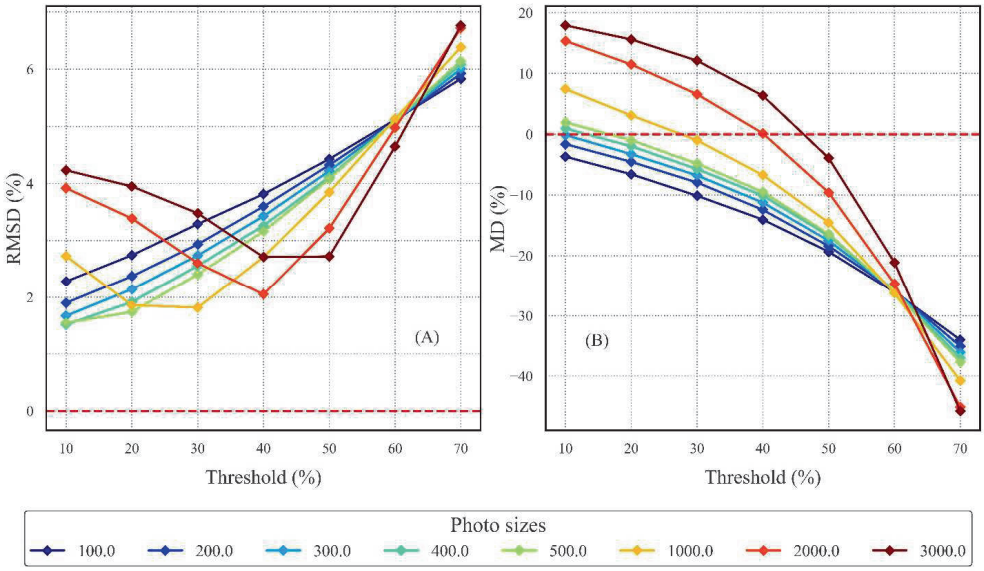

Figure 9. (A) RMSD% (relative root mean square difference) and (B) MD% (relative mean difference) of the photo-based CC data using the different photo sizes (different colours; see legend) and classification thresholds (x-axes) compared with the point-based data. The dashed red horizontal lines represent the ideal values for the absence of any differences in CC between the photo-based and point-based methods.

Figure 10 shows a very strong relationship in the mean CC estimates between the point-based and photo-based methods using the identified photo sizes and thresholds. The photo-based estimates at the 10% threshold had stronger correlations with the point-based data (0.95, 0.96, and 0.96 for the photo sizes of 300 × 300 pixels, 400 × 400 pixels, and 500 × 500 pixels, respectively). The estimates using the same respective photo sizes at the 20% threshold had correlation coefficients of 0.92, 0.94, and 0.95 with the point-based data (Pearson's correlation test; p-value < 0.05 for all).

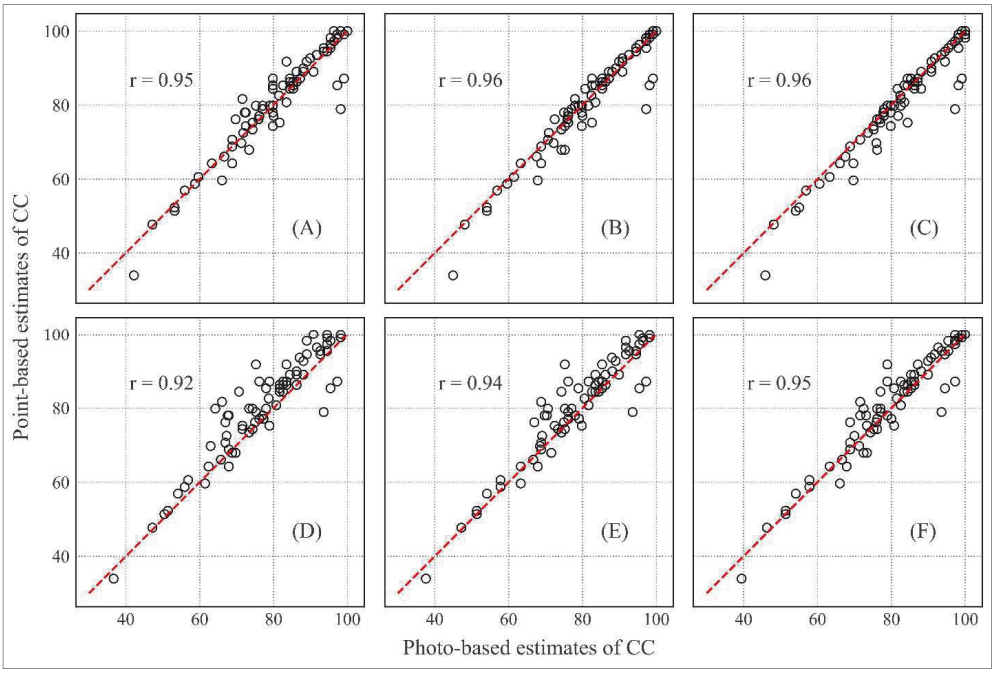

Figure 10. Relationship of the point-based and photo-based estimates of CC using 10% threshold for the photo sizes of (A) 300 × 300 pixels, (B) 400 × 400 pixels, and (C) 500 × 500 pixels and 20% thresholds for photo sizes of (D) 300 × 300 pixels, (E) 400 × 400 pixels, and (F) 500 × 500 pixels. The dashed red diagonal lines represent the identical (1:1) lines of each subplot.

In Table 3, we see that the results of the 10% threshold of the canopy fractions from the photo sizes of 500 × 500 pixels slightly overestimated the CC (82.5%) but was not significant. This was a more precise estimate than the other options (with a standard deviation of 12.6%). The use of a 20% threshold underestimated CC for all of the three photo sizes compared with their 10% equivalents. Similarly, the estimates with a 20% threshold for all the three photo sizes were less precise than their counterparts with the 10% threshold were. The CV for the 500 × 500 pixels photo size with a 10% threshold was the smallest of all the possible combinations. The MD% followed a similar pattern. For the identified optimum photo sizes, the estimates with a 10% threshold had a relatively smaller MD% than the 20% threshold equivalents. The CC with 10% threshold for photo sizes of 400 × 400 pixels and 500 × 500 pixels were 0.9% and 1.9% (respectively) beyond the point-based

CC. However, the 20% threshold had negative MD% for all the three optimum photo sizes indicating underestimation. Generally, the results showed an underestimation of CC for thresholds greater than or equal to the 20% and photo sizes smaller than or equal to 500 × 500 pixels, which represent the relatively less distorted sections of the digital photos. The MD% of all the identified optimum combinations of the photo sizes and thresholds were not significantly different from zero at a 95% confidence level. The results for the photo size of 300 × 300 pixels at the 10% threshold had the least MD% (-0.13).

Table 3. The estimates of mean, SD, and coefficient of variation (CV) of the photo-based CC using the selected photo sizes and thresholds and their relative mean differences (MD%) from the point-based data. The unit of all the estimators is percentage.

Optimum combinations of thresholds and photo sized for CC estimation	Mean CC	SD	CV	MD% [d]
10% threshold and 300 × 300 pixels	80.4	13.0	16.1	-0.1
10% threshold and 400 × 400 pixels	81.5	12.7	15.6	0.9
10% threshold and 500 × 500 pixels	82.5	12.6	15.3	1.9
20% threshold and 300 × 300 pixels	77.3	13.1	17.0	-3.3
20% threshold and 400 × 400 pixels	78.6	13.0	16.6	-2.0
20% threshold and 500 × 500 pixels	79.6	13.1	16.5	-1.0
Point-based data	80.6	13.5	16.8	---

[d] *the MD% were insignificant at 95% level of confidence.*

4. Discussions

4.1. Otsu thresholding for photo segmentation and time of canopy photography

A visual check of the performance of the Otsu thresholding method indicated that it misclassified atypical photos. This could be because the timing of photo capture in those SPs where the atypical photos were taken was not in the ideal diffuse sky condition as recommended by Anderson (1964). A direct penetration of sunlight through the forest canopy influenced the quality of the photos. These results were in agreement with the recommendations of previous studies (Rich, 1990; Chianucci, 2020). The fieldwork for canopy photography should be adjusted during the time of the day when the sky is uniformly overcast or when there is a perfectly diffuse sky condition although

this may increase inventory costs. Cloudy days, overhead sun and darkness/shadow should be avoided during photo taking for canopy cover estimation to eliminate possible discard of data. Therefore, inventory planning should account for appropriate scheduling for enhancing technical and financial efficiency.

4.2. Effect of photo size and classification threshold on canopy cover

The results indicated that photo size had a significant effect on the forest CC estimates. The increase in CC with increasing photo size might be due to the distortions in the outer sections of the photos. The photos towards the edges have distorted geometries, coarse pixel resolutions, and are blocked by tree trunks, which minimize the canopy gap fraction (Gonsamo et al., 2010; Gonsamo et al., 2013). The results revealed that removing the distorted outer parts of the photos significantly affected the CC estimates. The bigger photos gave larger estimates of CC, which is in line with previous studies that exhibited similar patterns when using digital photos for CC estimation (Korhonen et al., 2006; Gonsamo et al., 2013; Bianchi et al., 2017). Despite the increasing trend with an increase in photo size, all of the photo-based estimates across the photo sizes were smaller than the point-based CC. The deviation might be because the point-based estimates were based on counts of either 1 or 0 at each sampling location whereas the processed photos, most of which represented dense CC, had gap elements that contributed to smaller canopy fractions above the point of observation. The canopy fractions computed from the digital photos with all the different sizes were less precise and deviated from the point-based data. This was the motivation for the classification of the canopy fraction values.

Classification of the canopy fraction data with the different thresholds gave a logical comparison of the CC estimates and enabled the identification of feasible thresholds for a more precise estimation of CC. When photo size is not taken into consideration, the CC estimates at 10% and 20% thresholds were slightly larger than the point-based CC. This could be because the photos that had a significant amount of canopy gaps were classified as canopy (1) since the thresholds were small. This effect of overestimation at the specified thresholds increased tremendously with an increase in the size of the photos. The CC estimates from the full-size photos analysed with different thresholds had extreme values, indicating the huge uncertainty associated with the use of the entire photo for CC estimation.

The CC estimates using the central slices of the photos were more precise than the larger photos indicating the higher confidence associated with the use of these portions of the photos for generating information about forest CC. This was supported by the small MD% and RMSE% values associated with estimates using these photo sizes. Only a small central part of the vertical photo (less than 3% of the size of the original photo) was useful for CC estimation. Objects in this central portion of the photos are relatively free from distortion and the CC estimates had a strong coherence with the point-based method. They preserved the geometry of canopy gaps and resulted in a minimal deviation from the point-based data. This result was supported by other research findings that recommended a narrow-angle of view to obtain a reliable CC estimation using photographic techniques (Korhonen et al., 2006; Paletto and Tosi, 2009; Chianucci, 2016). Paletto and Tosi (2009) described the advantages of using narrow-angle photographic methods that they are simple to perform and suitable for CC estimation.

Photo sizes smaller than 300 × 300 pixels underestimated CC for all the thresholds. This could be due to under-sampling of the canopy fractions in which the canopy elements were not adequately represented (Gonsamo et al., 2013). Hence, these small photo sizes could not provide comparable estimates of CC with the point-based method. This may also be attributed to greater vulnerability to the effect of solar illumination close to the nadir location that exaggerated canopy gap fraction estimates (Gonsamo et al., 2013). The effect was more pronounced in the photos acquired during midday when the sun was overhead. This could be a critical challenge as Rich (1990) indicated that sunlight shining through tiny holes in a forest canopy could make it difficult to find a consistent estimate of CC.

Underestimation of CC for distortion-free photo sizes when the threshold values were greater than or equal to 30% suggests the irrelevance of such thresholds for classifying the canopy fraction into canopy and sky (non-canopy) classes in such dense forests. The suitability of 10% and 20% thresholds for classifying the canopy fractions could be attributed to the fact that most SPs had large CC. The photos had a significant proportion of canopy that did not contribute to omission error for the canopy class, which could enhance correct classification at these thresholds. Therefore, the main concern in the use of these small thresholds should be controlling misclassification of non-canopy photos into the canopy class (commission error) that could easily be made. Therefore, cautions such as careful planning of the fieldwork and adhering to schedules of photo acquisition are needed for conducting canopy photography (Frazer et al., 2001).

4.3. Evaluation of the selected photo-based canopy cover estimates

The observed strong linear relationship between the point-based data and the selected photo-based estimates of CC indicates the potential of digital photography for CC assessment in the study forest type. The possibility of choosing different combinations of photo sizes and thresholds for optimum estimation of CC offers flexibility to the photo-based methods. This in turn improved the precision of the estimates. The optimum photo sizes and thresholds were able to yield standard deviations smaller than that of the point-based data. This might be due to the objective sampling and photo processing in the photo-based methods.

Among the optimum variable combinations, the slightly overestimated CC at 10% threshold for the point-based method could be due to the presence of inter-crown gaps that might be recorded open (gap fraction) in the point-based method while it could be misclassified into the canopy fraction in the photo-based method at this small (10%) threshold level (i.e., commission error). The results of the evaluation of the photo-based estimates of CC with the point-based data revealed that smaller thresholds provide estimates with better precision. This could also justify the appropriateness of the photo segmentation using Otsu thresholding.

The strong intercorrelation among the photo-based CC estimates using the identified optimum thresholds and photo sizes revealed the suitability of the photo-based method for precise estimation of CC. The photo-based method introduced in this study provided flexibility to choose a range of photo sizes and classification thresholds to enhance the precision of CC estimates.

5. Conclusions

Setting up a strict photo processing procedure is important for estimating CC from photos captured using ordinary digital cameras. The use of the central less distorted section of digital photos for CC estimation demands setting a reasonable threshold for classification of the canopy fractions into canopy and sky classes. For dense forests like the ones in this study area, 1-3% of the central part of the photos and 10% or 20% thresholds were found to yield a meaningful relationship with the point-based data. The photo-based techniques using the optimum photo sizes and thresholds showed a very strong correlation with the point-based data, which ranges from 0.92 to 0.96, indicating the possibility of using digital photography for precise estimation of CC. These photo sizes and classification thresholds provided a more precise estimation than the intensive-sampling

point-based method. Further research is needed to test the efficiency of this method against other accurate measurement techniques like the use of the Cajanus tube.

The camera lens used in this study was so wide that there were canopy gap distortions in the photos, which affected the quality of the photo-based CC data. For this technique to be effective, narrow-angle camera lenses are recommended for capturing relevant canopy photos. This is particularly useful for avoiding distortion close to the edges and improving sampling resolution at the central sections of the canopy photo (Gonsamo et al., 2010; Chianucci, 2020). Therefore, further research is needed to identify suitable focal length ranges for a more efficient assessment of canopy cover in different forest canopy conditions. The photo processing and data analysis workflow should also be automated to avoid subjectivity. The recent advances in digital cameras and data processing applications can contribute to improving the data quality and automating the processing routines of a large number of photos.

The methods of CC estimation used in this study could be relevant for supporting silvicultural management in tropical species-rich forests where light competition is severe. It can also provide useful information like the availability of adequate shade trees for agro-forestry systems like the traditional forest-coffee production practices in Ethiopia. The method is important for supporting forest monitoring and inventory in developing countries. It can also contribute to advancing the techniques of CC estimation in different forest types.

Acknowledgements

We are grateful for the logistics support we got from Hawassa University - Wondo Genet College of Forestry and Natural Resources. We also thank the field crew members for their contribution to the successful data collection.

Funding

This work was financially supported by the Norwegian Embassy in Ethiopia under the Mekelle/Hawassa/NMBU collaboration programme [ETH 14/0002 to H.T.].

Competing Interests

The authors have declared that no competing interests exist.

References

Akike, S. and Samanta, S., 2016. Land use/land cover and forest canopy density monitoring of Wafi-Golpu project area, Papua New Guinea. *Journal of Geoscience and Environment Protection*, *4*(08), 1-14, http://dx.doi.org/10.4236/gep.2016.48001.

Alivernini, A., Fares, S., Ferrara, C. and Chianucci, F., 2018. An objective image analysis method for estimation of canopy attributes from digital cover photography. *Trees*, *32*(3), pp.713-723, https://doi.org/10.1007/s00468-018-1666-3.

Anderson, M.C., 1964. Studies of the woodland light climate: I. The photographic computation of light conditions. *J. Ecol.,* pp.27-41, https://doi.org/10.2307/2257780.

Bellows, R.S., Thomson, A.C., Helmstedt, K.J., York, R.A. and Potts, M.D., 2016. Damage and mortality patterns in young mixed-conifer plantations following prescribed fires in the Sierra Nevada, California. *For. Ecol. Manage., 376*, pp.193-204.

Bianchi, S., Cahalan, C., Hale, S. and Gibbons, J.M., 2017. Rapid assessment of forest canopy and light regime using smartphone hemispherical photography. *Ecol. Evol., 7*(24), pp.10556-10566, https://doi.org/10.1002/ece3.3567.

Borlaf-Mena, I., Tanase, M.A. and Gómez-Sal, A., 2019. Methods for tree cover extraction from high-resolution orthophotos and airborne LIDAR scanning in Spanish dehesas. *Revista de Teledetección, 53*, 17-32. https://doi.org/10.4995/raet.2019.11320.

Bosiers, J.T.; Dillen, B.G.M.; Draijer, C.; Kleimann, A.C.; Polderdijk, F.J.; de Wolf, M.A.R.C.; Klaassens, W.; Theuwissen, A.J.P.; Peek, H.L. and Folkerts, H.O., 2003. "A 35-mm format 11 M pixel full-frame CCD for professional digital still imaging," in *IEEE Trans. Electron Devices, 50*(1), pp.254-265, https://doi.org/10.1109/TED.2002.806477.

Brown, C.E., 1998. Coefficient of variation. In *Applied multivariate statistics in geohydrology and related sciences* (pp.155-157). Springer, Berlin, Heidelberg. https://doi.org/10.1007/978-3-642-80328-4_13.

Brown, P.L., Doley, D. and Keenan, R.J., 2000. Estimating tree crown dimensions using digital analysis of vertical photographs. *Agric. For. Meteorol.*, *100*(2-3), pp.199-212.

Calder, I., Hofer, T., Vermont, S. and Warren, P., 2008. Towards a new understanding of forests and water. *UNASYLVA-FAO-*, *229*, p.3.

Calder, I.R., 2001. Canopy processes: implications for transpiration, interception and splash induced erosion, ultimately for forest management and water resources. *Plant Ecol., 153*, pp. 203-214.

Cao, S., Lu, C. and Yue, H., 2017. Optimal tree canopy cover during ecological restoration: a case study of possible ecological thresholds in Changing, China. *Bioscience*, *67*(3), pp.221-232.

Cescatti, A., 2007. Indirect estimates of canopy gap fraction based on the linear conversion of hemispherical photographs: Methodology and comparison with standard thresholding techniques. *Agric. For. Meteorol., 143*(1-2), pp.1-12, https://doi.org/10.1016/j.agrformet.2006.04.009.

Chianucci, F., 2016. A note on estimating canopy cover from digital cover and hemispherical photography. *Silva Fenn., 50*(1), pp.1-10, https://doi.org/10.14214/sf.1518.

Chianucci, F., 2020. An overview of in situ digital canopy photography in forestry. *Can. J. For. Res., 50*(3), pp.227-242, https://doi.org/10.1139/cjfr-2019-0055.

Chianucci, F., Chiavetta, U. and Cutini, A., 2014. The estimation of canopy attributes from digital cover photography by two different image analysis methods. *IForest., 7*(4), p.255, https://doi.org/10.3832/ifor0939-007.

Ćosović, M., Bugalho, M.N., Thom, D. and Borges, J.G., 2020. Stand structural characteristics are the most practical biodiversity indicators for forest management planning in Europe. *Forests*, *11*(3), p.343, https://doi.org/10.3390/f11030343.

Curran-Everett, D., 2010. Explorations in statistics: correlation. *Adv. Physiol. Educ., 34*(4), pp.186-191, https://doi.org/10.1152/advan.00068.2010.

Dawson, T.P., Curran, P.J., North, P.R.J. and Plummer, S.E., 1999. The propagation of foliar biochemical absorption features in forest canopy reflectance: a theoretical analysis. *Remote Sens. Environ.*, *67*(2), pp.147-159, https://doi.org/10.1016/S0034-4257(98)00081-9.

Deichmann, J. L., Hernandez-Serna, A., Delgado C., J. A., Campos-Cerqueira, M., & Aide, T. M., 2017. Soundscape analysis and acoustic monitoring document impacts of natural gas exploration on biodiversity in a tropical forest. *Ecol. Indic., 74*, pp.39-48. https://doi.org/10.1016/j.ecolind.2016.11.002.

FAO (Food for Agriculture Organization of the United Nations). 2000. On definitions of forest and forest change. Forest Resources Assessment Programme, Working Paper 33. FAO, Rome, Italy.

FDRE (Federal Democratic Republic of Ethiopia). 2016. Ethiopia's forest reference level submission to the UNFCCC (United Nations Framework Convention on Climate Change). Available online: https://redd.unfccc.int/files/ethiopia_frel_3.2_final_modified_submission.pdf (accessed on 03 August 2020).

Fitzgerald, S.A., 2005. Fire ecology of ponderosa pine and the rebuilding of fire-resilient ponderosa pine ecosystems.

Frazer, G.W., Fournier, R.A., Trofymow, J.A. & Hall, R.J., 2001. A comparison of digital and film fisheye photography for analysis of forest canopy structure and gap light transmission. *Agric. For. Meteorol.*, *109*(4), pp.249-263, https://doi.org/10.1016/S0168-1923(01)00274-X.

FVC (Fractional vegetation cover). 2020. In: Liang S. and Wang J. (eds) *Advanced Remote Sensing*, pp. 477-510, https://doi.org/10.1016/B978-0-12-815826-5.00012-X.

Gemmell, F., 1999. Estimating conifer forest cover with Thematic Mapper data using reflectance model inversion and two spectral indices in a site with variable background characteristics. *Remote Sens. Environ., 69*(2), pp.105-121, https://doi.org/10.1016/S0034-4257(99)00004-8.

Goldsmith B. 1991. Vegetation monitoring. In: Goldsmith B. (eds) *Monitoring for Conservation and Ecology*. Conservation Biology, vol. 3. Springer, Dordrecht, the Netherlands, https://doi.org/10.1007/978-94-011-3086-8_5.

Gonsamo, A., D'odorico, P. and Pellikka, P., 2013. Measuring fractional forest canopy element cover and openness – definitions and methodologies revisited. *Oikos*, *122*(9), pp.1283-1291, https://doi.org/10.1111/j.1600-0706.2013.00369.x.

Gonsamo, A., Walter, J.M.N. and Pellikka, P., 2010. Sampling gap fraction and size for estimating leaf area and clumping indices from hemispherical photographs. *Can. J. For. Res.*, *40*(8), pp.1588-1603, https://doi.org/10.1139/X10-085.

Goodenough, A.E. and Goodenough, A.S. 2012. Development of a rapid and precise method of digital image analysis to quantify canopy density and structural complexity. *ISRN Ecol.*, *2012*, pp.1-11, https://doi.org/10.5402/2012/619842.

Hofhansl, F., Chacón-Madrigal, E., Fuchslueger, L., Jenking, D., Morera-Beita, A., Plutzar, C., Silla, F., Andersen, K.M., Buchs, D.M., Dullinger, S. and Fiedler, K. 2020. Climatic and edaphic controls over tropical forest diversity and vegetation carbon storage. *Sci. Rep.*, *10*(1), pp.1-11, https://doi.org/10.1038/s41598-020-61868-5.

Hwang, B., Hundera, K., Mekuria, B., Wood, A. and Asfaw, A., 2020. Intensified Management of Coffee Forest in Southwest Ethiopia Detected by Landsat Imagery. *Forests*, *11*(4), pp.1-21, https://doi.org/10.3390/f11040422.

Jennings, S.B., Brown, N.D. and Sheil, D., 1999. Assessing forest canopies and understorey illumination: canopy closure, canopy cover and other measures. *Forestry: An International Journal of Forest Research*, *72*(1), pp.59-74, https://doi.org/10.1093/forestry/72.1.59.

Johansson, T., 1985. Estimating canopy density by the vertical tube method. *For. Ecol. Manage.*, *11*(1-2), pp.139-144, https://doi.org/10.1016/0378-1127(85)90063-5.

Kern, C.C.; Burton, J.I.; Raymond, P.; D'Amato, A.W.; Keeton, W.S.; Royo, A.A.; Walters, M.B.; Webster, C.R. and Willis, J.L. 2017. Challenges facing gap-based silviculture and possible solutions for mesic northern forests in North America. *Forestry: An International Journal of Forest Research*, *90*(1), pp.4-17, https://doi.org/10.1093/forestry/cpw024.

Korhonen, L. and Heikkinen, J., 2009. Automated analysis of in situ canopy images for the estimation of forest canopy cover. *Forest Science*, *55*(4), pp.323-334, https://doi.org/10.1093/forestscience/55.4.323.

Korhonen, L., Ali-Sisto, D. and Tokola, T., 2015. Tropical forest canopy cover estimation using satellite imagery and airborne LIDAR reference data. *Silva Fenn.*, *49*(5), pp.1-18, http://dx.doi.org/10.14214/sf.1405.

Korhonen, L., Korhonen, K.T., Rautiainen, M. and Stenberg, P., 2006. Estimation of forest canopy cover: a comparison of field measurement techniques, *Silva Fenn., 40*(4), pp.577-588, https://www.doi.org/10.14214/sf.315.

Korhonen, L., Korpela, I., Heiskanen, J. and Maltamo, M., 2011. Airborne discrete-return LIDAR data in the estimation of vertical canopy cover, angular canopy closure and leaf area index. *Remote Sens. Environ.*, *115*(4), pp.1065-1080, https://doi.org/10.1016/j.rse.2010.12.011.

Landert, K.A., 2016. Comparing Photographic and GIS-based applications for estimating canopy cover in Southern Appalachian Bogs, *Proceedings of the National Conference on Undergraduate Research*, University of North Carolina, Asheville, North Carolina.

Ligot, G., Balandier, P., Courbaud, B. and Claessens, H., 2014. Forest radiative transfer models: which approach for which application? *Can. J. For. Res.*, *44*(5), pp.391-403, https://doi.org/10.1139/cjfr-2013-0494.

Macdonald, H. and Macdonald, G., 2016. *HabitApp*. Available online: https://play.google.com/store/apps/details?id=com.scrufster.habitapp (accessed on 27 July 2020).

Makkar, H. and Pundir A. 2014. Image Analysis Using Improved Otsu's Thresholding Method. *International Journal IJRITCC. 2*(8), pp.2122 – 2126.

McRoberts, R.E., Tomppo, E.O. and Czaplewski, R.L., 2015. Sampling designs for national forest assessments. *Knowledge Reference for National Forest Assessments; FAO: Rome, Italy*, pp.23-40.

Mello, J.M.D., Scolforo, H.F., Raimundo, M.R., Scolforo, J.R.S. and Oliveira, A.D.D., 2015. Estimating precision of systematic sampling in forest inventories. *Ciênc. Agrotec., Lavras, 39*(1), pp.15-22, https://doi.org/10.1590/S1413-70542015000100002.

Næsset, E. 1997. Estimating timber volume of forest stands using airborne laser scanner data. *Remote Sens. Environ.*, *61*(2), pp.246-253, https://doi.org/10.1016/S0034-4257(97)00041-2.

Nobis, M. and Hunziker, U., 2005. Automatic thresholding for hemispherical canopy-photographs based on edge detection. *Agric. For. Meteorol.*, *128*(3-4), pp.243-250, https://doi.org/10.1016/j.agrformet.2004.10.002.

Otsu, N., 1979. A threshold selection method from gray-level histograms. *IEEE Trans. Syst. Man Cybern., 9*(1), pp.62-66, https://doi.org/10.1109/TSMC.1979.4310076.

Palace, M., Sullivan, F.B., Ducey, M. and Herrick, C., 2016. Estimating tropical forest structure using a terrestrial LiDAR. *PLoS One*, *11*(4), p.1-19, https://doi.org/10.1371/journal.pone.0154115.

Paletto, A. and Tosi, V., 2009. Forest canopy cover and canopy closure: comparison of assessment techniques. *Eur. J. For. Res., 128*(3), pp.265-272, https://doi.org/10.1007/s10342-009-0262-x.

Penman, J., Gytarsky, M., Hiraishi, T., Krug, T., Kruger, D., Pipatti, R., Buendia, L., Miwa, K., Ngara, T., Tanabe, K. and Wagner, F., 2003. Good practice guidance for land use, land-use change and forestry. URL: https://www.ipcc-nggip.iges.or.jp/public/gpglulucf/gpglulucf_contents.html.

Piper J., Pelc R. (2020) Consumer versus Dedicated Digital Cameras in Photomicrography. In: Pelc R., Walz W., Doucette J. (eds) Neurohistology and Imaging Techniques. Neuromethods, vol 153. Humana, New York, NY. https://doi.org/10.1007/978-1-0716-0428-1_13.

Pratt, D.J., Greenway, P.J. and Gwynne, M.D., 1966. A classification of East African rangeland, with an appendix on terminology. *J. Appl. Ecol.*, pp.369-382.

Python Software Foundation: https://docs.python.org/3.7/.

Rex, F.E., Silva, C.A., Dalla Corte, A.P., Klauberg, C., Mohan, M., Cardil, A., Silva, V.S.D., Almeida, D.R.A.D., Garcia, M., Broadbent, E.N. and Valbuena, R., 2020. Comparison of Statistical Modelling Approaches for Estimating Tropical Forest Aboveground Biomass Stock and Reporting their Changes in Low-intensity Logging Areas using Multi-temporal LiDAR Data. *Remote Sens., 12*(9), pp.1-21, https://doi.org/10.3390/rs12091498.

Rich, P.M., 1990. Characterizing plant canopies with hemispherical photographs. *Remote sensing reviews*, *5*(1), pp.13-29, https://doi.org/10.1080/02757259009532119.

Sezgin, M. and Sankur, B., 2004. Survey over image thresholding techniques and quantitative performance evaluation. *J. Electron Imaging, 13*(1), pp.146-166, https://doi.org/10.1117/1.1631315.

Singh, M., Evans, D., Coomes, D.A., Friess, D.A., Suy Tan, B. and Samean Nin, C., 2016. Incorporating canopy cover for airborne-derived assessments of forest biomass in the tropical forests of Cambodia. *PloS one*, *11*(5), p.1-14, https://doi.org/10.1371/journal.pone.0154307.

Taubert, F., Jahn, M.W., Dobner, H.J., Wiegand, T. and Huth, A. 2015. The structure of tropical forests and sphere packings. *Proceedings of the National Academy of Sciences*, *112*(49), pp.15125-15129, https://doi.org/10.1073/pnas.1513417112.

Tichý, L., 2016. Field test of canopy cover estimation by hemispherical photographs taken with a smartphone. *J. Veg. Sci., 27*(2), pp.427-435, https://doi.org/10.1111/jvs.12350.

Topcon Positioning Systems Inc. Available online: https://www.topconpositioning.com/gb/ (accessed on 16 September 2019).

UNFCCC (United Nations Framework Convention on Climate Change). 2001. Report of the Conference of the Parties on its seventh session (COP7), Part 2: Action taken by the Conference of the Parties. Marrakesh, Morocco. 69 p.

Vilanova E. 2020. Silvicultural Practices in Venezuelan Natural Forests: A Historical Perspective and Prospects of Sustainable Forest Management [Online First], IntechOpen, DOI: 10.5772/intechopen.93279. Available from: https://www.intechopen.com/online-first/silvicultural-practices-in-venezuelan-natural-forests-an-historical-perspective-and-prospects-of-sus (accessed on 07 August 2020).

Willmott, C.J., 1981. On the validation of models. *Phys. Geogr., 2*(2), pp.184-194, https://doi.org/10.1080/02723646.1981.10642213.

Zhang, J. and Hu, J. 2008. Image Segmentation Based on 2D Otsu Method with Histogram Analysis. In *International Conference on Computer Science and Software Engineering, Hubei*, 2008, pp. 105-108, https://doi.org/10.1109/CSSE.2008.206.

Zhang, Z., Cao, L. and She, G., 2017. Estimating forest structural parameters using canopy metrics derived from airborne LiDAR data in subtropical forests. *Remote Sens.*, *9*(9), pp.1-26, https://doi.org/10.3390/rs9090940.

ISBN: 978-82-575-1792-2
ISSN: 1894-6402

Norwegian University
of Life Sciences

Postboks 5003
NO-1432 Ås, Norway
+47 67 23 00 00
www.nmbu.no

109406 / ANDVORDGRAFISK.NO